Defining the Cellular and Molecular Basis of Spondyloepiphyseal dysplasia tarda

Thesis

Defining the cellular and molecular basis of Spondyloepiphyseal dysplasia tarda

Francesca Zappa

Discipline: Life sciences

Affiliated research center: Telethon institute of genetics and medicine

Thesis submitted in accordance with the requirements of the Open University

for the degree of Doctor of Philosophy

November 2016

To Antonella,

your guidance made this journey possible.

List of contents

ABSTRACT

One third of the proteome is transported in membrane-encapsulated vesicles from the endoplasmic reticulum (ER) to the Golgi apparatus en route to the plasma membrane, other intracellular organelles and the extracellular matrix. After folding, newly synthesized proteins reach the Golgi apparatus through COPII carriers. COPII vesicles bud from sub-domains of the ER, named ER exit sites (ERES) and are composed of five rapidly cycling proteins: the small GTPase Sar1, the inner coat (Sec23/Sec24) and the outer layer (Sec13/31). The efficiency of COPII cycling is dispensable for the transport of small soluble cargoes or trans-membrane cargoes, yet is mandatory for the exit of "extra-size" proteins, such as procollagens. To facilitate the incorporation of procollagens into nascent COPII carriers, several adaptors work in cooperation at ERES. One of them is sedlin, a small protein that acts as a co-GAP for Sar1, thus increasing its kinetics. The idea that sedlin is important for collagen transport is enforced by the evidence that a rare Mendelian disorder, Spondyloepiphyseal dysplasia tarda (SEDT), is caused by sedlin mutations in which the main clinical manifestation is an alteration in collagen deposition.

With the aim to clarify sedlin functions in membrane trafficking, I followed two different approaches: (1) biochemical analysis of sedlin interactors and (2) the generation of a sedlin KO medaka model. Using mass spectroscopy approaches, several proteins were shown to interact with sedlin of which one of the most significant was CLIC1. Subsequent experiments showed that deletion of CLIC1 delayed protein secretion. Furthermore, this work showed that CLIC1 and sedlin, as well as the COPII inner coat, take part in the integrated stress response (IRS).

Upon perturbations that change cellular homeostasis such as heat shock, redox stress or unfolded protein accumulation, cells activate signalling pathways that result in translation inhibition by sequestering free mRNAs and ribonucleoproteins in cytosolic aggregates named stress granules (SGs).

I demonstrated that SGs control secretion by recruiting key components of ER-to-Golgi trafficking and thus inhibit anterograde transport. This suggested that the ISR regulates protein metabolism on two levels: translationally and post-translationally, by sequestering mRNAs and inhibiting protein export from the ER, respectively. Additionally, by using TALEN technology, I edited the sedlin gene in medaka to create a SEDLIN KO stable line (Sedl-/-). Sedl-/- fish have severe skeletal defects, which are similar to those observed in human SEDT patients, and die soon after birth suggesting that sedlin has an essential role in early postnatal medaka growth.

To investigate the molecular pathways altered in sedlin-/- vertebrates I performed a Transcriptomic analysis on whole larvae highlighting that eye and cartilage are the two most affected organs and led to the hypothesis of a common pathogenetic mechanism.

These findings provide evidence that sedlin is involved in different molecular pathways and when mutated can contribute to the pathogenesis of SEDT. Thus, my thesis work has shed light on a new control mechanism that involves ER-to-Golgi transport and establishes the first SEDT animal model, a suitable tool to find SEDT correctors.

List of figures

List of tables

Chapter1

Introduction:

Cells rapidly adapt to environmental changes that affect homeostasis by activating catabolic pathways such as autophagy as well as attenuating anabolic pathways such as DNA replication, protein translation and synthesis.

Another key anabolic pathway is protein transport through the secretory pathway. It has been estimated that one-third on the transcribed genome enters the secretory pathway (Kanapin et al., 2003) suggesting that the machinery dedicated to this process needs to be finely tuned to guarantee efficient protein secretion. Once synthetized in the endoplasmic reticulum, cargoes fold, accumulate and then reach the Golgi complex through COPII-coated carriers. Five components are sufficient to bud a COPII vesicle *in vitro* but a set of protein adaptors is required to modulate ER export *in vivo.* However, how the minimal requirements of a COPII vesicle and the activity of accessory factors are modulated to meet the different needs of cellular metabolism is not completely understood.

1.1 Principles of ER-export: COPII-coated vesicles

Proteins that need to be modified in the Golgi complex possess an N-terminal signal sequence, the signal recognition particle (SRP), which co-translationally or post-translationally drives the nascent polypeptide chain into the endoplasmic reticulum (ER) lumen. The environment in the ER is optimized for the folding and maturation of proteins to be packaged for export (Braakman & Bulleid 2011). Conditions in the ER are oxidizing, ATP is available as an energy source, and the ionic environment is neutral with a high concentration of calcium. The lumen is filled with molecular chaperones, thiol oxidoreductases,

prolyl isomerases, and N-linked glycan–modifying enzymes. The total concentration of protein in the ER has been estimated to be equal to or even exceed 100mg/mL, which means that the space in the ER lumen is extremely crowded (Booth & Koch 1989). Once properly folded, protein cargo is sorted in a specific sub-domain of the smooth endoplasmic reticulum, known as ER exit sites (ERES), from which they are transported to the Golgi complex. The machinery dedicated to this process was first identified in yeast in an elegant genetic screen for proteins necessary for secretion (Novick et al., 1980). Subsequently, Schekman and colleagues characterized ER-to-Golgi transport by reconstituting vesicle formation from ER membranes using the minimal requirements for vesicle budding (Salama et al., 1993). They further demonstrated that vesicles budding from the ER are coated and have a diameter of 60-65 nm, distinct from COPI-coated vesicles (responsible for the retrieval of cargo from the Golgi to the ER) and were cleverly coined COPII-coated vesicles (Barlowe et al., 1994). Currently, it is known that COPII-coated vesicle formation is initiated by the activation of the cytosolic small GTPase Sar1 by an ERES-localized guanine nucleotide exchange factor (GEF) called Sec12, exposing a hydrophobic helix that inserts into the ERES microdomain that actively bends the membrane to begin vesicle formation. Activated Sar1 binds the inner coat composed of Sec23/24, which in turn recruits the outer coat, Sec13/31. Structural analysis of the Sec23/24-Sar1 interaction revealed a bow-tie-shaped complex with a concave surface aptly shaped for binding the membrane vesicle and further demonstrated this interaction is stabilized by the binding of a GTP molecule (Bi et al., 2002). The Sec13/31 assembly unit is a heterotetramer comprising Sec13/Sec31-Sec31/Sec13, the “architectural core” of which is

organized to form a 28-nm long rod. Twenty-four copies of this rod assembly are required to form the COPII cuboctahedron (Stagg et al., 2006). Rapid GTP hydrolysis on Sar1 requires Sec23/24, which is the GTPase-activating protein (GAP) for the reaction (Yoshihisa et al., 1993), and its activity is accelerated 10-fold by interacting with the Sec13/31 complex (Antonny et al., 2001). Thus, the GTP hydrolysis reaction on Sar1 is programmed in the COPII budding process so as to couple coat assembly with disassembly. Budding is mediated by a Sar1 hydrophobic helix that creates membrane asymmetry and guarantees fission (Fig 1.1).

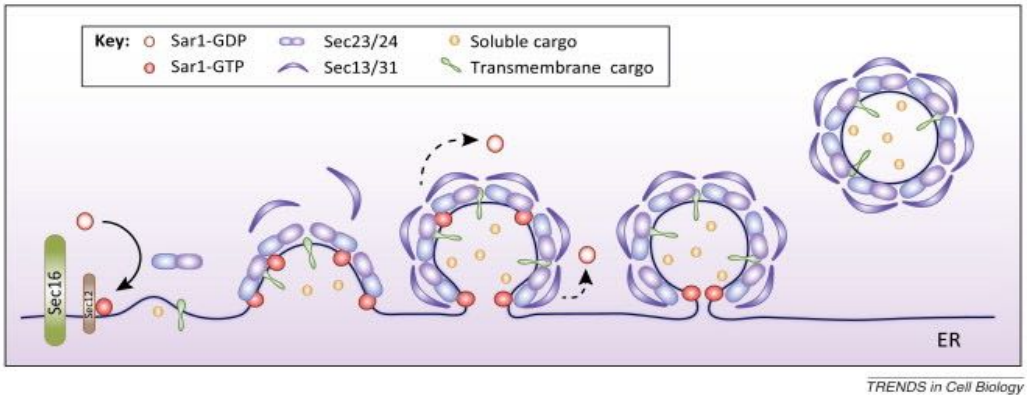

Figure 1.1 COPII budding at ERES. Sar1 is inactivated through the GAP activity of the inner coat subunit Sec23, which is further enhanced by the outer COPII layer comprising the Sec13/31 tetrameric complex. The Sec13/31 complex is recruited to the prebudding complex and forms cage-like structures that impose membrane curvature and have an organizational role by conferring structural rigidity to the COPII coat. The next step in COPII carrier biogenesis is membrane fission, a process driven by the ability of the amphipathic N-terminal helix of Sar1-GTP to insert into the membrane and induce surface asymmetry between the outer and inner membrane leaflet, thus initially promoting curvature and subsequently creating lipid-packing defects in the inner leaflet that result in hemifusion and fission. (Adapted from Venditti et al., 2014)

1.2 Mechanisms of cargo capture or bulk flow in COPII vesicles

Cargo molecules can be packaged into COPII carriers using different

mechanisms: (I) bulk-flow; (II) cargo capture or (III) the direct binding to Sec24.

(I) Bulk flow export is a passive means of ER secretion where soluble or membrane-associated proteins are stoichiometrically sequestered into COPII vesicles by default. The cargo molecules are simply included as components of the bulk membrane and fluid.

(II) Cargo capture is a process by which, after proper folding, proteins are released from chaperones and bind to specific receptors localized on ERES that mediate their capture and packaging into COPII-nascent carriers.

(III) Trans-membrane cargoes can be exported out of the ER by binding directly to the inner COPII coat component Sec24. To accommodate the diversity of cargo that must transit through the ERES, cells express multiple isoforms of the Sec24 adaptor protein, each with up to four non-overlapping cargo recognition sites (Barlowe, 2016).

1.3 Pathways of COPII megacarrier formation

Whereas coat subunits bind to these subdomains dynamically (with a half-time $t_{1/2}$ of ~3 s), ERES can be visually tracked as stable domains for minutes by live-cell fluorescence imaging (Forster et al., 2006). Over time, ERES can form de novo, fuse, and divide. In addition to changes in size, the total number of ERES per cell varies from one to several hundred, depending on cell type and status (Stephens, 2003). The dynamic structure of ERES is consistent with their function as a major sorting hub in the secretory pathway. The COPII coat performs a critical role not only in carrier vesicle formation but also in selective loading of cargoes. Given its role, it seems reasonable to expect that COPII coat dynamics have to be finely tuned. A question that has remained open for years

in the field, and has now been partially addressed, regards the plasticity of the nascent vesicles to accommodate comparatively large molecules (e.g. procollagens or chylomicron particles) that exceed the size of "typical" COPII-coated vesicles. Studies on collagen secretion and COPII architecture postulated that the megacarriers needed to transport such large cargo would need accessory proteins for their formation. Another limiting factor is represented by membrane source at ERES, since larger COPII vesicles would likely require an additional source of membrane. Malothra and co-workers proposed a model in which TANGO1, an ERES-localized trans-membrane protein essential for procollagen export, first binds to procollagen in the ER lumen and then subsquently dimerizes with cTAGE that concentrates Sec12 at ERES to further recruit more Sec23/24 inner coat protein (Saito et al., 2009). The TANGO1-Sec24 interaction leads to a conformational change of the cargo protein that allows for the exposure of a TAAR domain that binds to the ER-Golgi intermediate compartment (ERGIC) trans-membrane protein ERGIC-53. The fusion of ERGIC membranes with procollagen VII-enriched domains provides a means for the growth of a mega export carrier commensurate for a larger cargo. This process of carrier biogenesis is fundamentally different from the mechanism by which canonical COPII vesicles form at the ER to transport secretory cargoes (Santos et al., 2015). Another example of accessory proteins is represented by Sedlin (see below) and the Cul3 ubiquitinase that, upon calcium release from the ER, mediates Sec31 modification allowing for the formation of COPII megacarriers that promote collagen secretion (McGourty et al., 2016). An efficient COPII machinery is mandatory for collagen secretion since genetic mutations in Sar1B alter exclusively chylomicron secretion while Sec23A and

Sec24D affect only collagen export. However, it is still not clear whether megacarriers are coated, partially coated, or COPII proteins are only required at ERES but do not bud with collagen-containing carriers (fig. 1.2).

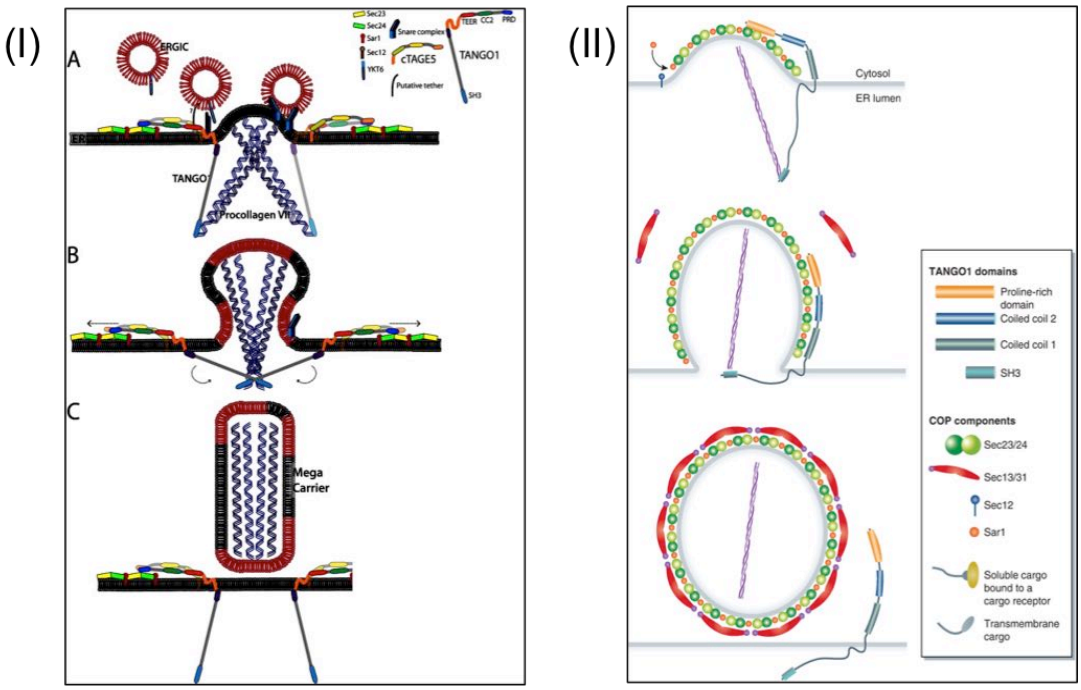

Figure 1.2 Proposed models for collagen export. (I) (**A**) A pool of ERGIC membranes fuse to the ER exit site enriched in procollagen. TANGO1 acts as a tether binding to recruit ERGIC membranes. (**B**) Binding of the proline-rich domain of TANGO1 on the cytoplasmic side to Sec23/24, prevents Sec13/31 recruitment, allowing continuous fusion of ERGIC membranes that result in the growth of the nascent bud into a mega-bud that is enriched in procollagen VII. (**C**) The SH3-like domain of TANGO1 dissociates from procollagen, which triggers the separation of the proline-rich domain from Sec23/24. This activates fission, to release the procollagen VII filled mega-carrier from the ER. TANGO1 remains at the ER exit site and not exported with the outgoing procollagen VII. (Adapted from Santos AJ 2015)
(II) (A) TANGO1 interacts with cTAGE5 and both proteins interact with Sec23/24 on COPII-coated carriers. **(B)** TANGO1 binds procollagen in the lumen of the ER, which may promote the subsequent binding to Sec23/24, retarding the recruitment of Sec13/31 to Sec23/24, thus delaying the completion of the COPII cage and promoting the growth of the larger COPII carriers that can accommodate the large procollagen fibrils **(C). (**Adapted from Malhotra and Erlmann 2011)

1.4 Regulation of COPII-coated vesicles

Although the structure of COPII vesicles have been broadly described, less is known about their regulation when cells are submitted to insults that change cell homeostasis. It has been reported that induction of the COPII recruitment cycle is slower in cells undergoing the unfolded protein response (UPR) compared to control cells, suggesting that ER export is partially impaired upon stress (Amodio et al., 2013). Recent work in yeast has shown that Sec24 is phosphorylated and targeted for autophagy upon starvation. This mechanism represents a limiting factor from the ER-export process (Davis et al., 2016) suggesting that ER-export can be modulated under stress conditions. Data in support of these ideas have been provided by the Rabouille laboratory who demonstrated that Sec16, a protein that gives identity to ERES, is less associated with membranes upon amino acid deprivation (Zacharogianni et al., 2011) thus leading to a defect in protein secretion. Furthermore, analysis of *Drosophila* cell lines postulated the existence of a transient, non-membrane bound ERES component reservoir (the "sec bodies") that form upon starvation. These aggregates are similar to other non-membrane bound aggregates, the stress granules (see below), but they are physically independent of each other (Zacharogianni et al., 2014). However, in the same experimental conditions, no sec bodies in mammalian cells have been observed suggesting that this mechanism is not conserved among evolution.

In conclusion, although some progress has been made, to date the mechanisms through which COPII formation/kinetics are regulated remain elusive.

1.5 The TRAPP complex

The TRAnsport Protein Particle (TRAPP) was first identified in yeast in 1998. The study focused on the protein Bet3, previously identified in a large-scale genetic screen as an essential gene that genetically interacts with ER-to-Golgi SNAREs but is not part of a SNARE complex (Rossi et al., 1995). Using Bet3 as a probe and using a combination of genetic and biochemical studies, the core components of the yeast TRAPP complex were identified. TRAPP components were named with the pre-fix "trs" (transport subunits) followed by a number corresponding to the molecular weight of each protein: Trs20, Trs23, Trs33, Trs31 and Trs18 (more commonly known as Bet5). The complex was proposed to participate in ER-to-Golgi trafficking since depletion of Bet3 caused an impairment in the arrival of COPII vesicles to the Golgi complex. Furthermore, the trafficking defect could be overcome by over-expression of an ER-to-Golgi specific SNARE suggesting that the TRAPP complex acts upstream of COPII fusion with Golgi membranes (Sacher et al., 1998). Following the identification of an additional four sub-units (Trs65, Trs85, Trs120, and Trs130) and the observation that orthologs are present in mammals (Sacher et al., 2000), a role for TRAPP as a tethering factor that acts during the docking of COPII vesicles with the Golgi was proposed (Barrowman et al., 2000). The interest in TRAPP became stronger in the community when Wang et al. (2000) demonstrated that the multi-molecular complex is able to bind and activate the small GTPase Ypt1. Ypt1 belongs to the Ypt/Rab family that exchange GDP for GTP, thus activating the protein. The cycle is achieved by nucleotide exchange and GTP hydrolysis. Since the intrinsic rate of nucleotide exchange and GTP hydrolysis are low for most of

small GTPases, accessory proteins that stimulate these reactions are required. Guanine nucleotide exchange factors (GEFs) and GTPase activating proteins (GAPs) are therefore mandatory to guarantee efficient Rab function (Barr and Lambright, 2010). YPT1 is an essential gene in yeast and once activated the protein is recruited onto ER membranes and subsequently promotes the recruitment of a set of downstream effectors responsible for vesicle formation, movement, tethering, and fusion of ER-derived vesicles (Morsomme et al., 2002). In 2001, Sacher and co-workers postulated the existence of two different TRAPP complexes. TRAPPI, the core that functions in ER-to-Golgi trafficking by docking COPII vesicles with Golgi membranes and subsequently activating Ypt1, and the larger TRAPPII complex that contains additional sub-units. TRAPPII is required for intra-Golgi trafficking since mutations in Trs130, a TRAPPII specific sub-unit, show defects in hydroxylase carboxyl-peptidase (CPY) maturation. CPY is a vacuolar protein that enters into the secretory pathway and can be followed easily biochemically through the secretory pathway. CPY is considered to be in its p1 form when in the ER, p1' after it enters the *cis*-Golgi, p2 once it arrives at the *trans*-Golgi, and, finally, it localizes to the vacuole as the mature form. While CPY is in its ER form in Bet3 mutants, the cargo is blocked at the *cis*-Golgi in Trs130 mutants, suggesting that TRAPPII-specific components are required for the intra-Golgi trafficking (Sacher et al., 2001). However, in the same year in which it was shown that TRAPP acts as a GEF, the exclusivity of the complex as a Ypt1 exchange factor was refuted. In the Nava Segev laboratory, the activity of purified TRAPP on both Ypt1 and Ypt31/32 was demonstrated *in vitro.* Whether TRAPP is able to activate either Ypt1 on the

cis-Golgi or Ypt31/32 on the *trans*-Golgi has been an issue broadly debated in the field (Jones et al., 2000; Morozova 2006; Barrowman et al., 2010) despite strong evidence supporting that TRAPPII specific subunits are required for the specificity switch of a Ypt GEF to coordinate Golgi entry and exit (Morozov et al., 2006). Currently it is well accepted that the yeast TRAPP complex can stimulate both Ypt1 (TRAPPI) and YPT31/32 (TRAPPII) (Kim et al., 2016) and that the minimal requirements for binding and activating Ypt1 (Bet5, Trs23, Bet3 and Trs31) (Kim et al., 2006) are masked by TRAPPII specific sub-units that indeed confer specificity for Ypt31/32.

However, understanding the functionality of the different TRAPP assemblies is still confounding the field.

So far, in addition to TRAPPI and TRAPPII, another two TRAPP complexes have been identified (TRAPPIII and TRAPPIV). Trs85 is the TRAPP sub-unit that gives specificity to TRAPPIII (Lynch-Day et al., 2010). TRAPPIII is targeted to the pre-autophagosomal structure (PAS) and it is mandatory for autophagy. Autophagy defects are not due to CPY mis-trafficking to the vacuole but rather to an active role of TRAPPIII through Trs85 on the PAS (Nazarko et al., 2005; Meiling-Wesse et al., 2005). TRAPPIII is recruited to the PAS through Atg9-containing vesicles and stimulates Ypt1 that, in turn, activates the autophagic kinase Atg1 and/or the coiled-coil Atg11 on the PAS (Karuta et al., 2012; Wang et al 2013; Lipatova 2012). Interestingly, Ypt1 mutant autophagic defects are not fully mimicked by trs85Δ raising the possibility that other Ypt1 GEFs could participate in autophagy. Very recently Lipatova et al. (2016) have demonstrated the existence of another form of the TRAPP complex that they named TRAPPIV. While TRAPPII indirectly participates in autophagy through its activity on

Ypt31/32 (Zou at al., 2013), TRAPPIII and TRAPPIV are required for the Ypt1-Atg11 autophagy module (Lipatova et al., 2016) (fig. 1.3).

Moreover, it has been demonstrated that TRAPPII, but also TRAPPIII, are required for trafficking from early endosomes to the late Golgi (Cai et al., 2005; Shirahama-Noda et al., 2013)

Although not completely clarified, to date the picture in yeast shows that, depending on their assembly, different TRAPP complexes act at different stages of membrane trafficking either stimulating the small GTPases Ypt1 and Ypt31/32 or acting as tethering factors to allow membrane fusion (fig. 1.4).

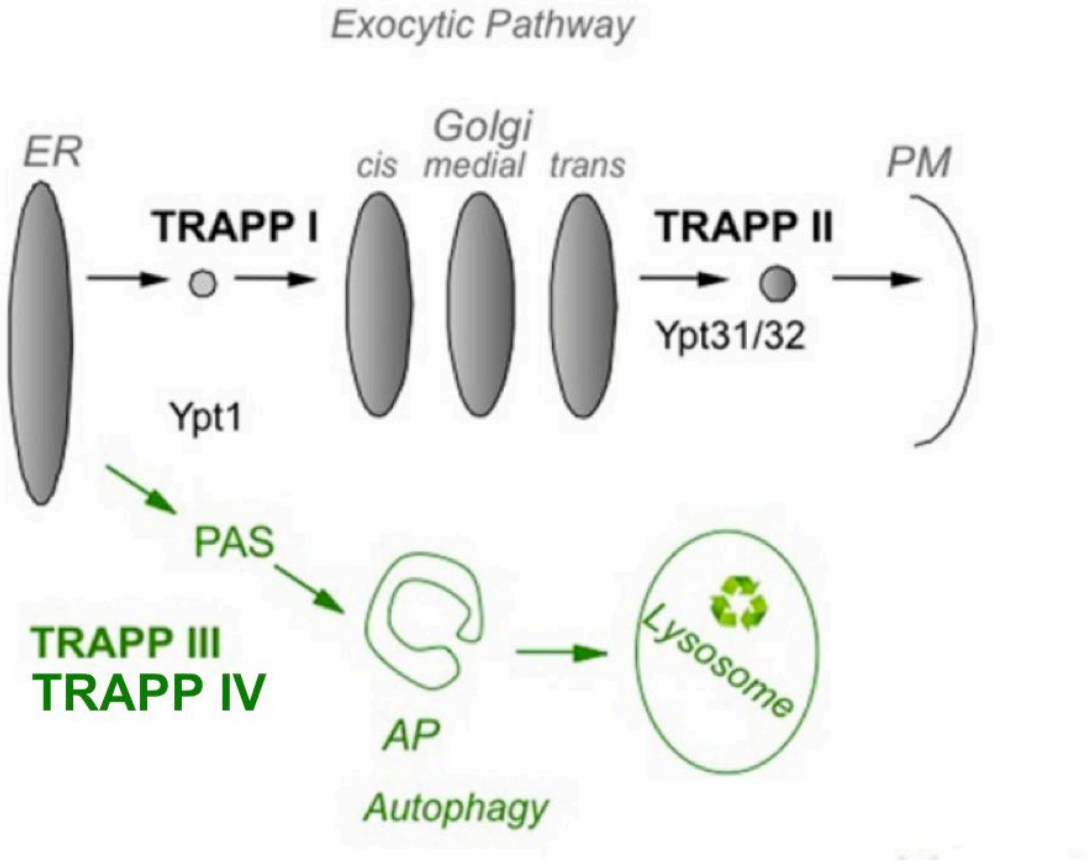

Figure 1.3 The role of TRAPP complexes and their Ypt substrates in yeast intra-cellular trafficking. In the exocytic pathway (top), TRAPP I activates Ypt1 to regulate ER-to-Golgi transport, whereas TRAPP II activates Ypt31/32 to regulate Golgi-to-PM transport. In autophagy (bottom), a cellular recycling pathway (in green), TRAPP III and TRAPP IV activate Ypt1 to regulate the assembly of PAS, the first step of autophagy. PAS is required for the formation of the double-membrane autophagosome (AP), which delivers cargo for degradation in the lysosome (Adapted from Kim et al., 2016).

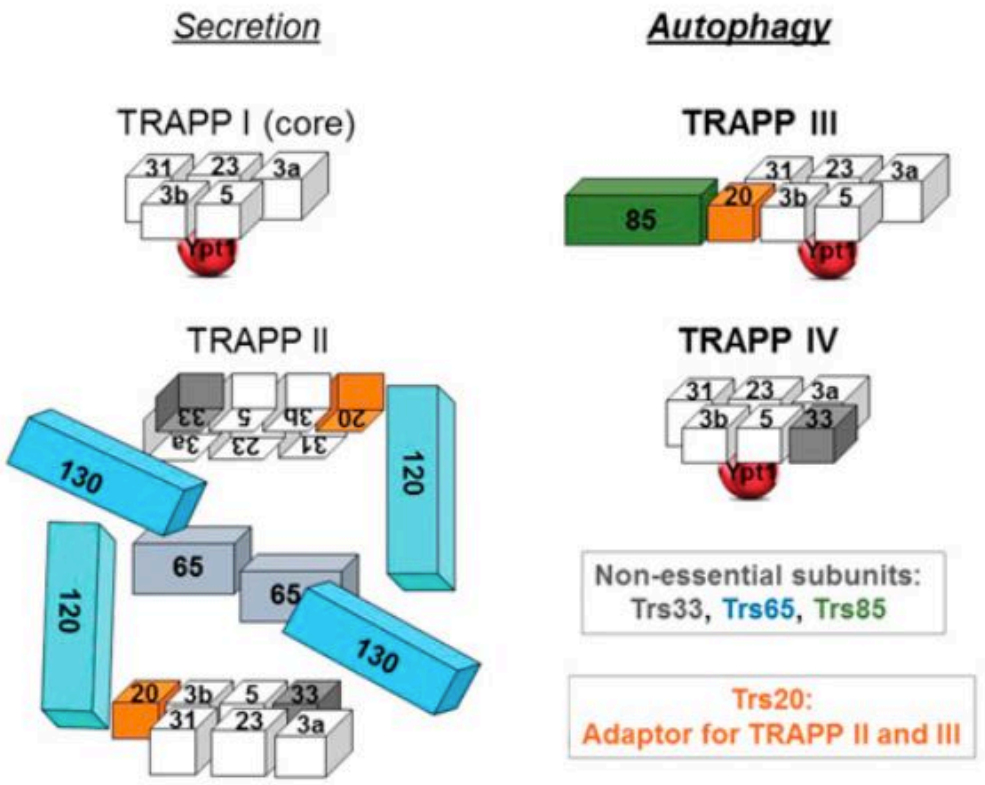

Figure 1.4. Different assemblies of yeast TRAPP complexes. (A) Core TRAPP, which contains four small subunits with two copies of Bet3 (3a and 3b), self assembles, binds Ypt1 through Bet5 and Trs23 and acts as a Ypt1-GEF. TRAPP I contains core TRAPP, Trs20 and Trs33. However, it is not clear that the presence of the latter two subunits is required for its function. **(B)** TRAPP II contains TRAPP I, including Trs20 and Trs33, and three large subunits: Trs120, Trs130, and the non-essential Trs65. Trs20 is required for the interaction of TRAPP I with Trs120, and either Trs65 or Trs33 are required for assembly of TRAPP II *in vivo*. TRAPP II is depicted here as a dimer. The cubes representing the subunits are roughly proportionate to their size. **(C)** TRAPP III contains core TRAPP, Trs20, which is required for its assembly with Trs85 and its function in autophagy**. (D)** TRAPP IV contains the core TRAPP and the not essential subunit Trs33. (Adapted from Lipatova et al., 2016).

1.6 The Mammalian TRAPP complex

The first evidence of a functional role of TRAPP in mammalian cells came in 2005 from Loh and colleagues. Mammalian Bet3 (mBet3) distribution was analysed, and was found to be prevalently cytosolic with a minor fraction (about 15%) associated with Golgi membranes. Transport assays on semi-intact cells

showed that the acute inhibition of Bet3 with an inhibitory antibody blocked the arrival of VSV-G (a cargo reporter) to the Golgi (Loh et al., 2005).

In mammals, once budded, COPII carriers can either fuse with each other (homotypic fusion) or tether and fuse with the intermediate compartment (heterotypic fusion), a pre-Golgi compartment that is absent in yeast.

Yu et al. (2006) showed that mBet3 is localized on ER exit sites and is required for homotypic fusion. Thus, mBet3 depletion/inactivation blocks cargoes in COPII-positive structures. Consistent with the proposal that mBet3 is needed for intermediate compartment biogenesis, Yu and al. found an alteration of Golgi architecture in mBet3-depleted cells (Yu et al., 2006). Although evidence concerning the localization of mBet3 are very detailed and convincing, the functional analyses performed upon protein depletion are less clear. Furthermore, observations from others (Venditti et al., 2012) refuted the model proposed by Yu et al. regarding mBet3-dependent intra-Golgi trafficking. Moreover, studies performed by depleting or inactivating mBet3 have not clarified which TRAPP complex is being effected since mBet3, present as a double copy, represents the core of the complex, a minimal requirement shared by all TRAPP isoforms (Kim et al., 2006). Two different TRAPP complexes have been identified in mammals, TRAPPII (Yamasaki et al., 2009) and TRAPPIII (Bassik et al., 2013) but the existence of other TRAPPs cannot be excluded. mTRAPPs are composed of 11 sub-units (table 1.1) and the sub-unit composition (C9 and C10 for TRAPPII and C8, C11, C12 and C13 for TRAPPIII) determines complex identity.

YEAST TRAPP SUBUNIT	MAMMALIAN TRAPP SUBUNIT
Bet5p	TRAPPC1
Tva17p	TRAPPC2L
Trs20p	TRAPPC2
Bet3p	TRAPPC3
Trs23p	TRAPPC4
Trs31p	TRAPPC5
Trs33p	TRAPPC6a,b
Trs65p	
Trs85p	TRAPPC8
Trs120p	TRAPPC9
Trs130p	TRAPPC10
	TRAPPC11
	TRAPPC12

Table 1.1 Mammalian and yeast TRAPP nomenclature. TRAPPII specific sub-units (blue), TRAPPIII-specific sub-units (green).

mTRAPPII binds γCOPI and stimulates Rab1 activity (the orthologue of yeast Ypt1) and depletion of mTRAPPII specific sub-units inhibit Golgi-to-PM trafficking (Yamasaki et al., 2009). Binding of mTRAPPII with γCOPI is also necessary for localization of the complex on lipid droplets (LDs) where it activates another small GTPase, Rab18. Mutations in Rab18 or its GEFs/GAPs are associated with a neurological genetic disorder (Warburg–Sjo–Fledelius syndrome (WARBM)) in which the only abnormal feature observed in cells derived from patients is the accumulation of lipid droplets. Interestingly, transient depletion or genetic ablation of mTRAPPII mimic the phenotype observed in WARBM cells opening the possibility that mTRAPPs can act on different Rabs in distinct compartments (Li et al., 2016). TRAPPII has also been found to indirectly activate Rab8 on the centrosome of the primary cilium. Rabin8 is the Rab8 GEF that shuttles from a Rab11-positive compartment

(recycling endosomes) to the centrosome. Westlake et al., demonstrated that TRAPPII is required for rabin8 localization and depletion of TRAPPII specific sub-units partially impairs ciliogenesis (Westlake et al., 2011). On the other hand, TRAPPIII has been found to regulate ER-to-Golgi export since knock down of TRAPPIII-specific subunits (TRAPPC11/C12) blocks cargoes in a brefeldin A-resistant compartment meaning that under these conditions, newly synthetized proteins are not able to reach the Golgi complex. To date, the precise molecular mechanisms that underlie these phenotypes have not been determined. More recently, TRAPPIII has been associated with the autophagic pathway since alteration of the complex III leads to an impairment of autophagosome biogenesis (Imai et al. 2013; Lamb et al., 2016). However, differently from yeast in which the involvement of TRAPPIII/IV in the pre-autophagosomal compartment (PAS) formation is independent from anterograde or retrograde transport, in mammals it is still unclear whether mTRAPPIII has a direct role in autophagosome formation or if it affects this catabolic process indirectly by regulating endosomes-to-Golgi trafficking of Atg9 vesicles. (fig.1.5)

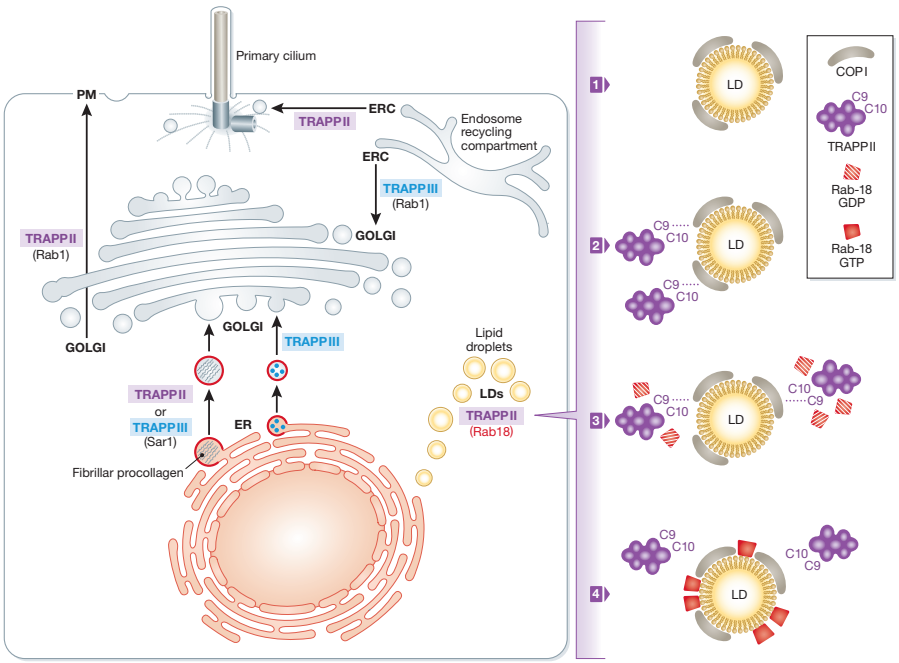

Figure 1.5 Functions of mammalian TRAPPs. Two TRAPP complexes have been identified in mammalian cells, TRAPPII and TRAPPIII, which share common core subunits (TRAPPC1, C2, C3, C4, C5) but differ in the peripheral subunits: TRAPPII contains TRAPPC9 and C10 while TRAPPIII contains C8, C11, C12 and C13. The scheme illustrates the different steps along the anterograde and retrograde membrane trafficking pathways that are under control of each TRAPP complex. In anterograde trafficking, TRAPPC2 is required for the ER export of fibrillar procollagens indicating a cargo-specific role for TRAPPII and/or TRAPPIII in this step, TRAPPIII is required for ER-to-Golgi trafficking, while TRAPPII controls intra-Golgi and/or Golgi to plasma membrane trafficking and the trafficking of ciliary proteins from endosomes to the primary cilium. In the retrograde pathway TRAPPIII controls the trafficking from endosomes to the Golgi complex of different cargoes including ATG9, a key component of the autophagic machinery. The report by Li et al. (2016) highlights a novel site of action for TRAPPII at lipid droplets. Also indicated are the Rabs activated by TRAPPII and by TRAPPIII at their different sites of action.

1.6.1 TRAPP in mammalian diseases

1.6.1.2 TRAPPC11

TRAPPC11 omozygous mutations have been found in some patients with triple A syndrome (Koehler et al., 2016). The disease spectrum includes cerebral

atrophy, mental retardation, scoliosis and muscular dystrophy. Recessive mutations also cause a disease with a milder phenotype that partially overlap with triple A disorder. Fibroblasts obtained from patients show defects in early Golgi trafficking and alteration in Lamp1 (a trans-membrane lysosomal protein) glycosylation (Bo¨gershausen et al., 2013). Studies performed using TRAPPC11*mut* zebrafish as an animal model revealed that in addition to alterations in protein secretion, TRAPPC11 is required for glycosylation in the endoplasmic reticulum, a protein function completely independent from its role in membrane trafficking. The authors speculated that this finding could be relevant for human disease since abnormal glycosylation has been found in patients with muscular dystrophy and mental retardation. This idea is enforced by evidence that mis-regulation of the glycosylation pathway causes lipid dysfunction, and TRAPPC11*mut* human fibroblasts show an accumulation of lipid droplets and some patients present steatosis (Liang et al., 2015).

1.6.1.2 TRAPPC9

Homozygous mutations in the TRAPPC9 gene cause intellectual disability and microencephaly (Ganeshwaran et al., 2009). Interestingly, TRAPPC9 was first identified as a a positive regulator of the NF-κb pathway (Zhang et al., 2015), but if the defect observed in the brain is associated with protein mistrafficking or to an hyperactivation of the NF-κb pathway has yet to be explored.

1.6.1.3 TRAPPC2

Mutations in TRAPPC2 (*SEDL*), which encodes the protein called sedlin, cause Spondyloepiphyseal dysplasia tarda. SEDT is a late-onset X-linked recessive genetic disorder characterized by disproportionately short stature with short

trunk and arm span significantly greater than height. At birth, affected males are normal in length and have normal body proportions. Patients exhibit retarded linear growth beginning around age six to eight years. Final adult height is typically 137-163 cm. Progressive joint and back pain with osteoarthritis ensues; hip, knee, and shoulder joints are commonly involved but to a variable degree. Hip replacement is often required as early as age 40 years. Interphalangeal joints are typically spared. Motor and cognitive milestones are normal. Various mutations essentially result in an apparent loss of function, and a complete unaltered sedlin protein is absolutely essential for normal bone growth (Gedeon et al., 2012). Interestingly, seven *SEDL* pseudogenes were detected in the human genome: *SEDLP1* on chromosome 19q13.4; *SEDLP2,* another retropseudogene (not transcribed) on chromosome 8; and five truncated pseudogenes, *SEDLP3–SEDLP7,* on chromosome Yq11.23 (Gecz et al., 2000).

Northern blot analysis and RT (reverse transcription)–PCR experiments revealed ubiquitous expression of both the x-linked *SEDL* and *SEDLP1* chromosome 19 with a transcript size of approximately 2.8 kb. There are only six nucleotide differences in the ORFs of the two sequences, but the encoded amino acid sequences are identical.

So far, more than 30 different mutations in the human sedlin gene have been identified (Gecz et al., 2000). The first functional studies were performed on the yeast orthologue Trs20, which is an essential gene (Sacher et al., 1998). It was observed that over-expression of disease-causing mutations in TRS20 temperature-sensitive mutants does not rescue cell viability (Gecz et al., 2003) suggesting that a full-length completely functional sedlin is needed.

Interestingly, Trs20 is shared by all TRAPP complexes but it is not required for Ypt1 activation (Kim et al., 2006) and Trs20 mutants do not show any defect in ER-to-Golgi or intra-Golgi trafficking but an alteration in the endocytic-recycling compartment (Mahfouz et al., 2012; Brunet et al., 2013). The protein structure shows high similarities with SNARE proteins but a role for sedlin in mediating vesicle fusion has not been observed. Instead, it seems to be a protein adaptor by which TRAPPII can switch into TRAPPIII by binding Trs85 and Trs120/130 (TRAPIII specific proteins) (Taussig et al., 2014). Trs20-D46Y (analogous to the human-causing mutation sedlD47Y) causes defects in endocytosis, and in selective and non-selective autophagy suggesting that TRAPPIII complex integrity is compromised in trsD46Y.

Human sedlin has been found to interact with several transcription factors (MBP1; PITX1 and SF1 and MRG14 through PAM14). However, the molecular consequences of the lack of interaction between sedlin and the transciption factors and its pathological relevance for SEDT have not been elucidated.

The first and unique connection between sedlin protein function and the pathogenesis of SEDT was described in Antonella De Matteis' lab in 2012. It was demonstrated that sedlin, through TRAPP, controls the ER-export of fibrillar collagens by directly binding the small GTPase Sar1. Binding of sedlin to Sar1 promotes GTP hydrolysis, thus increasing the efficiency of the COPII machinery. Procollagens are very big cargoes that need a "special" machinery to enter into COPII carriers, thus sedlin is not required for the trafficking of small soluble cargoes and/or transmembrane cargoes but is mandatory for collagen secretion (Venditti et al., 2012). The proposed model is reflected in the clinical signs of the disease that only affects endochondral ossification and cartilage. However,

sedlin is ubiquitously expressed and why mutations in the TRAPPC2 gene alter only bones remain to be addressed. Sedlin is also highly conserved throughout evolution and its absence in yeast leads to lethality, so it is plausible that it could have other as yet unidentified biological roles. However, the lack of an animal model for SEDT makes it difficult to address the question as to whether the procollagen type II export defect is the only pathogenic cause of SEDT.

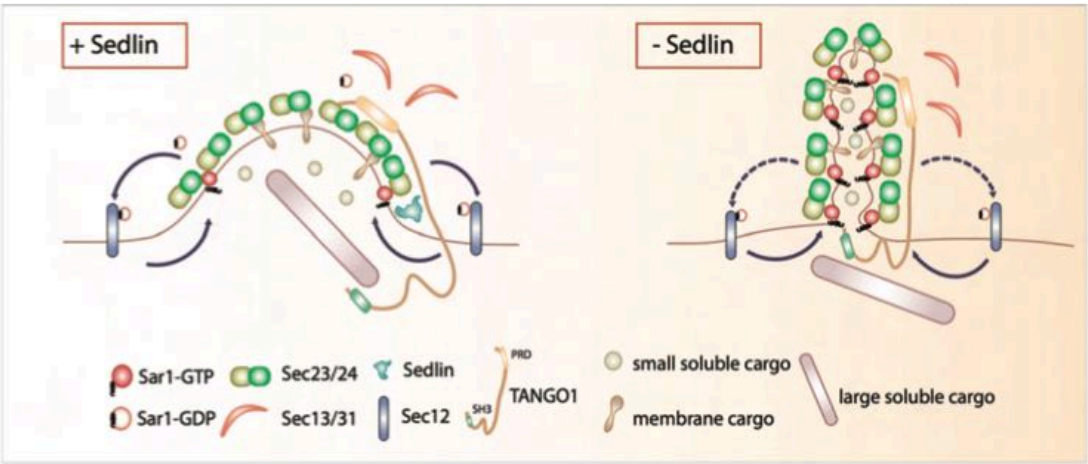

Figure 1.6 Model of the role of Sedlin in the biogenesis of PC transport carriers.
Left: the activation of Sar1 by Sec12 initiates the recruitment of the COPII complex (*1*). TANGO1 assists the packaging of PC by binding PC in the ER lumen and Sec23 in the cytosol and preventing the interaction of Sec23/24 with Sec13/31 (*3*). Preventing Sec13/31 recruitment can have contrasting consequences on carrier biogenesis. On the one hand, by postponing the membrane deformation induced by Sec13/31 (*35*), it would allow the assembly of large platforms of the inner COPII layer (as required for a megacarrier) but on the other it would also slow down the Sar1 cycle and accumulate Sar1-GTP that, by inducing membrane constrictions, would antagonize the growth of megacarriers. However, TANGO1 also recruits Sedlin and Sedlin promotes Sar1 inactivation/release. Hence, the combined action of TANGO1/Sedlin coordinates the stabilization of the inner COPII layer (mediated by TANGO1) with efficient Sar1 cycling (through Sedlin) to prevent membrane constriction thus allowing the growth of the nascent carriers and the incorporation of the large PC prefibrils. **Right:** upon Sedlin depletion or mutation the Sar1 cycle is slowed down and Sar1-GTP accumulates on the nascent carrier inducing membrane constrictions. The carriers formed under these conditions are unsuited to host large cargoes, but are still able to accommodate small cargoes. Adapted from Venditti et al., 2012.

1.7 Medaka as a model to study SEDT

The physiology, embryology and genetics of Medaka fish have been widely studied in the past 100 years. Already in 1913, the Medaka fish was used to show Mendelian inheritance in vertebrates (Ishikawa, 2000). In addition, the complete sequencing of its genome has greatly contributed to the use of this model to study various biological processes underlying embryonic development. Different comparative studies among vertebrates have demonstrated a high conservation in terms of genomic sequences and molecular processes, also in model systems such as teleosts (*Danio rerio*/Zebrafish and *Oryzias latipes*/Medaka fish). Zebrafish and Medaka are ideal organisms for genetic studies as they display many advantages such as the simple use of different genetic engineering techniques. They have a short generation time (8-10 weeks for Zebrafish and 6-8 weeks for Medaka fish). Moreover, Zebrafish/Medaka fish biology allows ready access to all developmental stages, and the optical clarity of embryos and larvae allow real-time imaging of developing pathologies. (Furutani-Seiki and Wittbrodt, 2004).

In particular, Medaka fish has several advantages. Medaka fish is very hardy and tolerates a wide range of salinities and temperatures (10–40 °C); it is easy to breed and highly resistant to common fish diseases. For all the above-mentioned reasons, Medaka fish is easier to keep and maintain in aquaculture than Zebrafish and it is easier to handle. Early Medaka fish development is slower than in Zebrafish: Zebrafish larvae hatch after 2–3 days, whereas Medaka fish embryos are enclosed in a tough chorion that protects them in their natural habitat until they hatch as feeding young adults after 8 days (fig 1.7).

The slower development at the early phases allows to better define and characterize developmental processes and defects (Iwamatsu et al., 2004).

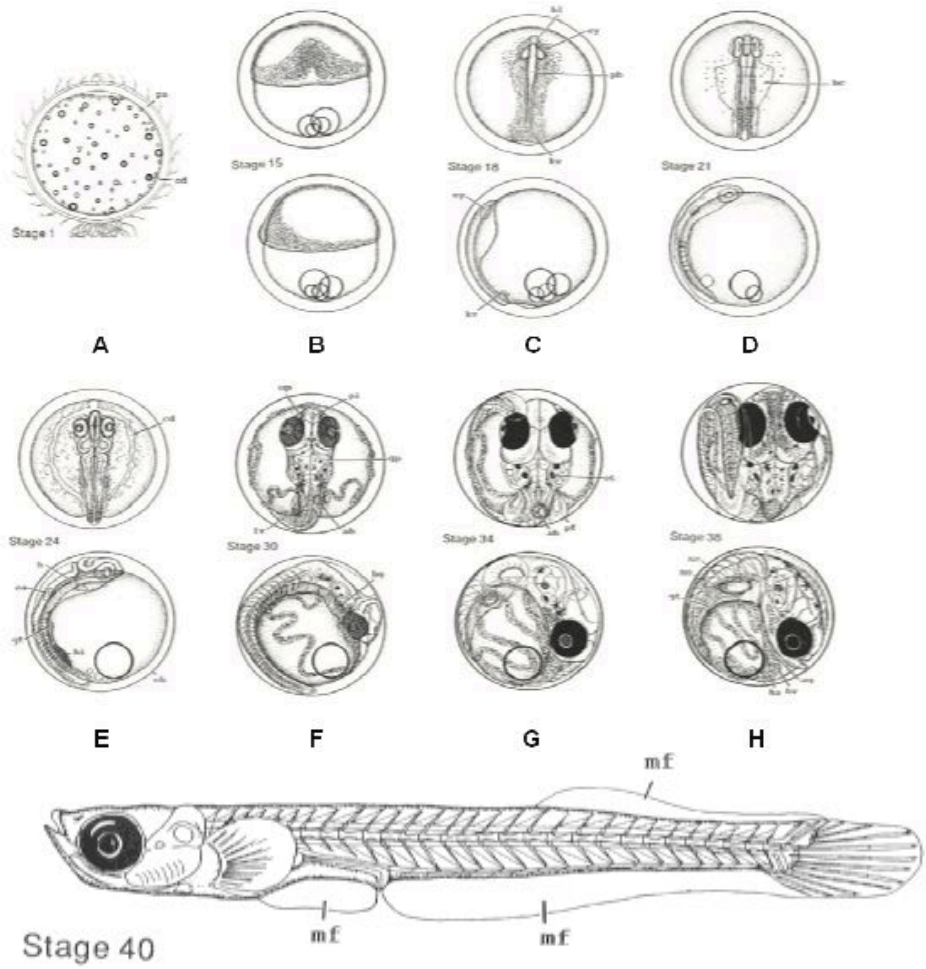

Figure 1.7 Selected stage of Medaka development (A) Stage 1 (3 min post fertilization) Activate egg stage. **(B)** Stage 15 (17 hours post fertilization) Mid gastrula stage. **(C)** Stage 18 (1 day and 2 hours post fertilization) Late nerula stage. **(D)** Stage 21(1 day and 10 hours post fertilization) 6 somite stage, brain and otic vesicle formation. **(E)** Stage 24 (1 day and 20 hours post fertilization) 16 somite stage, formation f tubular heart. **(F)** Stage 30 (3 days and 10 hours) 35 somite stage, blood vessel development. **(G)** Stage 34 (5 days post fertilization) Pectoral fin blood circulation. **(H)** Stage 38 (8 days post fertilization) Spleen developmental stage (Differentiation of caudal fin begins) (**Stage 40)** (9 days post fertilization) This period extends from hatching until fin rays appear in the caudal and pectoral fins.

From the experimental point of view, however, the two model systems are completely equivalent. In both systems, reverse-genetic analyses are also facilitated by assays of gene function using transient rather than stable misexpression, which is technically easier than in mice. In fish model systems, antisense morpholinos are widely used to transiently interfere with gene function (Bill et al., 2009). These typically 25-bp-long oligos specifically interfere with gene function based on their complementarity with the target sequence either by blocking translation initiation or by interfering with splicing. The nonribose-based back-bone renders morpholinos insensitive to enzymatic degradation. These antisense morpholinos are injected into fertilized eggs at the one-cell stage to ensure a ubiquitous distribution to all cells of the developing embryo. If thus applied, they interfere with gene function during early development. In the last years, several tools that allow specific manipulations of the genome have been developed that are applicable to many organisms, including medaka. These tools are based on sequence-specific binding of a nuclease that cleaves the genomic double-stranded DNA (dsDNA), thereby inducing a double strand break (DSB). Subsequently, the DSB repair by nonhomologous end joining (NHEJ) introduces small insertion/deletions (indels) at high frequency and thus introduces mutations. In addition to introducing mutations, exogenous DNA can be inserted into the site of the DSB via NHEJ or homology-directed repair (HDR). Two types of sequence-specific nucleases are used for these purposes. ZFNs (Zinc-Finger Nucleases) as well as transcription activator-like effector nucleases (TALENs) have a bipartite structure with a flexible and modular DNA binding domain fused to the effector FokI nuclease. A modular set of ZFNs or TALENs can be designed to bind a specific sequence in the genome and induce a DSB at that site. Recently, it was

shown that sequence-specific binding of a guide RNA coupled to a nuclease can very efficiently induce DSBs (Cong et al. 2013; Mali et al. 2013). This CRISPR (Clustered Regularly Interspaced Short Palindromic Repeats)/Cas9-based system uses a single guide RNA (sgRNA) that targets the nuclease Cas9 in a sequence-specific manner to generate a DSB. Importantly, the use of TALENs and the CRISPR/Cas9 system has been greatly simplified. Initial reports of targeted mutagenesis in medaka demonstrated the ZFN- and TALEN-mediated knockout of an EGFP transgene (Ansai et al. 2012) as well as endogenous genes (Ansai et al. 2013; Ansai and Kinoshita, 2014) (fig.1.8).

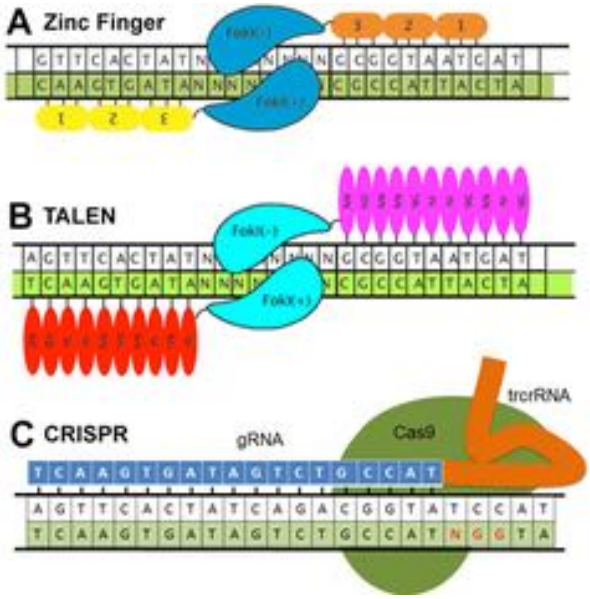

Figure 1.8 Different technologies for genome engeenering. **(A)** Zinc finger (ZNF) domains are relatively small protein motifs that contain multiple finger-like protrusions that make tandem contacts with their target DNA molecule. ZNC finger have been fused with the endonucleases Fok1 to produce a double strand-break. **(B)** TAL effector TAL are proteins that are secreted by Xanthomonas bacteria when they infect plants. The DNA binding domain contains a repeated highly conserved 33–34 amino acid sequence with divergent 12th and 13th amino acids. These two positions, referred to as the Repeat Variable Diresidue (RVD), are highly variable and show a strong correlation with specific nucleotide recognition. A pair of TALEN, as ZNF, is thus fused to the endonucleases Fok1. **(C)** CRISPR (Clustered RegularlyInterspaced Short Palindromic Repeat) are short nucleic acid sequence that can guide a set of endonucleases (Cas9) to cleave the genoms.

Of note, teleosts are powerful tools to study skeletal and cartilage development. Great strides in understanding the role of the secretory machinery in skeletal development have been made studying zebrafish cartilage-defective mutants. Interestingly, mutations in some COPII components causative of human genetic diseases show phenotypes that resemble patients' clinical signs (Melville and Knapik, 2011).

The above reasons demonstrate that fish represent mainstream models in developmental biology. Their attributes have propelled the rise of fish as a

model in developmental biology and human disease research, allowing an enhanced understanding of the basic cell-biological processes that underlie the development and the disease phenotype of the specific genetic diseases (Lieschke and Currie, 2007).

1.8 The sedlin interactor CLIC1

In a work aimed to study SEDT, sedlin was used as a probe to perform a two-hybrid screen and the protein CLIC1 was fished as a sedlin physical interactor. The interaction was then confirmed in a mammalian system by immuno-precipitation experiments but the functional relevance of the interaction was not addressed. CLorhide Intracellular Channel 1 (CLIC1), like the other members of CLIC family, are very enigmatic proteins since they are thought to be localized in the cytoplasm under physiological conditions while homo-dimerized and translocate to the plasma membrane to form a channel pore under redox stress (Averaimo et al., 2010) (figure 1.9). To date a broad spectrum of sub-cellular localizations has been found (Littler et al., 2010)).

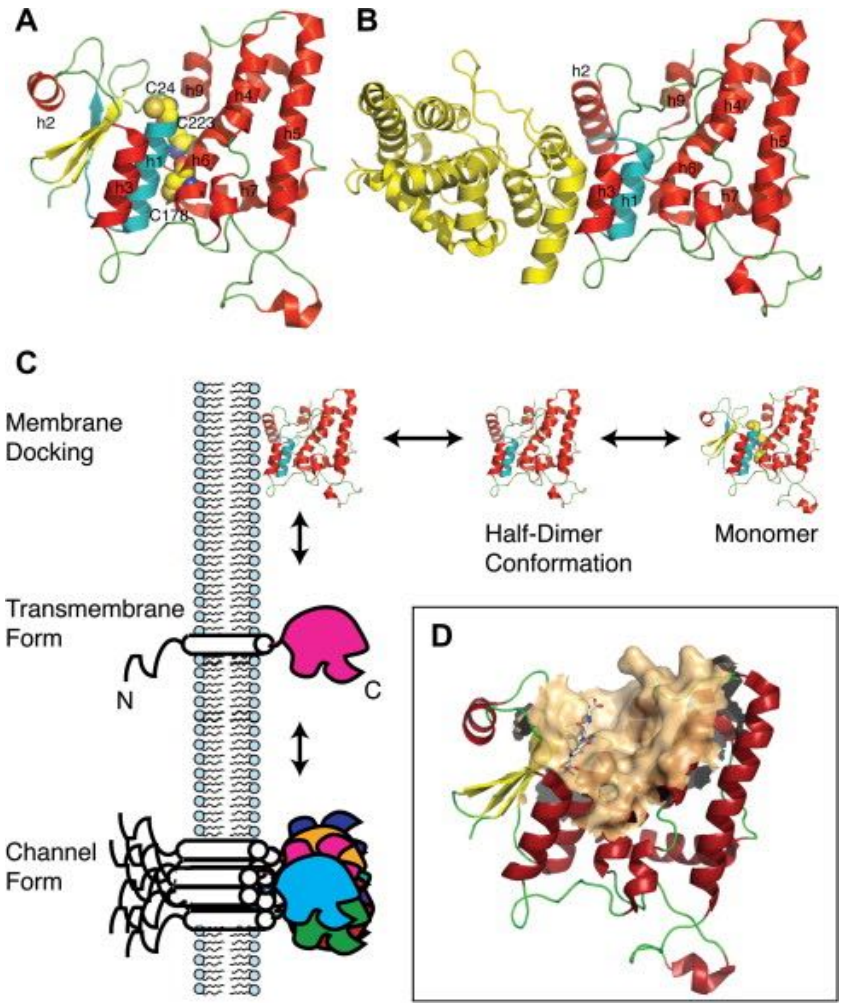

Figure 1.9 Structure of CLIC protein. (A) The structure of CLIC1 in the soluble, reduced monomeric form coloured by secondary structure (helices in red, strands in yellow, loops in green). The putative TM region is shown in cyan (residues 25–46). The N-domain is on the left (β-sheet plus helices h1, h2 and h3) and the all-helical C-domain is on the right (helices h4–h9). The three cysteines (Cys24, Cys178 and Cys223) that are conserved in all vertebrate CLIC proteins are shown as CPK models. **(B)** The crystal structure of the oxidised CLIC1 dimer. The left hand side subunit is coloured yellow, while the right hand side subunit is coloured and oriented as per the CLIC1 monomer in panel **(A). (C)** A proposed model for the transition between the soluble form of CLIC1 and the integral membrane ion channel form. **(D)** Glutathione (stick model) covalently bound to CLIC1, where the

A function of CLICs as soluble proteins was described in 2015 when Al Khamici and co-workers demonstrated that CLIC1, 2 and 4 conserve a glutatione-S-transferase (GSTs) domain with enzymatic activity in vitro. The GSTs can exist

largely as dimeric proteins in the cytosolic environment of cells. They are well known for their ability to catalyse the conjugation of glutathione (GSH) to exogenous toxins and xenobiotics, and therefore vital in detoxification processes within cells. They are also involved in the synthesis of prostaglandins and facilitate the intracellular transport of hydrophobic compounds. Interestingly, the enzymatic activity of the proteins is blunted by the use of the inhibitor IAA-94, a drug broadly used to block CLIC channel activity (Al Khamici et al., 2015). CLICs also interact with a set of cytoskeleton proteins and, of note, CLIC2 was found in a genome-wide screening as an inhibitor of the early secretory pathway (Simpson et al., 2012). Additionally, CLIC1 has been proposed as a marker for different types of cancer (Peretti et al., 2015), whether it functions as an enzyme, chloride channel, a second messenger or an activator of conventional anion channels is still debated.

1.9 Stress granules

1.9.1 General properties of SGs

Stress granules are non-membrane bound aggregates containing stalled mRNA and RNPs (ribonucleoproteins) that from in stressed cells to inhibit translation. Originally, cytoplasmic stress granules were described in tomato cell lines submitted to heat shock. Masses of regularly ordered 30-40 nm particles were found as a result of heat shock and of the ensuing translational arrest (Nover et al., 1983). However, mammalian stress granule size depends on the stimulus applied to the cells. Usually, arsenite-induced stress granules range between 1.5-2 μm (Moutaoufik et al., 2014) while over-expression of SG components in the absence of further stress leads to formation of larger aggregates that range

from 3 to 4 μm (Souquere et al., 2009). Although there are several stress granule-inducer stimuli (e.g. osmotic, oxidative or endoplasmic reticulum stress, viral infection, proteasome inhibition, inhibition of translation initiation factors, ultraviolet light, cadmium chloride as well as certain anti-cancer and antifungal drugs) that activate different upstream signals, sodium arsenite represents the most common used drug to visualize SGs in cultured cells (Panas et al., 2015; Aulas and Valde Velde, 2015).

SGs contain proteins rich in prion-like domains and low complexity domains that drive the formation of a liquid-liquid separation phase in the cytosol that strongly contributes to stress granule formation (Molliex et al., 2015; Gilks et al., 2004) (fig. 1.10)

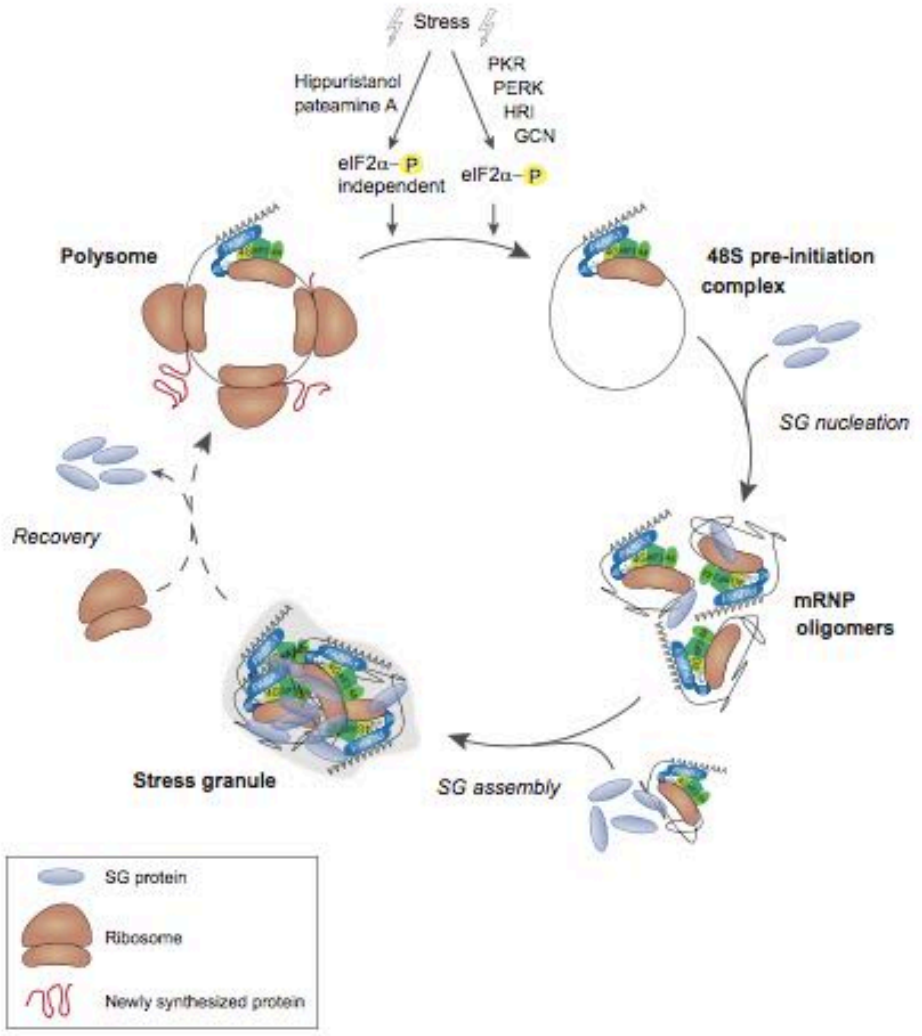

1.10 Stress granules life cycle. Under physiological conditions, several ribosomes that translate mRNA into protein are bound to an mRNA molecule, forming a polysome. Upon cellular stress, elongating ribosomes run-off the transcript as a result of the reduced availability of eIFs, leaving behind a circularized mRNP (48S pre-initiation complex). SG nucleation is initiated by the recruitment of SG-associated proteins, such as TIA- 1, G3BP and tristetraprolin (blue), which triggers the aggregation of mRNPs. Subsequently, protein–protein interactions and cross-linking via PABP-1, as well small ribosomal subunit, facilitate the assembly of the aggregated mRNPs into SGs. During recovery from stress, SG proteins dissociate from the SG, allowing ribosomes to bind and re-form a translating polysome. Adapted from Bentmann et al., 2014)

1.9.2 Distinct models of SG assembly

A major step forward in understanding SG biology was provided by Jain and co-workers who isolated the aggregates biochemically. SGs were found to be

composed of a stable core and a shell in which proteins shuttle in and out dynamically in an ATP-dependent fashion (Jain et al., 2016). So far, there are two models for discrete phases of stress granule assembly: (I) in the "Liquid–Liquid Phase Separation (LLPS) First" model, the formation of large stress granules precedes core assembly. The first phase of this model is the nucleation of translationally repressed RNPs into initial phase-separated droplets held together by weak dynamic interactions. The second phase is the growth of the initial droplets by the addition of translationally repressed RNPs. The third phase of assembly is core formation within phase-separated granules due to the high local concentration of proteins within the droplets. (II) in the "Cores First" model, cores precede the assembly of large stress granules. The first phase of assembly is the nucleation of translationally repressed ribonucleoproteins (RNPs) into oligomers. The second phase of assembly is the growth of these oligomers into larger assemblies by the addition of more translationally repressed RNPs. The third phase of assembly is the fusion of these core assemblies and recruitment of the dynamic shell to form the large, microscopically visible granules typically observed in cells; (Wheeler et al., 2016) (figure 1.11).

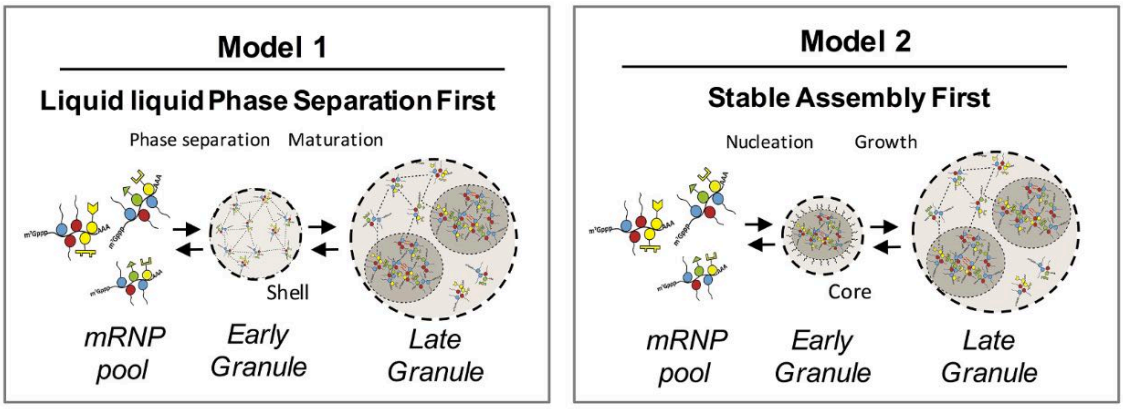

Figure 1.11 Two models for stress granule assembly. **(1)** An increase in a pool of untranslated mRNAs with bound proteins containing IDRs, could lead to the formation of a LLPS based on weak, dynamic IDR-IDR interactions and over time core formation occurs as a second phase due to the supersaturation of local concentration of core components. **(2)** Untranslating mRNAs with bound proteins containing IDRs could initially oligomerize into stable cores that provide a platform for LLPS and eventual coalescence of multiple cores results in formation of a larger LLPS assembly. (Adapted from JR Wheeler et al., 2016)

1.9.3 The role of post-translational modifications in the assembly of stress granules

Different post-translational modifications have been found linked to SG components. In 2008 a genome-wide screen identified O-linked-N-acetylglycosylations, a feature common to several SG proteins. The O-glycosyl transferase (OGT), a cytosolic enzyme that mediates the reaction, was found on SGs. Moreover, depletion of OGT causes a severe impairment in SG formation and mass spec analysis revealed several SG-related proteins conjugated to O-GlcNAc residues (Ohn et al., 2008). Phosphorylation have also been liked to SGs since the reprogramming of protein translation observed in stressed cells is initiated by the phosphorylation of ser51 on eIF2alpha and de-phosphorylation

of G3BP is a critical step for its assembly into SGs (Tourriere et al., 2003). Moreover, a requirement for poly (ADP-ribose) in the assembly of SGs has been described (Leung et al., 2011). Hypusination is an unusual posttranslational modification mediated by the polyamine biosynthetic pathway that is involved in many cellular processes including cell proliferation and the stress response. It has been shown that alteration in hypusination of eIF5alpha alters SG assembly in cells subjected to adverse environmental conditions (Li et al., 2010). Methylation of lysine and arginine residues regulates many different cellular processes including the DNA damage response, chromatin remodeling, and RNA metabolism. Methylation of the RGG domain of FMRP (Fragile X-Mental Retardation Protein) has been implicated in SG assembly. FMRP, which exhibits a punctate cytoplasmic distribution under non-stressed conditions, quantitatively relocalizes to SGs in response to heat or arsenite-induced oxidative stress. Treatment with a methylation inhibitor increases the assembly of FMRP-containing aggregates at baseline, inhibits arsenite-induced SG assembly, and prevents the recruitment of FMRP to SGs. Thus, methylation of FMRP appears to be required for both recruitments onto SGs and optimal SG assembly. Methylation of the cold-inducible RNA-binding protein (CIRP) is also required for the assembly of SGs. In contrast to FMRP, methylation of CIRP promotes the re-localization of the protein from the nucleus to the cytoplasm of stressed cells. Unlike FMRP, methylation inhibitors do not promote the cytoplasmic aggregation of CIRP, suggesting that methylated CIRP may not be sufficient to induce SG-independent protein aggregation. More recently, sumoylation and NEDDylation have been also identified as post-translational modifications needed for stress granules assembly (Jayabalan et al., 2016; Wang

T. et al., 2016 jongjitwimol et al., 2016). Although several post-translational modifications have been determined, it is likely that the identification of new types of modifications, additional modified target proteins, and upstream signaling pathways will be essential to fully understand the functions of SGs.

1.9.4 Functions of SGs

Stress granule formation is expected to affect biological reactions in two ways. On one hand, due to the high local concentration of components, the equilibria of interacting molecules will shift towards associated states. For example, during viral infections stress granules recruit numerous antiviral proteins including RIG-1, PKR, OAS, and RNaseL, stimulating their activation, and thereby enhance the induction of the innate immune response and viral resistance (Reineke et al., 2015; Reineke and Lloyd 2015). Given this function, many viruses employ mechanisms to block stress granule induction, including proteolytic cleavage of G3BP, a well characterized stress granule component (Reineke and Lloyd., 2015). A second manner by which stress granules may affect biological reactions is by limiting the interactions of sequestered components with the bulk cytosol. In this manner, stress granules have been proposed to modulate signaling pathways by sequestering components of TORC, MAPK, or TRAF2 signaling pathways (Takahara and Maeda, 2012; Thedieck et al., 2013; Wippich et al., 2013; Kim et al., 2005; Arimoto et al., 2008). Because stress granules also sequester numerous proteins involved in RNA physiology and/or metabolism, the formation of stress granules is likely to have broad effects on the physiology of cells. However, it should be noted that how stress granule assembly fully affects the regulation of mRNA function and/or other aspects of cell physiology remains to be established.

1.9.5 Stress granules in diseases

Of note, mutations in genes causing amyotrophic lateral sclerosis (ALS), frontotemporal lobar degeneration (FTLD) (Ramaswami et al., 2013) and some myopathies result in the formation of aggregates in a persistent stress granule-like structure in the absence of stress. Interestingly, in many cases mutations are in RNA-binding proteins (e.g., hnRNPA1, FUS, TDP-43, Atx2, TIA1) increasing their ability to self-assembly. While the relationship between aggregate formation and the pathogenesis of the disease is still under investigation (fig. 1.11), a model proposed for the persistence of the aggregates is that these disease states increase the probability of the prion-like domains of stress granule components forming very stable beta-amyloid structures, which might be largely irreversible in cells. Consistent with this hypothesis, it has been shown that the liquid-liquid separation phase shows an increased tendency to form beta-amyloid like fibrillar structures (Molliex et al., 2015).

A correlation between SGs and cancer has also been exploited. Some chemotherapeutic drugs trigger SG formation and would be expected to cause cell mortality by inhibiting translation. On the other hand, mutations or over-expression of SG components that cause SG assembly have been found in some tumors. Although apparently conflicting, these findings are perfectly in line with the diverse mechanisms by which stress granules can affect cell signalling and survival under stress conditions.

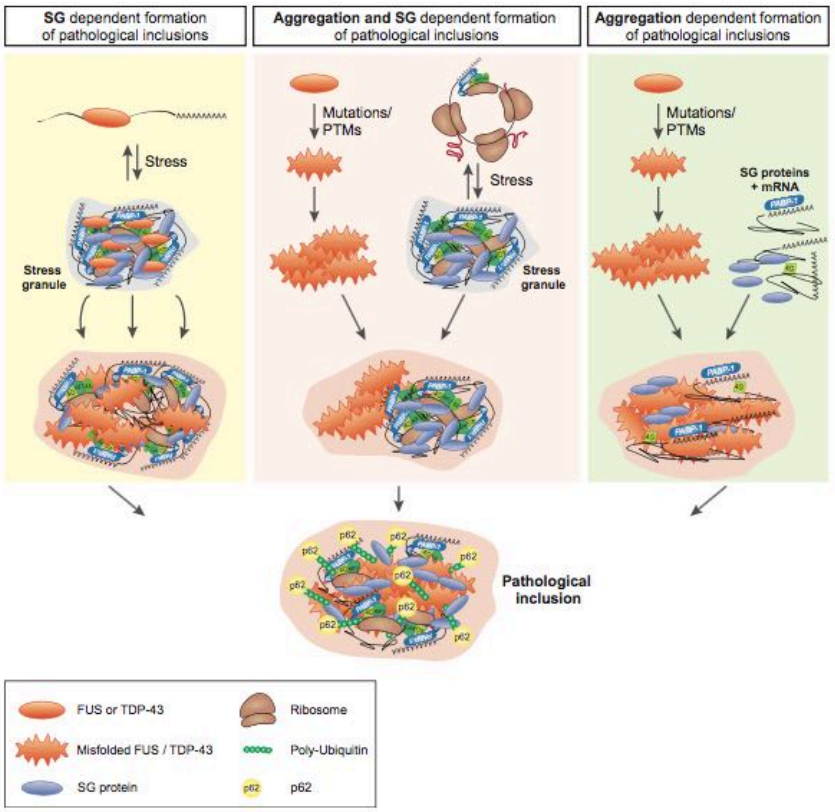

1.11 Alternative models for the formation of SG marker-positive pathological inclusions. The first model **(left)** proposes that SGs are the origin of pathological TDP-43/FUS inclusions. Upon cellular stress, TDP-43/FUS are sequestered into SGs together with their mRNA targets. This is a reversible process, although the high local concentration of these aggregation-prone proteins within SGs and/or the presence of RNA as a templating agent might trigger the aggregation of TDP-43/FUS. Additionally, defects in SG disassembly (e.g. caused by inhibition of DYRK3 or Hsp70 or by chronic stress) could contribute to the conversion of SGs into pathological inclusions. In the alternative second model **(middle)**, aggregation of FUS/TDP-43 or other aggregation-prone proteins, such as tau, SOD1 and poly Q Htt, is triggered by mutations or post-translational modifications (PTMs). These aggregates and/or external stress stimuli elicit the formation of SGs, which are then sequestered by pre-formed FUS/TDP-43 aggregates via protein–protein or protein–RNA interactions. In the third model **(right)**, inclusions form completely independently of stress and SGs. Mutations and/or PTMs that enhance the intrinsic aggregation propensity of FUS, TDP-43 and other aggregation-prone proteins result in misfolded protein aggregates. Subsequently, SG marker proteins, such as TIA-1 or PABP-1, may be recruited into these aggregates together with their bound mRNA. The presence of ubiquitin and p62 in these SG marker-positive pathological inclusions **(bottom)** may indicate that a defect in the clearance of these aggregates by the protein degradation machinery contributes to inclusion formation. Adapted from Bentmann et al., 2014)

Aims

Sedlin is a sub-unit of a multimolecular complex called TRAPP whose role in membrane trafficking has been broadly described. Sedlin, when mutated, gives rise to a genetic disorder, Spondyloepiphyseal dysplasia tarda (SEDT) that specifically affects cartilage. The protein, through TRAPP, binds to Sar1, a small GTPase responsible of ER-export, modulating collagen secretion. However, sedlin is highly conserved during evolution suggesting that it could exert other functions other than its effect on procollagen transport. Thus, the specific aims of my project were:

- To identify other biological roles of sedlin by the identification of its interactome
- To generate an animal model to study sedlin in an *in vivo* system

Chapter 2

Materials and Methods

2.1 Cell culture

HeLa cells and human fibroblasts were bought from American tissue type collection (ATCC, USA).

Rat chondrosarcoma chondrocytes were provided by J. Kimura and B. Vertel. HeLa cells were grown in DMEM supplemented with 4.5 g/l glucose, 2 mM L-glutamine (Thermoscientific, UK), 1 U/ml penicillin and streptomycin (Sigma Aldrich, Germany), and 10% FCS (Euroclone, UK). Rat chondrosarcoma chondrocytes were grown in DMEM supplemented with 4.5 g/l glucose, 2 mM L-glutamine and 1mM sodium pyruvate (Euroclone) 1 U/ml penicillin and streptomycin, and 10% FCS HF BJ-5Ta were grown in DMEM/M199 4:1 (Thermoscientific, UK) supplemented with 4.5 g/l glucose, 0.02 mg/mL hygromycinB, 1 U/ml penicillin and streptomycin, and 10% FCS.

All cell lines were grown in a controlled atmosphere in the presence of 5% CO_2 at 37°C. Cells were grown in a flask (corning, UK) to 80-90% confluence. The medium was removed and trypsin-EDTA solution (0.05% trypsin, 0.02% EDTA purchased from Sigma Aldrich, Germay) was added for 3-5 min at 37°C. The medium was added back to block the protease action, cells were collected into a plastic tube and centrifuged for 5 min at 800 x g. The pellet was resuspended in fresh medium and placed in a new plastic flask.

2.2 Preparation of recombinant proteins

The following procedures were carried out by M. Santoro (Telethon institute of genetics and medicine TIGEM, Italy).

The Xho1/BamHI (NEB, UK) restriction sites were inserted in the CLIC1 clone kindly provided by Dr. Mazzanti (University of Milan) by PCR reaction using the primers CGAGGATCCGTGGCTGAAGAACAACCGCAG (BamHI forward primer) and TGTCTCGAGTTATTTGAGGGCCTTTGCCAC (Xho1 reverse primer).

After its purification with the JET-QUICK PCR Purification Spin Kit (GENOMED, USA) the product of PCR-reaction was ligated in frame with the pEGFP-C vector, previously digested with the same restriction enzymes, by using the T4 DNA ligase (30 fmol of the product of PCR-reaction were ligated with 10 fmol of the purified PstI/BamHI pre-digested vector).

The products of ligation were used to transform competent bacteria. On the following day, some isolated bacterial colonies for each construct were picked up and used to inoculate 2 ml of LB-broth containing 50 µg/ml of ampicillin. The culture was incubated at 37 °C overnight. Seven hundred and fifty µl of sterile glycerol were added to 750 µl of bacterial culture and stored at -80 °C. Bacteria cultures were used to prepare plasmids and these were digested for 3 h at 37 °C with the respective restriction enzymes in order to verify the presence of the inserts. Moreover, the obtained plasmids were sent to be sequenced by MWG Biotech (Italy).

Competent bacterial cells were prepared by M. Santoro (Telethon institute of genetics and medicine TIGEM, Italy).

A single colony of XL-1 Blue *E. coli* bacteria was picked from a LB-agar plate (10 g/l NaCl, 5 g/l yeast extract, 10 g/l tryptone peptone and 15 g/l agar) and used to inoculate 10 ml of LB-broth (10 g/l NaCl, 5 g/l yeast extract and 10 g/l tryptone peptone). Bacteria were grown overnight, then diluted in 190 ml of fresh LB broth

and incubated at 37 °C until the optical density (OD) reached 0.5 (at λ=600 nm). Bacteria were harvested by centrifugation at 6,000 rpm in a JA10 rotor for 10 min at 4 °C. The bacterial pellet was resuspended in 40 ml of 30 mM potassium acetate, 100 mM RbCl, 10 mM $CaCl_2$, 50 mM $MnCl_2$, 15% (v/v) glycerol, pH 5.8, and left on ice for 2 h. After centrifugation and resuspension of the pellet in 4 ml of 10 mM MOPS, 75 mM $CaCl_2$, 10 mM RbCl, 15% (v/v) glycerol, pH 7, cells were stored at -80 °C in 400 µl aliquots.

The plasmid cDNA of interest (10 ng) was added to 200 µl of competent bacteria previously thawed on ice. After gentle mixing, cells were left on ice for 30 min, heat shocked for 90 sec at 42°C and, after addition of 800 µl LB broth, incubated with shaking at 37 °C for 45 min. Bacteria were plated on LB-agar containing the appropriate selective antibiotic and incubated overnight at 37°C. The following day, an isolated bacterial colony was picked and used to inoculate 2 ml of LB-broth containing the appropriate antibiotic. The culture was incubated at 37°C overnight. For storage, 750 µl of sterile glycerol were added to 750 µl of bacterial culture and stored at -80 °C.

2.3 Cell transfection and RNA interference

2.3.1 Preparation of plasmid DNA and transfection of DNA

To produce pilot sample of DNA preparation a single colony of XL-1 Blue E. Coli bacteria, transformed with the plasmid of interest was used to inoculate 2 ml of LB-broth containing the selective antibiotic. After 15-20 h incubation with shaking at 37 °C, bacteria were collected by centrifugation at 14,000 rpm in a Microfuge®18 centrifuge [Beckman Coulter (USA)] for 1 min at RT and processed accordingly to the mini-plasmid preparation protocol of the “SIGMA- plasmid-

miniprep kit". The cDNA obtained was resuspended in 10 mM TRIS-HCl pH 8 and stored at 4 °C or, for long-term, at -20 °C.

To produce large scale DNA preparation a single colony of XL-1 Blue E. Coli bacteria, transformed with the plasmid of interest was used to inoculate 500 ml of LB-broth containing the selective antibiotic. After 15-20 h incubation with shaking at 37 °C, bacteria were collected by centrifugation at 6,000 rpm in a JA10 rotor for 10 min at 4 °C and processed according to the maxi-plasmid purification protocol of the "Qiagen-plasmid-kit". The cDNA obtained was resuspended in TE buffer (10 mM TRIS-HCl, 1 mM EDTA pH 7.5) to a final concentration of 1 mg/ml and stored at 4 °C or, for long-term, at -20 °C.

2.3.2 TransIT-LT1-reagent-based cell transfection

HeLa cells were seeded into 24-well or in a 15 cm plates at a concentration suitable to have 50%-70% confluence for transfection. The transfection mixture was prepared in a polypropylene tube: for each well, 0.3 µl TransIT-LT1 (Mirus, Germany) transfection reagent was diluted in 50 µl OptiMEM culture medium. The mixture was shaken and incubated at RT for 5 min. Then 100 ng of total DNA was added to the transfection mixture, which was shaken and kept at RT for 15 min, to allow the DNA-TransIT-LT1 (Mirus, USA) complex to form. The cells were then incubated with the transfection mixture at 37 °C in the presence of 5% CO_2 for 16-20 h.

CLIC1-GFP was produced by Michele Santoro as indicated in session 2.2.2. Sedlin-3Xflag and Rab1B-GFP have been previously produced in Antonella De Matteis lab. G3BP-GFP was purchased from Origene (USA). TDP-43, 35 and 25 2Xflag were kindly provided by Prof. Poletti (University of Milan)

2.3.3 siRNA duplexes

SiRNA oligonucleotides for sedlin, Bet3 and CLIC1 were purchased from Sigma (USA). Non-targeting siRNA sequences were used as controls; the siRNAs sequences are listed in **Table 2.1**.

Name	Sense sequence 3'-5'	Species	Company
Sedl n°1	GGGCAUAUGAGGUUUAUUA	human	Sigma
Sedl n°2	GAGCUUCUACUUUGUAAUU	human	Sigma
Sedl n°3	ACAUGUGGCUAUCGAACAA	human	Sigma
Sedl n°4	CAUAAGACAAGAAGAUGGA	human	Sigma
Bet3	GGGCAUCACUCCAAGCAUU	human	Sigma
CLIC1 n°1	GAACAACCGCAGGUCGAAU	human	Sigma
CLIC1 n°2	AGAUCGAGCUCGCCUAUGA	human	Sigma
CLIC1 n°3	GGACCGAGACAGUGCAGAA	human	Sigma
CLIC1 n°4	GGAGUCACCUUCAAUGUUA	human	Sigma
CLIC1 n°1	GAACAACCUCAGGUCGAAU	rat	Dharmacon
CLIC1 n°2	AGAUAGAGCUGGCCUAUGA	rat	Dharmacon
CLIC1 n°3	GGACAGAGACGGUACAGAA	rat	Dharmacon
CLIC1 n°4	GGAGUCACCUUCAACGUUA	rat	Dharmacon

Table 2.1 List of siRNA used in this study

2.3.4 siRNA-duplex transfection

HeLa cells were transfected using Oligofectamine (Invitrogen, USA), Rx chondrocytes LipoFectamine 2000 (Invitrogen, USA).

HeLa cells were plated in 24-well plates to subconfluent density on glass coverslips, in antibiotic-free medium. The day after, a transfection mixture was prepared: for each well, specific siRNA duplexes were diluted in 40 µl of OptiMEM (Gibco, UK) culture medium in a polypropylene tube to the final concentration of 50 nM. In a separate polypropylene tube, for each well, 1.25 µl of Oligofectamine Reagent was diluted in 8.75 µl of the same medium. The mixtures were first

shaken and incubated at RT for 5 min, then combined, shaken and kept at RT for 20 min, to allow the siRNA-Oligofectamine complex to form. The cells were incubated with the transfection mixture at 37 °C in the presence of 5% CO_2 for 72 h.

A similar protocol was adopted for Rx chondrocytes. SDS-PAGE, Western blotting and densitometry analyses were carried out to evaluate the efficiency of siRNA treatment for each experiment.

2.4 Immunofluorescence Confocal Microscopy

2.4.1 Immunofluorescence procedures

HeLa, HFs and Rx chondrocytes were grown to subconfluent density on glass coverslips and treated as follows. They were fixed with 4% paraformaldehyde for 10 min at RT and washed twice in PBS. Blocking buffer (0.05% saponin, 0.5% BSA, 50 mM NH_4Cl in PBS) was then added to the cells for 20 min, followed by a 1-h incubation with the primary antibody in blocking reagent (see Table 2.1 for the dilutions used). When required, cells were permeabilised with 0.01% Triton-X 100 in PBS. The cells were then extensively washed with PBS and incubated with secondary antibodies (1:400) and with DAPI (where indicated, at a final dilution of 1:1000 from a 1 mg/ml stock) for 45 min, diluted in blocking solution. After immuno-staining, the cells were washed three times in PBS and once in sterile water, to remove salts. The coverslips were then mounted on glass microscope slides (Carlo Erba, Italy) using Mowiol. The antibodies used in this studies are listed in table 2.2.

Antibody	Company or other source	Animal source	Dilution
AP-2	Pierce	mouse	1:200
CLIC1	Sigma	mouse	1:100
EEA-1	Cell Signaling	rabbit	1:200
FAPP1	G. Di tullio CMNS	rabbit	1:200
FAPP2	G. Di tullio CMNS	rabbit	1:100
flag	Sigma	mouse	1:200
G3BP	BD	mouse	1:1000
G3BP	Bethil	rabbit	1:1000
GIANTIN	G. Di tullio CMNS	rabbit	1:10000
GM130	G. Di tullio CMNS	rabbit	1:1000
golgin97	G. Di tullio CMNS	rabbit	1:1000
M6PR	novus	rabbit	1:200
OCRL	G. Di tullio CMNS	rabbit	1:200
p115	G. Di tullio CMNS	rabbit	1:1000
procollagen type I	Hybridoma Bank	mouse	1:100
procollagen type II	Hybridoma Bank	mouse	1:30
rab11	Transduction	mouse	1:100
rab1B	Santa Cruz	rabbit	1:200
rab8	Transduction	mouse	1:100
RACK1	Santa Cruz	rabbit	1:200
sar1A	Sigma	rabbit	1:400
sec16	Bethil	rabbit	1:200
sec16	Bethil	rabbit	1:200
sec23	Sigma	rabbit	1:100
sec24C	Sigma	rabbit	1:400
sec31	G. Di tullio CMNS	rabbit	1:1000
sedlin	G. Di tullio CMNS	rabbit	1:200
TGN-46	Serotech	sheep	1:750
TRAPPC1	Sigma	rabbit	1:200
VSVG	Bethil	rabbit	1:1000
VSVG LD	G. Di tullio CMNS	mouse	1:1000
β-COP	G. Di tullio CMNS	mouse	1:1000

Table 2.2 List of antibodies used in this study

2.4.2 Immunofluorescence analysis by laser scanning confocal microscopy

IF samples were examined under a confocal laser microscope (Zeiss LSM710,

LSM700 and Leica SP5 confocal microscope systems) equipped with 63x1.4 NA oil objective. Optical confocal sections were taken at 1 Airy unit with a resolution of 1024×1024 pixels. Images were composed using Power Point.

2.4.3 Immunofluorescence analysis by super resolution microscopy

IF samples were examined using LSM880 equipped with 63x1.4 NA oil objective and images exported as TIFF and composed using power point.

2.4.4 Image processing and quantification of colocalisation on fixed cells

For quantification experiments, 10-15 randomly chosen fields each containing 8-10 cells were scanned with the same microscope settings (i.e. laser power and detector amplification) below pixel-saturation. Images were analysed using Columbus software. All experiments were repeated at least three times.

2.5 Immunoprecipitation assay

$15*10^6$ HeLa cells were seeded in 15 cm dishes. Transient transfection of sedlin3Xflag and CLIC1-GFP using 3Xflag anf GFP as a control was performed using 30 µg and 90 µL of TransIT-LT1 DNA as indicated in session 2.3.3. After 16 hrs of transfection, cells were washed with cold PBS and lysed with 1 mL of lysis buffer (25mM TRIS pH 7.4, 100 mM NaCl, 1 mM EDTA, 0.5% lauryl maltoside, supplemented with protease and phosphatase inhibitors cocktail (Roche)). Cells were harvested 15 minutes at 14,000 rpm at 4°C. Anti FLAG-M2 (Sigma- Aldrich, Germany) or anti-GFP (Consorzio Mario Negri Sud) were added to the samples for 6 hrs at 4°C. Samples were then incubated with protein A Sepharose (Sigma-Aldrich, Germany) for GFp-overexpressing cells and protein G Sepharose (Sigma-Aldrich, Germany) respectively, for 1 hr. The immunoprecipitates were washed 6

times in lysis buffer and 2 times in the same buffer with out detergent and eluted in 2X sample buffer by denaturating at 95°C. Eluates were sent to to the Central Proteomics facility (South Parks Rd., Oxford) for mass spectrometry analysis.

2.6 Nocodazole treatment

HeLa cells were washed three times with DMEM and equilibrated with DMEM supplemented with HEPES. Nocodazole (Sigma Aldrich, Germany) was added in DMEM w/o FCS at final concentration of 33 μM and cells were incubated 5 min at 4°C and then shifted at 37°C for 3 hrs.

2.7 CLIC1 inhibitor treatment

HeLa cells were treated with IAA-94 (Sigma Aldrich, Germany) at final concentration of 100 μM in DMEM supplemented with HEPES for 90' at 37°C.

2.8 Transport assays

2.8.1 PCII transport assay

To follow PC-II in RCS, cells were incubated for 3 hrs at 40°C in DMEM supplemented with 1% serum and 20mM HEPES pH 7.2 (Euroclone, UK), then shifted to 32°C in the presence of cycloheximide (100 μg/ml) and ascorbate (50 μg/ml). Then, the cells were fixed and processed as described above.

2.8.2 VSV-G transport assay

HeLa cells were infected with VSV-G 1 hr at 32°C in serum free DMEM buffered with HEPES. Cells were then washed three times in DMEM and incubated at 40°C for 3 hrs in growth medium supplemented with HEPES. Finally, cells were shifted at 32°C in presence of cycloheximide (50 μg/ml) for the indicated times. In case of

treatment with CLIC1 inhibitor, IAA-94 was added at final concentration of 30 μM to the infection mix, supplemented during the incubation time at 40°C and refresh during the chase at 32°C.

2.8.3 Tf recycling

Cells were serum starved for 1 hr at 37°C in serum-free DMEM, washed twice in cold PBS, 1% BSA, and then incubated for 1 hr at 4°C in the continuous presence of 50 μg/mL Alexa-Fluor-488-Tf in serum free HEPES-buffered DMEM. The uptake of Tf and its movement along the endocytic pathway were followed by incubating the cells at 37°C for 15, 30 and 60 min in growth medium. Before being fixed, cells were washed with acid solution (0.150 M NaCl, 0.5% acetic acid pH 3.5) to remove Tf that is bound to the PM.

2.8.4 Shiga toxin internalization

Cells were equilibrated in 0.1% BSA HEPES-buffered DMEM for 5 min at 4°C and incubated with 14 μg/mL shiga toxin-Alexa-Fluor-568 in 0.1% BSA HEPES-buffered DMEM for 30 min. Cells were then washed washed three times in cold PBS and incubated in growth medium at 37°C for 30, 60, 120 and 240 minutes.

2.8.5 40-32 °C VSV-G transport assay upon arsenite/heat shock treatment

HeLa cells were infected with VSV-G for 1 hours, washed and incubated at 40°C for 2 hours and 30'. Then, cells where either treated with sodium arsenite (SIGMA) 300 μM at 40°C or incubated for 30' at 44°C. Finally, cells where shifted to 32°C for the indicated times and processed for IF. To follow PC-II in RCS or PC-I in HFs, cells were incubated for 2 hours and 30' 40°C in DMEM supplemented with 1% serum and 20mM HEPES pH 7.2, then treated with sodium arsenite, 300 μM or heat

shock, shifted to 32°C and then fixed at different times.

2.8.6 40-20-32 °C VSV-G transport assay under arsenite treatment

HeLa cells were as previously described. After infection, the cells were washed several times and shifted for 3 hrs at 40°C in complete medium and then incubated to 20°C for two hours. Then, cells were shifted at 32°C and treated with sodium arsenite, 300 μM for 30 min.

2.9 Stress granules induction

Sodium arsenite was purchase from SIGMA Aldrich and stocked in water (stock solution 20 mM). Cells were treated with sodium arsenite in growth media for the indicated concentrations and times or incubated at 44°C in growth media supplemented with HEPES for 30'. Alternatively, cells were transfected with GFP-G3BP or TDP-43 WT and mutants as described in session 2.3.3.

2.10 Microinjection experiments

HeLa cells were plated on glass coverslips in complete culture medium the day before injection. Pre-immune IgG and anti-Bet3 antibody (G. Di Tullio CMNS, rabbit) were injected (2 mg/ml) into cells using a 5246 transjector controlled by a 5171 micromanipulator (Eppendorf, Germany)

2.11 Western blot analysis

To assembly polyacylamyde gel two 16 x 15 cm glass plates were assembled to form a chamber using two 1.5 mm plastic spacers lined on the lateral edges of the plates. This chamber was fixed using two clamps and mounted on a plastic base that sealed the bottom (Hoefer Scientific instruments, Germany). The

polyacrylamide gel was then prepared using one solution of the desired polyacrylamide concentration (usually 13% to better separate the TRAPP subunits) or two solutions of 4 and 15% (v/v) polyacrylamide in a gradient maker device, to prepare a 4-15% (v/v) gradient gel.

Samples were prepared by adding sample buffer (0.125 M Trizma base, 4% (w/v) SDS, 20% (v/v) glycerol, 10% (v/v) β-mercaptoethanol, pH 6.8) and boiling for 5 min at 95 °C before loading onto the gel. The end wells were loaded with 3 µl of pre- stained molecular weight standards (Sigma, USA). The chamber was then assembled into the electrophoresis apparatus (Hoefer Scientific Instruments, Germany) and electrophoresis was carried out under a constant current of 8 mA (for overnight runs) or 30-40 mA (for 4 h runs).

To perform Western blot analysis the polyacrylamide gel was soaked for 15 min in transfer buffer, placed on a sheet of 3 MM Whatman paper and covered by a nitrocellulose filter (Schleicher & Schuell, USA). The filter was covered by a second sheet of 3 MM paper to form a "sandwich" that was subsequently assembled into the blotting apparatus (Hoefer Scientific Instruments, Germany). Protein transfer occurred at 400 mA for 4-5 h. At the end of the run, the “sandwich” was disassembled and the nitrocellulose filter was soaked in 0.2% (w/v) red Ponceau in 5% (v/v) acetic acid for 5 min to visualise the protein bands and then rinsed with 5% (v/v) acetic acid to remove the excess of the unbound dye. Nitrocellulose filters were then cut with a razor blade into strips. Strips containing the proteins of interest were incubated in blocking buffer for 30 min at RT and then with fresh blocking buffer containing the primary antibody at its working concentration (see Table 2.1 for the antibody dilution used).

After 2-3 h of incubation at RT, or overnight at 4 °C, the antibodies (table 2.3) were removed and the strips washed with TTBS 3 times, 3min each wash. Strips were incubated for 1 h with the appropriate HRP-conjugated secondary antibody (diluted 1:10,000 for ECL development) and washed 2 times, 3min each wash, with TTBS and 2 times, 3min each wash, with PBS. After washing, strips were incubated with the developing solution: Strips were incubated with the ECL (Euroclone, UK) developing solution for 1 min at RT and visualised by chemoluminescence.

Antibody	Company or other source	Animal source	Dilution
CLIC1	ABCAM	mouse	1:3000
β-actin	Sigma	rabbit	1:10000
sedlin	G. Di tullio CMNS	rabbit	1:3000
puromycin	millipore	mouse	1:1000
procollagen type II	Hybridoma Bank	mouse	1:1000
phospho-eIF2α	Cell Signaling	rabbit	1:2000
eIF2α	Cell Signaling	rabbit	1:2000
bet3	G. Di tullio CMNS	rabbit	1:2000

Table 2.3 List of antibodies used for Western blot in this study

2.12 Electron microscopy techniques

The following experiments were performed in collaboration with Elena Polishchuck (Tigem, Pozzuoli, Italy).

The cells were fixed by adding to the culture medium the same volume of a mixture of PHEM (10 mM EGTA, 2 mM $MgCl_2$, 60 mM PIPES, 25 mM HEPES, pH 6.9) buffer, 4% paraformaldehyde, 2% glutaraldehyde for 2 h, and finally stored in storage solution (PHEM buffer, 0.5 % paraformaldehyde) overnight. After washing with 0.15 M glycine buffer in PBS, the cells were scraped and pelleted by centrifugation, embedded in 10% gelatin, cooled on ice, and cut into 0.5-mm blocks

in the cold room. The blocks were infused with 2.3 M sucrose, which acts as a cryo-protectant, and then placed onto small specimen pins. The pins were frozen by immersion in liquid nitrogen, quickly transferred to a pre-cooled (–60 °C) cryo-chamber fitted onto an ultramicrotome (Leica Ultracut R) and trimmed to a suitable shape. The sections were cut at –120 °C using a dry diamond knife and collected on the knife surface. Sections were retrieved from the knife by picking them up on a small drop of a 1:1 mixture of 2.3 M sucrose and 2% methyl cellulose and transferred onto formvar- and carbon- coated specimen grids.

2.13 Medakafish Stocks

Wild type *Oryzias latipes* of the cab strain were maintained in an in-house facility in a constant re-circulating system at 28°C on a 14 hours light/10 hours dark cycle. Embryos were staged according to Iwamatsu 2004 (Iwamatsu, 2004).

2.14 Whole-Mount In Situ Hybridization

Whole-mount *in situ* hybridization was carried out using digoxygenin-labeled antisense RNA riboprobes. Antisense and sense cDNA templates were obtained by RT-PCR amplification of total RNA from *Oryzias latipes* at different stages of development with the appropriate oligonucleotide primers. These PCR products were then cloned into the Topo TA vector (Invitrogen). This vector contains two different promoter sequences (T7 and Sp6) for the expression of both the sense and antisense strands of the cloned product. The cDNA of the ol*sedl* gene were isolated by RT-PCR amplification with the following specific primers:

Forward

5’-AAC GAG TGG TTT GTC TCA GC-3’

Reverse

5’-CTG TAT AAC AAG CAC TAA GC-3’

Plasmids obtained were amplified and sequenced. Circular DNA were linearized using Not1 and BamH1 (NEB, USA). To synthesise RNA probes the reaction mix was set up as follow: 1µg of linearized plasmid/PCR product 2 µl of 10X transcription buffer (Roche) 2 µl of DIG-labelling mix (Roche) 2 µl of appropriate RNA polymerase (T7, SP6)-40 Units (Roche) 1 µl of RNase inhibitor DEPC H_2O. The reaction mix was incubated for two hours at 37°C, after which 2 µl (20 Units) of DNase-RNase free was added to the reaction mix and incubated for 15 minutes at 37°C to degrade template DNA. Products were separated by elettroforesis and bands representing sense and anti-sense probes, respectively were purified from acrylamide gel. Selected embryos were fixed in 10 ml of 4% paraformaldehyde prepared in 2X PTW (PBS containing 0.1% Tween) for 1 hour at room temperature and then 12 hours at 4°C. The embryos were dechorionated and washed 4 times with 1X PTW. Finally, embryos were dehydrated in methanol 100% and stored at -20°C (embryos in methanol endure to several months of storage without degeneration). Embryos were gradually rehydrated washing with 75% methanol/PTW, 50% methanol/PTW and 25%methanol/PTW. Than samples, were treated with 10mg/ml proteinase K in PTW for a different amount of time (from 5 to 90 minutes) depending on the specific embryonic stage and washed twice with freshly prepared 2mg/ml glycine in PTW. After the embryos were refixed in 4% paraformaldehyde/PTW at room temperature for 20 minutes and washed through five changes of PTW. The embryos were pre-hybridized for at least 1 hour at 65°C with hybridization buffer prepared as follow:

Formamide 100% 25ml SSC 20X (pH7.0) 12.5 ml Heparin (50mg/m) 150 l, Torula-RNA 250 mg

Tween20 10%. The probes were added and the samples were hybridized overnight at 65°C (42°C for microRNAs LNA-DIG-probes). After the hybr idization step, embryos were washed at 65°C (42°C for microRNAs LNA-DIG-pro bes) with 50% formammide/2xSSCT, 2xSSCT and 0.2xSSCT. Then the embryos were incubated at room temperature with a blocking solution (5% serum/PTW) for two hours in agitation. The samples were then incubated for 12 hours at 4°with 200 µl of anti-DIG antibody (1:4000 dilution). Then the samples were washed 3 times for 10 minutes with the SB solution (0.1M Tris pH 9.5, 0.1M NaCl, 50 mM, $MgCl_2$, 0.1% Tween). Subsequently the embryos were placed in the appropriate colour solution with specific reagents NBT / BCIP (Boehringer). The reaction was blocked with TE/Tween 0.1% solution, the embryos were again fixed in 4% paraformaldehyde/PTW for 20 minutes, washed with PTW1X and stored in glycerol. The embryos were embedded in a mix of BSA/Gelatine and sectioned with vibratome. Samples were imaged with Leica DM- 6000 microscope. ImageJ was used to adjust image brightness and contrast. A minimum of 20 embryos, obtained from independent injections were hybridized for each marker and condition.

2.15 Real Time PCR

RNAs were obtained from whole mount larvae at indicated stages by using RNeasy mini kit (Quiagen, UK). The cDNAs were generated by the Quantitect kit for the qRT-PCR analysis. The qRT-PCR reactions were performed with listed primers and carried out with the Roche Light Cycler 480 system. The PCR reaction was

performed using cDNA (200-500 ng), 10 ul of the SYBR Green Master Mix (ROCHE) and 400 nM primer, in a total volume of 20 ul. The PCR conditions for all the genes were as follows: preheating, 95°C for 5 min; cycling, 40 cycles of 95°C for 15 s, 60°C for 15 s and 72°C for 25 s. Quantification results were expressed in terms of cycle threshold (Ct). The Ct values were averaged for each triplicate. The ol*Hprt* and ol*Gapdh* genes were used as the endogenous control for the experiments. Differences between the mean Ct values of the tested genes and those of the reference gene were calculated as $\Delta Ct_{gene} = Ct_{gene} - Ct_{reference}$. Relative expression was analysed as $2^{-\Delta Ct}$. Relative fold changes in expression levels were determined as $2^{-\Delta\Delta Ct}$.

The sequences of oligonucleotide primers are summarized in Table 2.4.

Name	Forward	Reverse
Bet3	GAATTTCACATCCACGGCCA	ACAGCACCCTTGTCTACTCC
Sedlin	GTTACAGCAGGTCAAATCCG	CTTTCCTTTCAAATGCTGTGGAGCG
Col1a1	TCCGTTCATCTCACATCCTG	CTTTGTGGATATTCGGTTAGCG
Col2a1	AAAGGAGATGCCGGAGAG	CCCTTTCACCTCGCTGTC
Col2a2	AGTCAGATCGAGAACATGCG	TGGGATCAATCCAGAAGTCAC
Col10a1	GCCCATTGTGTTCACCTATA	GGATCTGGATGTAGACTGT
Col11a1	GCATATCGCATCACCAAGA	GCGTTCCTCACTTTAACTCT
HPRT	GATGTAGTCCAACAGGTCGG	TCTGGAGAGGGTGTACATCC

Table 2.4. List of the sequences of the primers used in qRT-PCR experiments.

2.15 Alizarin red staining

Larvae at stage 40 were fixed with 4% PFA in PTW2X for 3hrs at room temperature on a shaker. Samples were washed three times in PBS 1% tween and treated with 1% (p/v) KOH for 30 minutes. Alizarin red (Sigma Aldrich, Germany) was added to the samples at final concentration of 0.25 mg/mL for 30 minutes.

Samples were destained for 15-30 minutes with 1% (p/v) KOH.

2.16 Morpholinos (MO) injections

To inhibit sedlin function, specific morpholinos (MO) (Gene Tools) were designed on the two sedlin mature sequence as follow:

Mo-sedlin- TGTTGAAATTTGCTTCCTGGGAGTC (25b)

Control embryos were always co-injected with mismatch MOs to follow test possible defects associated with the injection procedures.

To inhibit sedlin morpholino were injected into one blastomere of the embryos at the one-two cell stage and the optimal MOs total concentration (0. 2 mM) were determined on the basis of morphological criteria.

2.17 Generation of sedl-/- medaka

Custom-designed transcription activator-like effector nucleases (TALEN) were used to induce targeted mutagenesis in sedlin medaka gene. Genomic sequence of medaka *sedlin* genes was retrieved from the Ensembl medaka genome browser (http://www.ensembl.org/Oryzias_latipes) and potential TALEN target sites in exon 3 of *sedlin* gene were identified using *TALEN Targeter* program at https://tale- nt.cac.cornell.edu/node/add/talen. The left (L) and right (R) recognition sequences and the spacer sequence were the following: L1 recognition sequence (16 bp): AGGATGATCACCGTCA; R1 recognition sequence (16 bp): CCAAGGCCGCGTGCGC; spacer sequence (16 bp): cctgaaccagttcatt (fig)

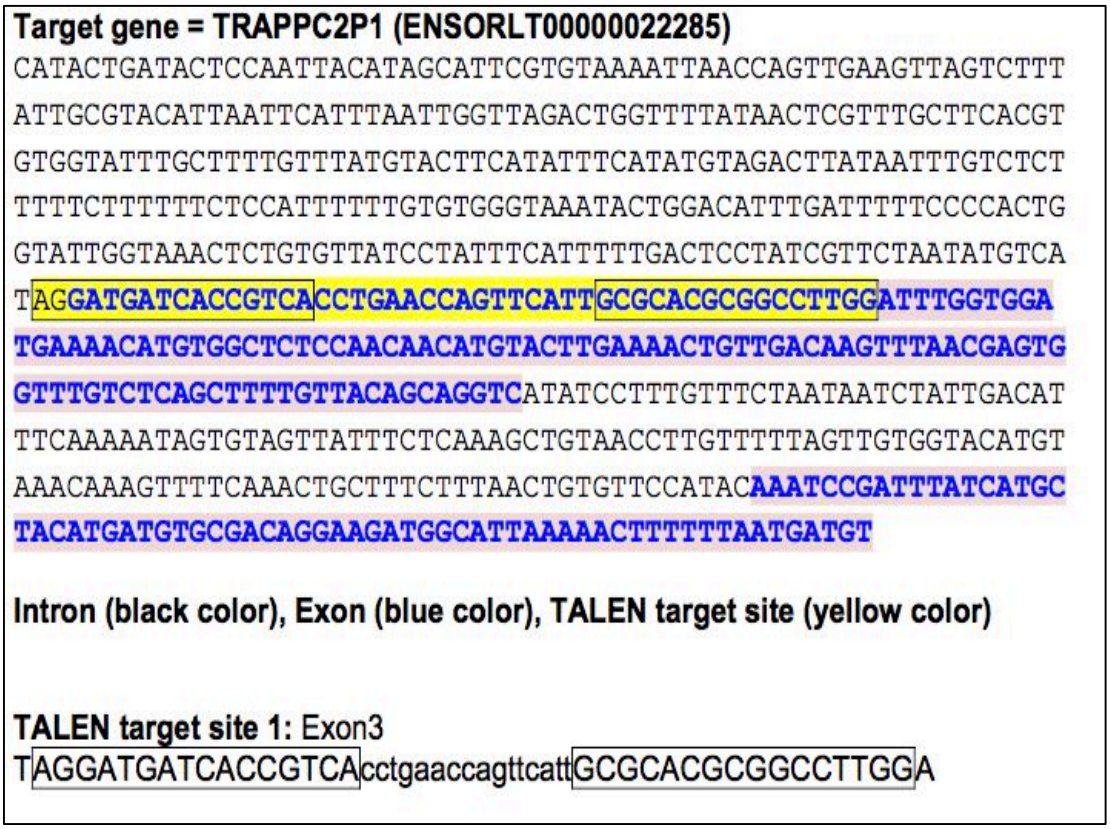

Figure 2.1 TALEN target sequence in Sedlin gene. The binding sites are in the black box.

Custom-designed TALEN vectors were assembled by ZGenebio (ZGenebio Biotech Inc, Taiwan). Two plasmids were produced, each one encoding a *Fok*I nuclease monomer and a TAL recognition domain able to recognize the left or right recognition sequence, respectively. The left (L) and right (R) plasmids (pZGB-3L and pZGB-3R) also included a SP6 promoter, an ampicillin-resistance gene, and a cDNA encoding the green or red fluorescent protein (figure 2.2).

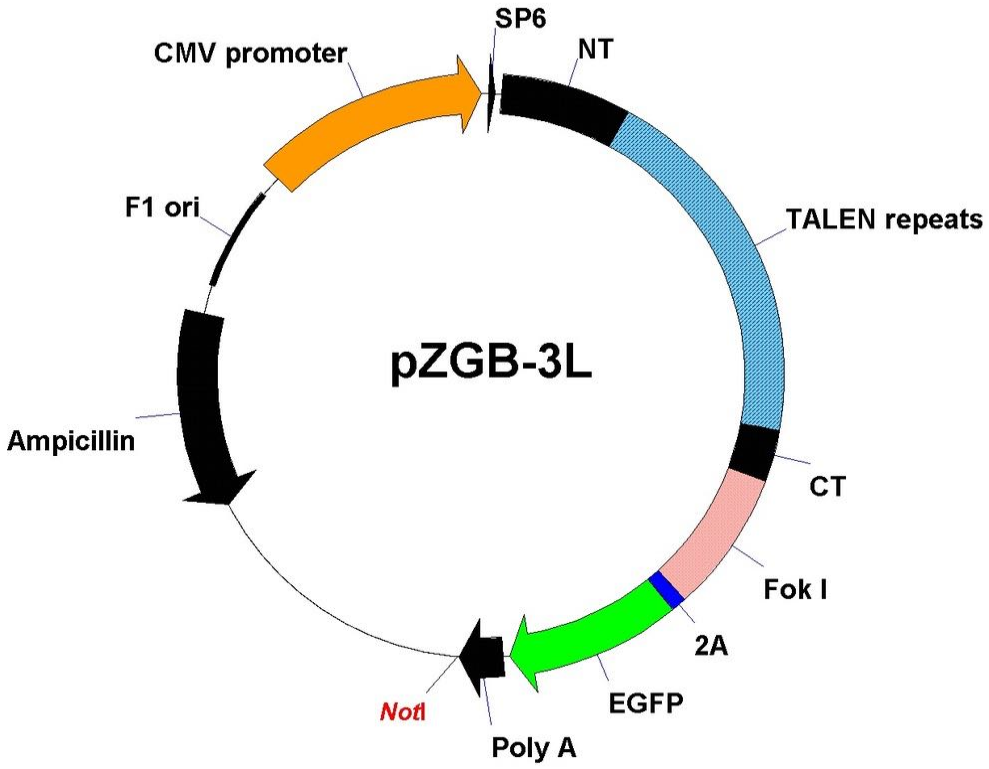

Figure 2.2 Schematic representation of the plasmid encoding TALEN proteins.

Competent DH5α bacteria were transformed with the two plasmids and 500 ml of bacterial suspension, deriving from a single clone, was grown in medium containing ampicillin for plasmid preparation. Linearized *Not*I plasmids were extracted from agarose gel using a commercial kit (QIAquick Gel Extraction Kit, QIAGEN). RNA was synthesized *in vitro* using a commercial kit (mMESSAGE mMACHINE SP6 Transcription Kit, Ambion, Life Technologies).

A pair of TALEN RNA for each target gene was injected into fertilized eggs at about 1-2 cell-stage, at a concentration of 100 ng/µl. Injected embryos were selected on the basis of GFP/RFP expression indicating successful translation of the injected RNA.

After hatching, a sample of more than 20 larvae were sacrificed and lysed for genomic DNA extraction. The target region on *sedlin* gene was amplified by PCR and sequenced to determine the presence of TALEN-induced genomic changes in mosaic state. Primers for PCR amplification of G0 and G1 generations of the target sequences were the following: ACTCGTTTGCTTCACGTGTGG (for) and TGCTACATGATGTGCGACAGG (rev). Samples were sequenced and selected to generate G2 populations. Sedlin-/- genotyping on G2 and G3 population was performed with the following primers GGAAGCAAATTTCAACAAAGG (for); GTGTAGTCTACCAATCACAC (rev) and screened for the ability to the restriction enzyme Xmn1 (NEB, USA) to cut the WT sequence.

2.18 Trancriptomic analysis

2.18.1 Samples preparation

About 50 stage 40 larvae (8 dpf) were lysed in 700µl Quiazol (Euroclone, UK) and tissues were distrupted by tissueLyser (Quiagen, UK). 140µl of Chloroform (Sigma Aldrich, Germany) were added to each samples, embryos were centrifuged at 14,000 rpm for 15 min, aqueous phase was carefully removed and saved at -80°C. 300µl of ethanol were added to the interphase and the phenol phase, samples were mixed gently by inversion and incubate at room temperature for 2-3- min. Samples were then centrifuge at 2000g for 2 minutes at 4°C to sediment DNA. Supernatants were discarded and DNAs were washed twice with 1 mL sodium citrate solution (0.1M sodium citrate in 10% ethanol v/v). 75% ethanol was added to pellet DNA, samples were incubated at room temperature for 20 minutes, mixing by inversion every 5 minutes. DNAs were pelleted at 2000g for 5 minutes, supernatants were discarded and pellets air-dried. DNAs were re-dissolved in 30µl of pure water. Finally, samples were processed for genotyping as described in session 2.17. WT

and KO aqueous phase were pulled, respectively and RNA extracted with RNeasy mini kit (Quiagen, UK). Purified RNAs quality was checked on agarose gel and RIN (RNA Integrity Number) was calculated. The above protocol was repeated three times. NGS analysis was performed with Illumina sequencer at TIGEM (Pozzuoli, ITALY).

2.18.2 Bioinformatic analysis

Gene expression profile was performed by Mario Failli (Ph.D. student in Antonella De Matteis lab) and the bioinformatics core at TIGEM (Pozzuoli, ITALY). Gene expression analysis was performed using TopHat and Cufflinks software. Of 20160 model genes annotated by Ensembl, 2831 were filtered out because their expression didn't reach the threshold of one count per million (cpm) in at least one replicate in each condition (WT and KO). The expression value of the remaining genes was normalized via trimmed mean of M-values (TMM) and differential expression analysis calculated.

Among 6193 significant differentially expressed genes (3408 down-regulated and 2785 up-regulated), 5071 had a human orthologous.

Genes excluded from the first analysis were annotated compairing their protein products with the human protein sequences database in search of identities of at least 30%. In this way, 218 genes more were associated with a human corresponding.

An enrichment analysis was carried out on the down-regulated genes below the 50^{th} percentile of the negative log fold change distribution.

2.19 Procollagen/WGA immunofluorescence on cryosections

Embryos were fixed with 4% PFA in PTW2X for two hours at room temperature or over night at 4°C. Samples were rince three times with PTW1X, incubated overnight in 15% sucrose/PTW at 4°C and than incubated overnight in 30%

sucrose/PTW at 4°C. Embryos were embedded in 50% sucrose in 50% gelatin and cut at cryostat with a thickness on 20 μm. Sections were rehydrated in PBS for 30 minutes, washed in PBS 0.1% triton and treated with antigen retrival (800 μg protease K (Sigma Aldrich, Germany), in 10 mM TRIS pH 8.0, 1mM EDTA (TE)) solution for 15 minutes at 37°C. Slides were then permeabilized with 0.5% triton in PBS for 20 minutes at room temperature, rinse in PBS 0.1% triton and block in 2% serum, 2% DMSO in PBS 0.1% triron for 20 minutes. Antibody anti collagen type II (Rockland, rabbit) was diluited 1:400 and incubated over night at 4°C. Samples were then rinsed three times in PBS 0.1% triton and incubated with Alexa Fluor anti-rabbit-568 (1:500), WGA (Invitrogen, UK) 1:500 and DAPI (1:1000) for one hour at room temperature. Sections were finally rinse fivr times in PBS 0.1% triton and mount with mowiol.

2.20 Rhodopsin/zpr1 immunofluorescence on cryosection

The following experiments were performed by Daniela Intartaglia in Ivan Conte laboratory. In brief, sections were rehydrated in PTW and blocked with 10% FBS in PTW for 1 hr at room temperature. Primary antibody anti-Rhodopsin or Zpr1 was diluted in PTW, 5% FBS and sections were incubated O.N. at 4°C. Thus, samples were washed three times in PTW and incubated with secondary antibody Alexa-fluor-488 and DAPI for nuclei staining. Finally, sections were washed with PTW (3X10' RT) and mounted with mowiol.

2.21 Whole mount immunostaining (anti phosphor histone H3)

Embryos were fixed in 4% PFA/PTW for 4 hrs at room temperature or alternatively, at 4°C over night and decorionated. Than samples, were treated with 1 μg /ml proteinase K and washed twice with freshly prepared 2mg/ml glycine in

PTW. After the embryos were refixed in 4% paraformaldehyde/PTW at room temperature for 20 minutes, washed through five changes of PTW and blocked 1-2 hrs with 1% FBS in PTW over night at 4°C. Embryos were incubates with anti-phospho histone H3 (1:400) in blocking solution over night at 4°C, washed three times in PTW and subsequently samples were incubated with biotin-anti-rabbit (1:200) in blocking solution for 2 hrs at RT. Signal was revealed with DAB lab mix and embryos re-fixed in 4% PFA O.N. at 4°C.

RESULTS:

3.1. Clic1 and Sedlin physically interact

To identify unknown molecular pathways involving sedlin, a biochemical approach was used to identify putative interacting partners. HeLa cell lysates overexpressing sedlin-FLAG and control FLAG-empty vector were immunoprecipitated with an anti-FLAG antibody. Samples were sent to the Central Proteomics facility (South Parks Rd., Oxford) for mass spectrometry analysis.

Mass spectrometry data revealed that in addition to TRAPP components and Sar1 interactions

1- one of the strongest sedlin interactors was the protein Clic1

2- a significant set of molecular partners comprised RNA binding proteins and proteins that are part of RNA metabolism pathways (Fig. 3.1).

A

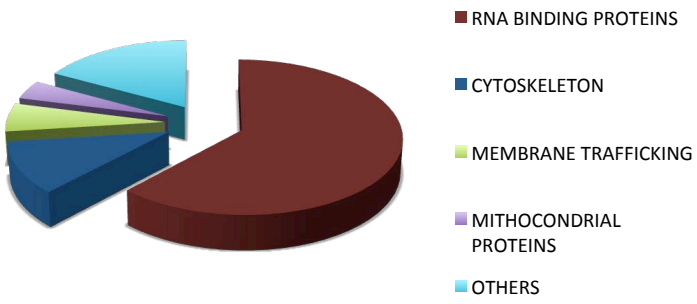

B

Member	Accession	Score	Mass	Num.. of.matches	Num.. of.significant.matches	Num.. of.sequences	Num. .of.significant.sequences	emPAI	Description
1	sp|Q15149-4|PLEC_HUMAN	11122	517822	316	290	227	210	6.69	Isoform 4 of Plectin OS=Homo sapiens GN=PLEC
2	sp|Q15149-8|PLEC_HUMAN	11083	515332	316	290	227	210	6.77	Isoform 8 of Plectin OS=Homo sapiens GN=PLEC
3	sp|P06310|KV206_HUMAN	4080	14811	88	77	3	3	1.57	Ig kappa chain V-II region RPMI 6410 OS=Homo sapiens PE=4 SV=1
1	sp|P53621-2|COPA_HUMAN	2978	140832	107	99	61	61	9.15	Isoform 2 of Coatomer subunit alpha OS=Homo sapiens GN=COPA
2	sp|P61978-3|HNRPK_HUMAN	2753	48760	82	73	24	23	14	Isoform 3 of Heterogeneous nuclear ribonucleoprotein K OS=Homo sapiens GN=HNRNPK
1	sp|Q13813-3|SPTN1_HUMAN	2509	282906	83	74	71	63	1.92	Isoform 3 of Spectrin alpha chain, non-erythrocytic 1 OS=Homo sapiens GN=SPTAN1
2	tr|H0Y711|H0Y711_HUMAN	1820	31706	47	37	10	9	2.79	Methylosome protein 50 (Fragment) OS=Homo sapiens GN=WDR77 PE=1 SV=1
1	sp|P35606-2|COPB2_HUMAN	1727	99839	50	46	35	32	4.5	Isoform 2 of Coatomer subunit beta' OS=Homo sapiens GN=COPB2
1	sp|O00299|CLIC1_HUMAN	1590	27248	69	58	13	13	8.42	Chloride intracellular channel protein 1 OS=Homo sapiens GN=CLIC1 PE=1 SV=4

Figure 3.1 Sedlin-flag interactors (A) HeLa cells over-expressing Sedlin-flag were immunoprecipitated with antibodies anti-flag, analyzed by MS/MS and interactors grouped according to cellular function **(B)** Sedlin partners were ranked based on their score. The chloride intracellular channel (CLIC1) represent one of the strongest sedlin interactor.

To corroborate the mass spectrometry data, I immunoprecipitated endogenous sedlin from cells overexpressing Clic1-GFP and was able to confirm this interaction (Fig. 3.2).

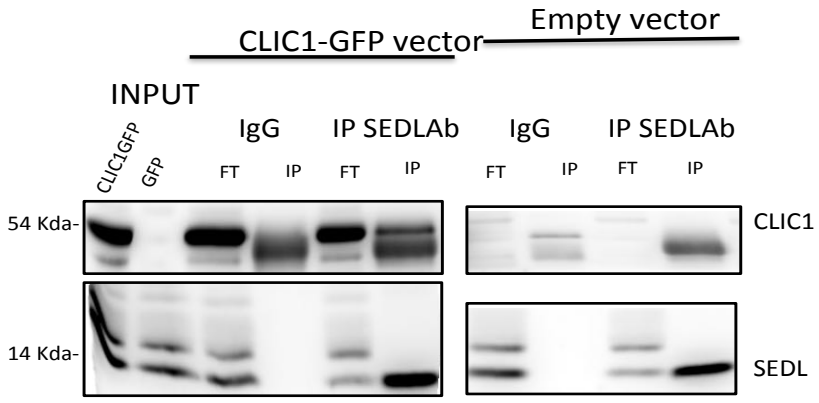

Figure 3.2 Endogenous Sedlin co-immunoprecipitates with CLIC1-GFP HeLa cells were transfected with CLIC1-GFP or GFP alone and immunoprecipitated with antibody anti-Sedlin. Western blot analysis shows a clear band at 54 KDa, the molecular weight of CLIC1-GFP absents in controls. Immunoprecipitations are indicated as (IP), flow through samples are indicated as (FT).

3.2. Study of the role of Clic1 in the secretory pathway

- *3.2.1 morphological studies*

To characterize Clic1 function in the secretory pathway, CLIC1-KD cells were analysed by immunoelectron microscopy under steady-state conditions. Morphometric analysis revealed severely fragmented Golgi complexes in CLIC1 KD cells (Fig. 3.3). The Golgi apparatus is the main hub of the secretory pathway. It is a very special organelle comprised of stacks of flattened, discrete, membrane-bound compartments called cisternae forming Golgi stacks. In mammalian cells, these stacks are laterally connected by membrane tubules to form a large Golgi ribbon capping the nucleus. Furthermore, the Golgi apparatus is polarized with a cis-entry site facing the ER and the ER-Golgi intermediate compartment (ERGIC), and a

trans-exit that faces the endosomal system (Polishchuk and Mironov, 2004).

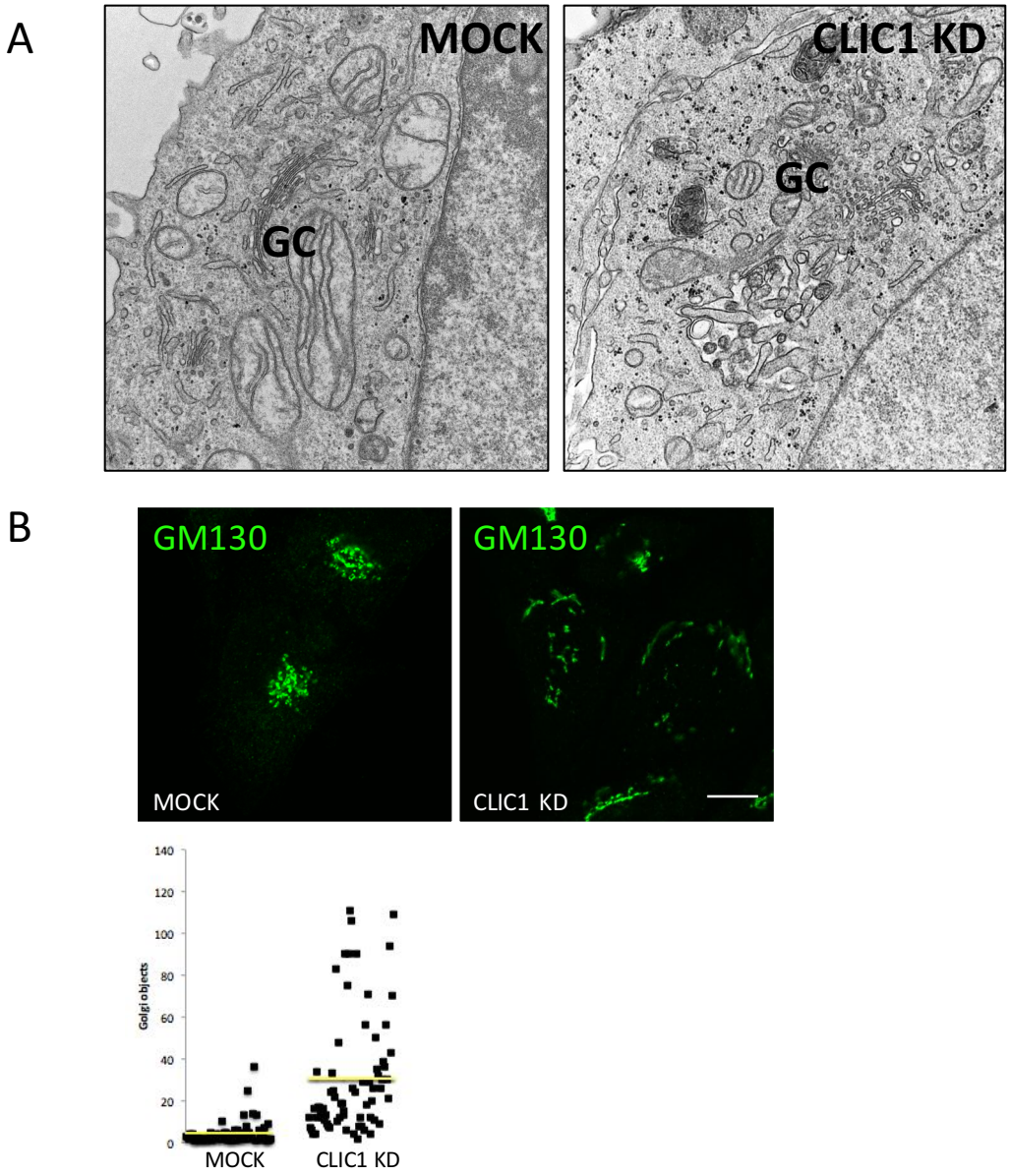

Figure 3.3 CLIC1 depletion affects the structure of the Golgi complex (A) HeLa cells were mock (CTRL) and CLIC1-siRNA treated for 72 hours and samples were processed for transmission electronmicroscopy analysis (TEM). **(B)** Quantification of Golgi objects by immunofluorescence using GM130 as a Golgi marker. Samples were visualized by confocal microscopy as described in methods and Golgi spots were measured by Imagej software. Data represent the number of Golgi spots per cell in Mock and CLIC1 KD, respectively. Both figure A and B show that CLIC1 depletion leads to Golgi fragmentation.

Therefore, I addressed whether the Golgi fragmentation observed in CLIC1-KD cells was also accompanied by alteration in Golgi polarity. To better visualize Golgi polarity, mock and CLIC1 KD cells were treated with the fungal metabolite Nocodazole that results in Golgi mini-stack formation due to actin depolymerisation, which allows for better visualization of Golgi subdomains (cis, medal, trans). Upon CLIC1 depletion the Golgi maintains the same polarity (Fig. 3.4) demonstrating that CLIC1 depletions does not alter Golgi compartmentalization. Thus, this finding rules out the hypothesis that CLIC1 is important for Golgi function.

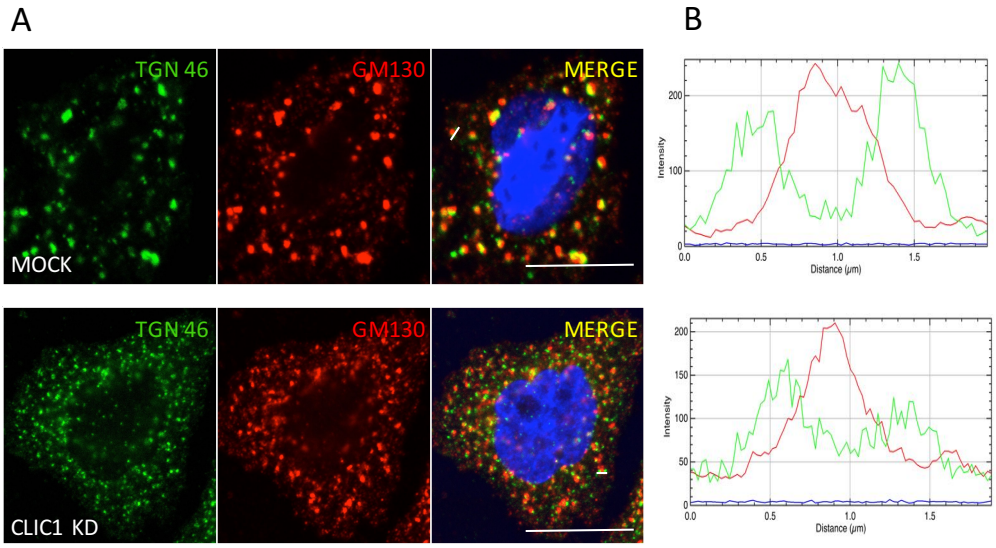

Figure 3.4 CLIC1 depletion does not alter Golgi polarity (A) Control (Mock) and CLIC1 KD cells were treated with nocodazole 33 μM for 3 hours then fixed and stained with a *cis*-Golgi marker (GM130) and TGN46 localized at *trans*-Golgi. Golgi polarity is maintained in CLIC1 KD cells. **(B)** Representative region are shown (white line). Intensity plots of signal intensity (y-axis) against distance in μm (x-axis) show occurrence of overlap between the two channels.

3.3.2 functional studies

Given the effects of sedlin depletion on PCII transport (Venditti et al., 2012), I asked whether also CLIC1 depletion could affect procollagen secretion. Rat chondrosarcoma chondrocytes (RCS) that normally express high levels of PCII were treated with CLIC1-specific siRNAs prior to a procollagen secretion assay. Procollagen secretion is very easy to monitor by immunofluorescence: the cargo get unfolded at 40°C thus accumulating in the endoplasmic reticulum. Temperature shift (from 40°C to 32°C) allows collagen proper folding and releasing from the ER. The analysis of procollagen trafficking of CLIC1 KD cells, revealed a strong delay in the exit of the procollagen from the ER (Fig. 3.5).

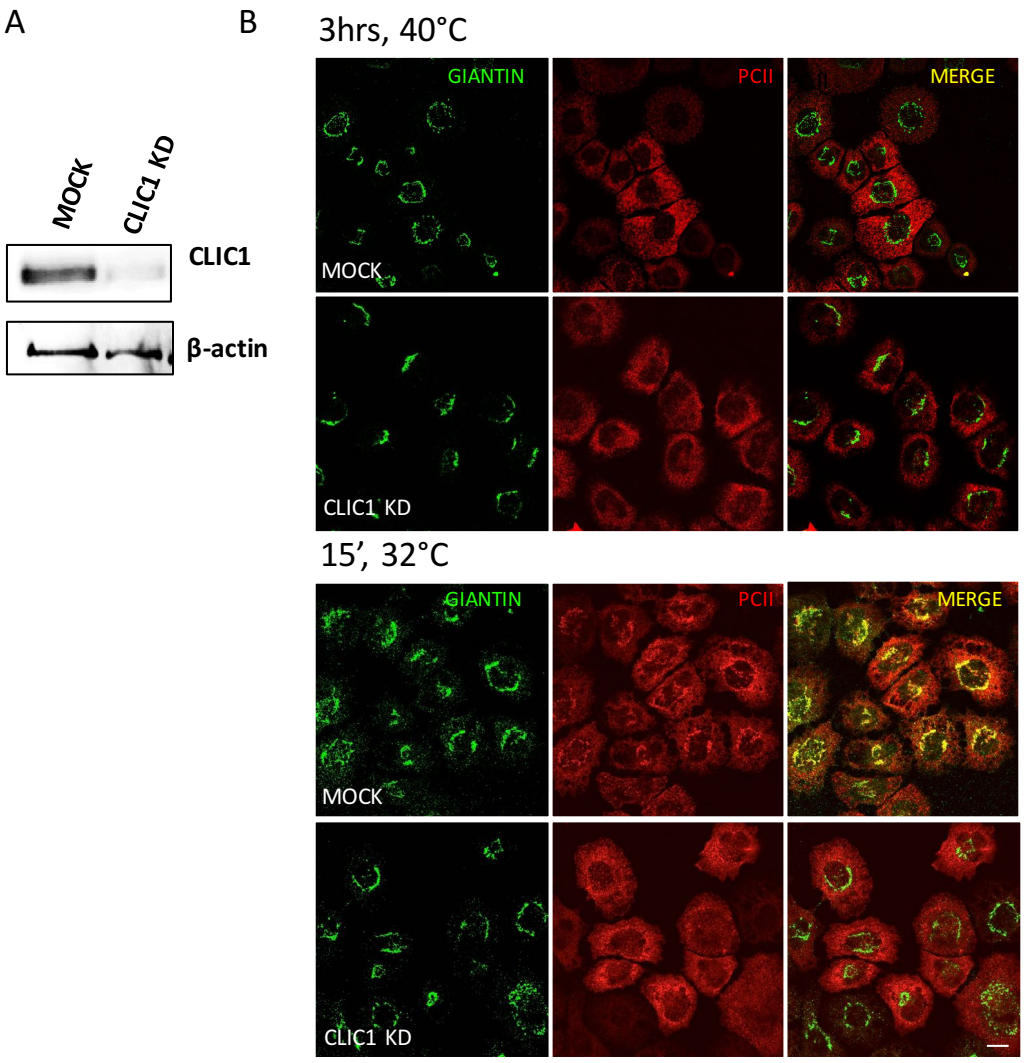

Figure 3.5 The exit of PCII is impaired in CLIC1 depleted cells (A) Rat chondrosarcoma chondrocytes expressing high level of procollagen type II were incubated at 40°C for 3 hours and fixed and imaged (A) or subsequentely shifted to the permessive temperature for 15 minutes. **(B)** Cells were stained using anti-Giantin (a Golgi marker) and anti-PCII. In control cells, PCII reaches the Golgi complex after 15 minutes, while in CLIC1 KD cells it fails to leave the ER. Scale bar 10 nm. (B) Western blot analysis show the reduction of CLIC1 protein level after siRNA treatment. 60 µg of total lysate from each sample were separated by SDS-PAGE (13%) gel.

Procollagen (PC) is a unique cargo due to its size (300nm), which exceeds the capacity of conventional COPII carriers (~65-85nm). The exit of PC from the ER requires a functional COPII machinery while small, soluble or transmembrane cargoes are still able to reach the Golgi when specific components of COPII vesicles are depleted (Townley et al., 2008). The reporter cargo VSV-G was used to investigate whether the effects on trafficking is restricted to "extra-size" cargoes or also encompasses general secretion. I analysed the trafficking of the cargo reporter tsO45-G, a modified form of a glycoprotein of vesicular stomatitis virus. The modification in a hydrophobic pocket of the protein (Gallione and Rose, 1985) results in thermo sensitivity and therefore can be used to synchronize this cargo. After infection with the virus and synchronization at 40°C, VSV-G is retained in the ER due to mis-folding that is rescued at 32°C allowing the protein to be packaged and secreted from the ER, traversing the biosynthetic pathway that ultimately terminates at the cell surface.

HeLa cells were treated with siRNA specific to human CLIC1 and a VSV-G trafficking assay was subsequently performed measuring the ratio of luminal versus total VSV-G levels. After one hour at the permissive temperature about 90% of VSV-G had reached the plasma membrane in control cells while in CLIC1-depleted cells a significant delay in the arrival of VSV-G at the plasma membrane (~70%) was observed (Fig. 3.6).

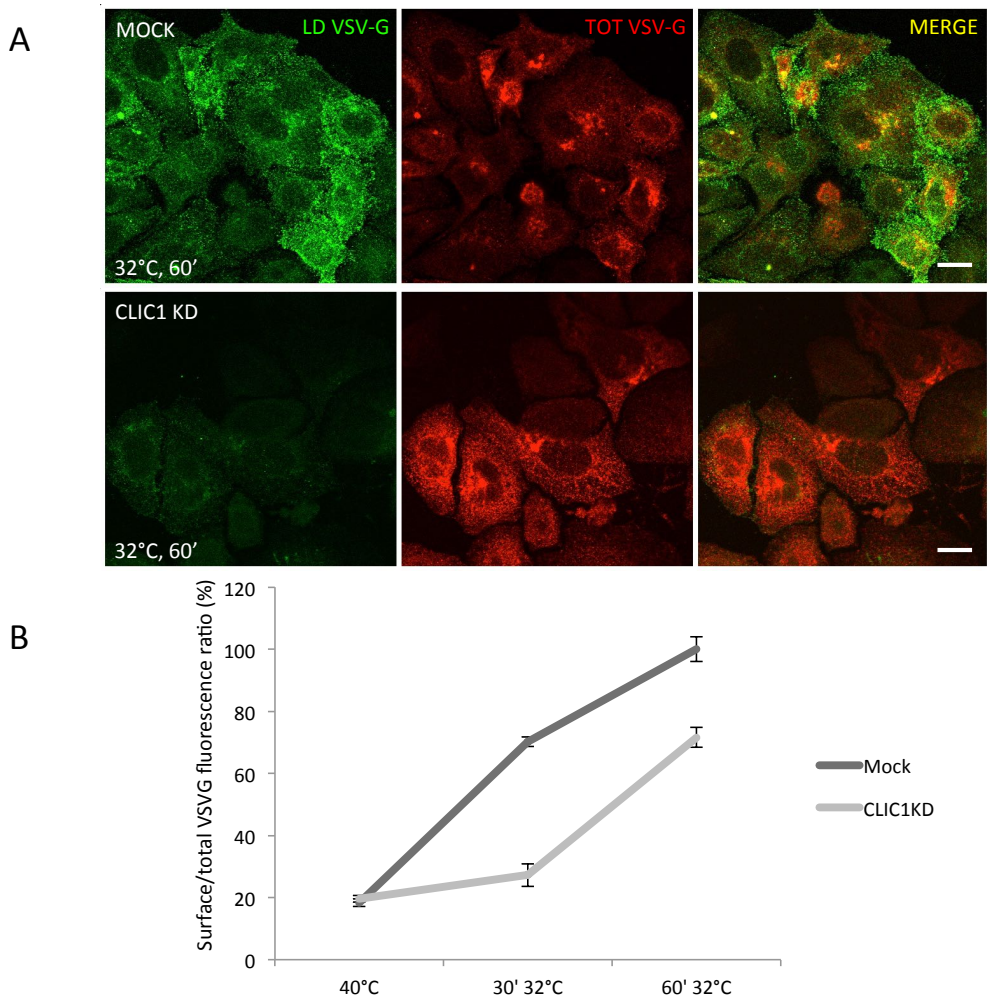

Figure 3.6 CLIC1 KD affects VSV-G arrival to the plasma mebrane (A) HeLa cells were mock (CTRL) and CLIC1 KD-siRNA transfected for three days. Cells were infected with VSVGtsO45 for 1 hour at 32°C and then shifted to 40°C for 3 hours, to accumulate VSV-G into the ER. Finally, cells were incubated at 32°C for 60' fixed and imaged. To measure the arrival of VSV-G to the plasma membrane (PM), a specific antibody recognising the VSV-G luminal domain was used before permeabilizing cells. Subsequently, cells were permeabilized with saponin 0.2% and stained with an antibody against a cytosolic portion of VSV-G (P5D4). Images were taken using the same laser parameters. Arrival of VSV-G to the PM is strongly delayed in CLIC1 KD cells. Scale bar 10 µm. **(B)** VSV-G arrival to the plasma membrane was measured by evaluating the ratio between VSV-G at the PM and the total ammount of the viral protein. The data are expressed as % of the control cells with VSVG at the PM. Mean values (±SD) from 3 independent experiments (n=100).

VSV-G travels through the secretory pathway through the Golgi complex until the plasma membrane. Thus, CLIC1 depletion could block VSV-G at different stages of the secretory pathway. Therefore, I performed the VSV-G assay following the exit of the viral protein from the ER.

Control and CLIC1-KD HeLa cells were infected with VSVG, fixed, and imaged at 15 minutes after the temperature shift. At 32°C the VSV-G protein is correctly folded, sorted at ER Exit Sites (ERES), and exits the ER via COPII carriers. After 15 minutes at 32°C, a clear staining of the Golgi appears in control conditions while CLIC1-depleted cells were not able to transport the viral protein, which accumulated in the ER (Fig. 3.7). Bet3-depleted cells accumulate cargo (VSV-G, CD-8) in vesicular tubular clusters (VTCs), an intermediate pre-Golgi complex that forms after COPII homotypic fusion (Yu et al., 2006; Cai et al., 2007) while knock down of TRAPPIII-specific subunits blocks cargoes in the intermediate compartment (Scrivens et al., 2011). These data and the fact that CLIC1 depletion results in ER cargo accumulation suggests that CLIC1 is epistatic to the TRAPP complex, which acts downstream mediating the homotypic fusion of COPII vesicles and activating Rab1.

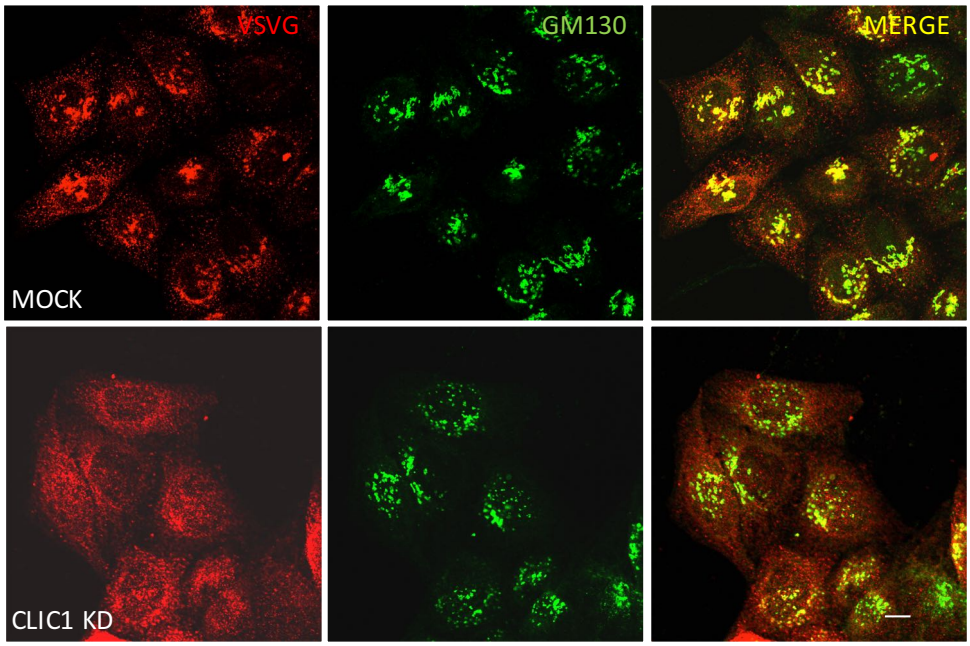

Figure 3.7 CLIC1 depletion impairs the exit of VSV-G from the ER HeLa cells were mock (CTRL) and CLIC1 KD-siRNA for three days. Cells were infected with VSVGtsO45 as previously described (figure 3). Samples were fixed 15' after permessive temperature (32°C) and stained with a cis-Golgi marker (GM130) and VSV-G antibody. Scale bar 10 μm.

3.3. Study of the role of Clic1 in the endocytic pathway

Data from CLIC1-KD cells suggested that CLIC1 functions early in the secretory pathway. To address if CLIC1's role is generally required for membrane trafficking events, analysis of recycling endosome dynamics was analyzed in CLIC1-depleted cells.

To this end, I looked at the dynamics of recycling endosomes in HeLa cells knocked down for CLIC1. Endocytosis follows multiple routes such as clathrin- or caveolin-dependent, or uncoated vesicles can transport cargoes from the plasma membrane into the cytosol (Elkin et al., 2016). I monitored the trafficking of transferrin to

address the effects of CLIC1 depletion on clathrin-mediated endocytosis (CME) and the trafficking of uncoated carriers looking at Shiga-toxin, respectively.

In both conditions I observed no differences in the transport of these cargoes, suggesting that CLIC1 is exclusively required for ER-to-Golgi trafficking (Figs. 3.8; 3.9).

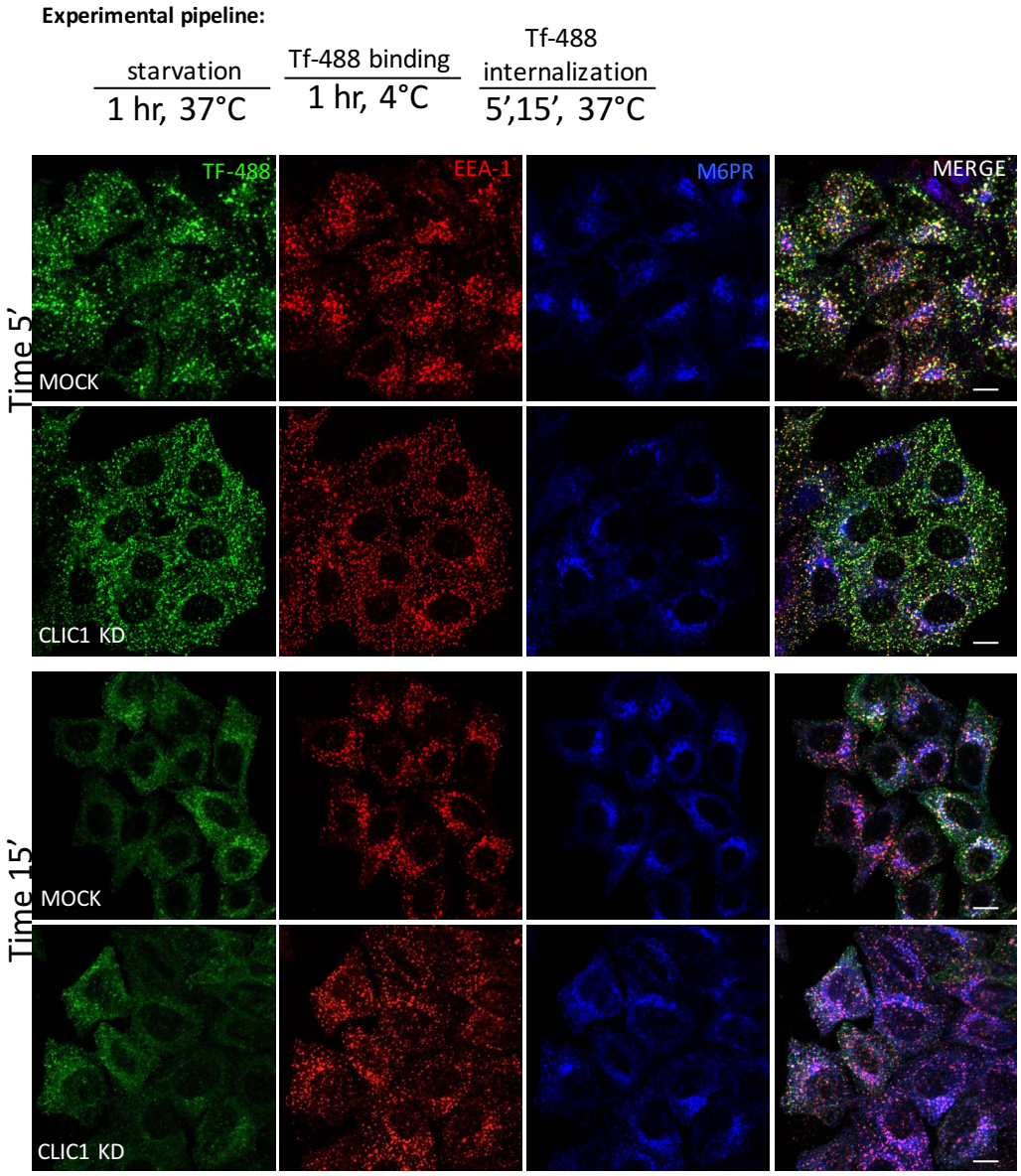

Figure 3.8 Transferrin recycling is not altered in CLIC1 KD cells. Fluorescent Tf internalization, uptake and recycling was evaluated in CTR and CLIC1 KD HeLa cells. Cells were serum starved and treated with A488-Tf for 1hr at 4°C and chase in complete medium for indicated times.

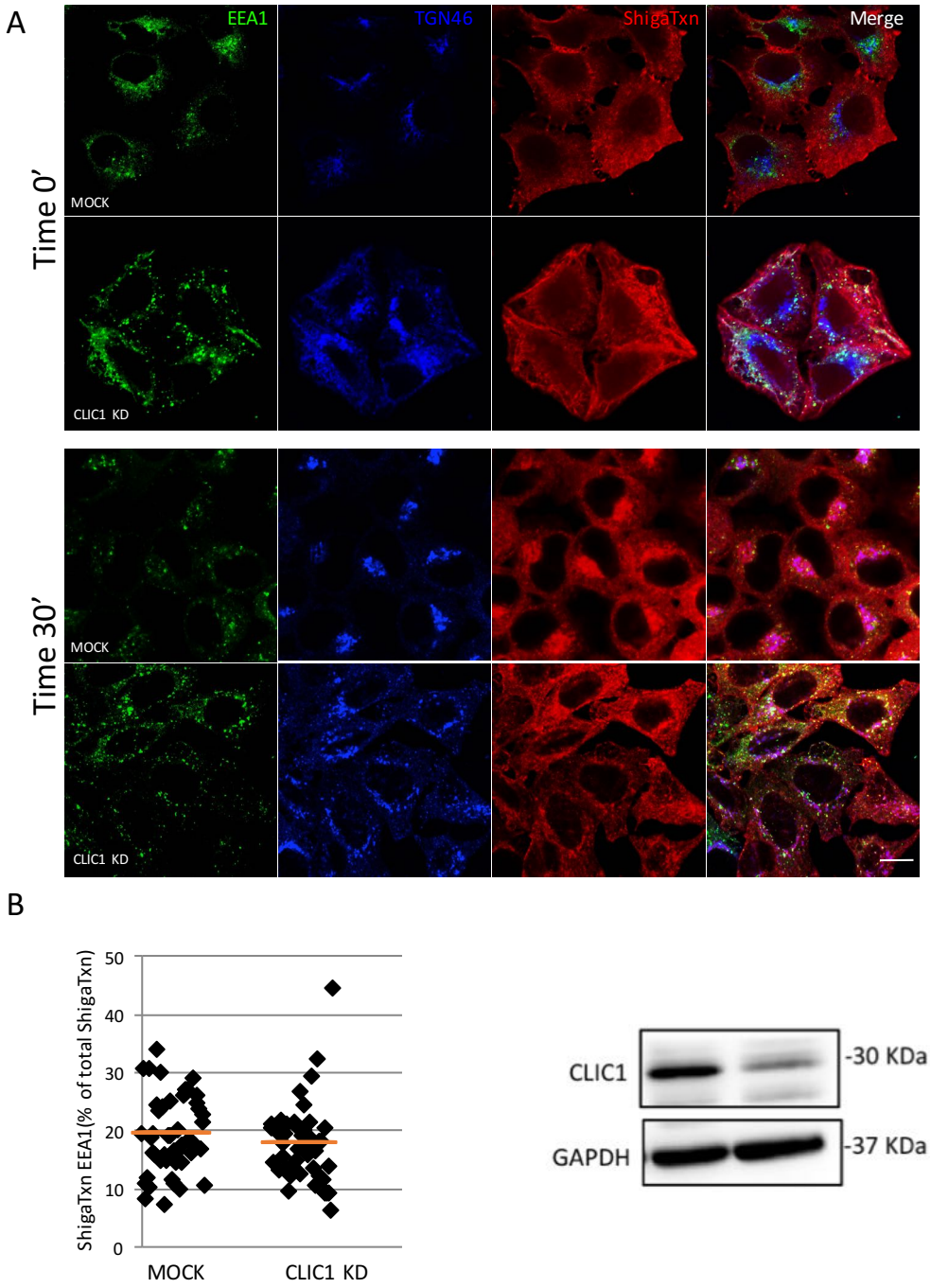

Figure 3.9 CLIC1 KD does not impact on Shiga toxin trafficking (A) Shiga toxin retrograde trafficking was assayed in Control (MOCK) and CLIC1 KD cells. Cells were loaded with shiga toxin for 30' at 4°C and fixed after 30' of internalization. **(B) (Left)** Shiga toxin mean intensity in EEA1-positive structures on total shiga toxin was quantified by ImageJ software. **(Right)** KD efficiency was evaluated by western blot analysis.

3.4 Chemical inhibition of CLIC1 leads to Golgi fragmentation and inhibition of ER-export

To evaluate whether the effect on the trafficking observed in CLIC1 KD cells was due to as secondary effect of the siRNA transfection or a consequence directly dependent from CLIC1 functions, HeLa cells were treated with a specific CLIC1 inhibitor, IAA-94 that acutely blocks CLIC1 function without affecting protein stability. CLIC1 loss of function after IAA-94 treatment led to Golgi fragmentation (Fig. 3.10) and inhibition in ER-to-Golgi trafficking, corroborating the knockdown data (Fig. 3.11). These data suggest that CLIC1 activity is crucial for ER-to-Golgi transport.

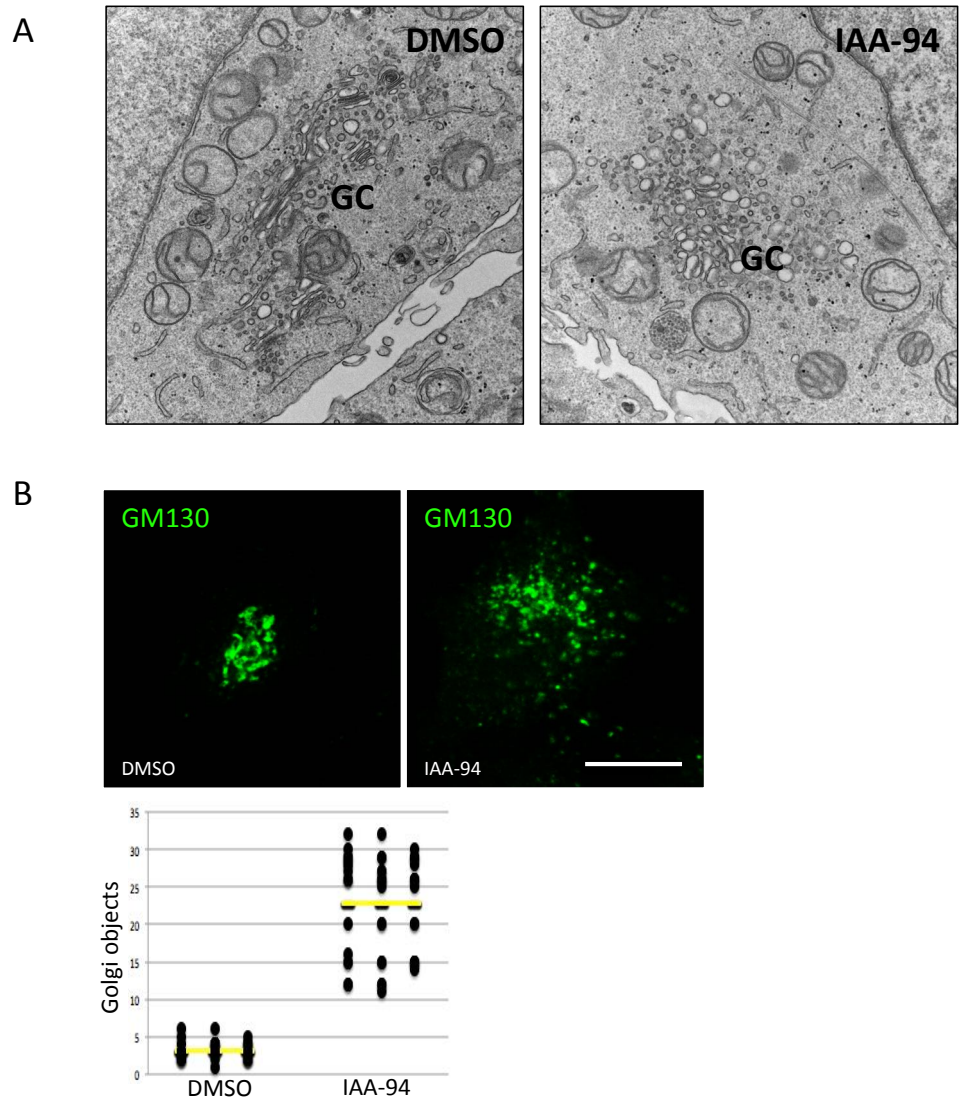

Figure 3.10 CLIC1 inactivation disrupts the structure of the Golgi complex (A) HeLa cells were treated for three hours with DMSO (CTRL) and IAA-94. Samples were processed for transmition electronmicroscopy analysis (TEM). **(B)** (Upper panel) DMSO (CTRL) and IAA-94 treated cells were fixed, stained for GM130 (a Golgi marker) and analysed at confocal. (Bottom panel). Quantification of Golgi objects by immunofluorescence using GM130 as a Golgi marker. Samples were visualized by confocal microscopy as described in methods and Golgi objects were measured by Imagej software. Data represent the number of Golgi spots per cell in Mock and CLIC1 KD, respectively. Scale bar 10μm.

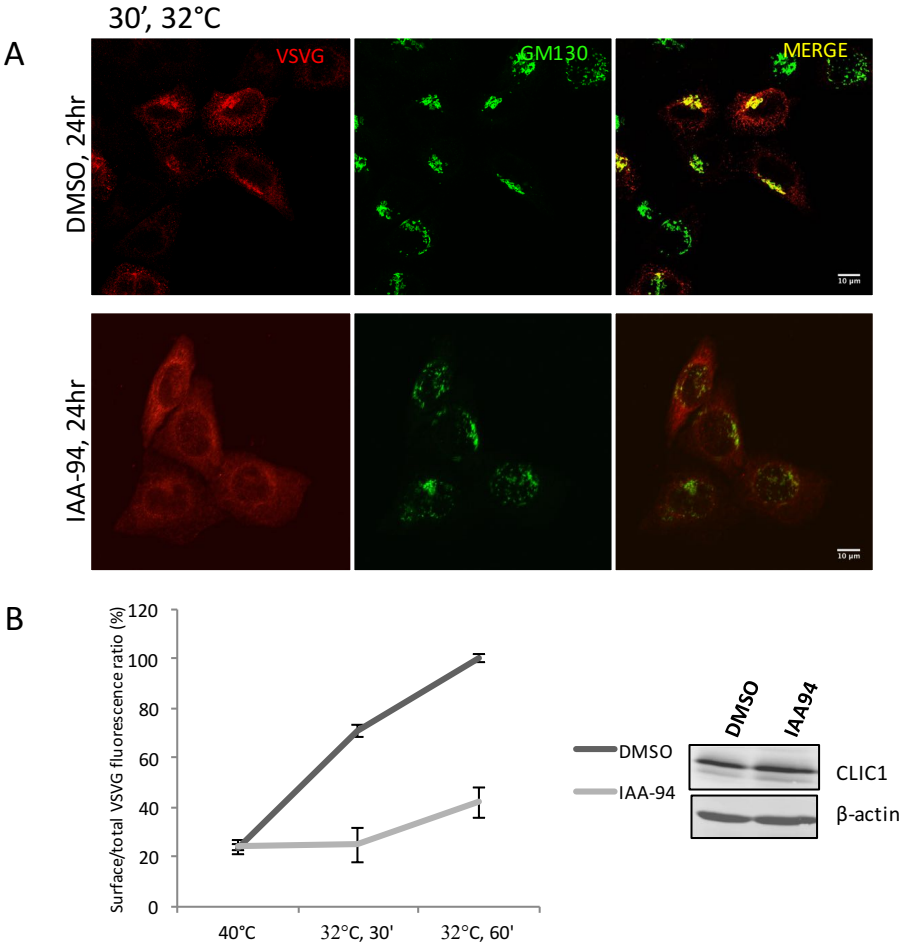

Figure 3.11 CLIC1 chemical inhibition impairs ER-to Golgi trafficking (A) HeLa cells were treated with the CLIC1-specific inhibitor, IAA94 (30μM) for 24 hours. Thus, cells were infected with VSV-G and samples processed as described before (figure 6) Scale bar 10μM. **(B)** (Left) VSV-G arrival to the PM was measured by evaluating the ratio between VSV-G at the PM and the total amount of the viral protein using a specific antibody that recognizes the luminal portion of VSV-G. The data are expressed as percentage of control cells with VSV-G at the PM. Mean values (±SD) from three independent experiments (n=100). Both the experiments show that VSV-G trafficking is impaired in the ER upon CLIC1 inhibition. (Right) Western blot analysis of CLIC1 protein levels upon IAA-94 treatment.

3.5 CLIC1 and sedlin are components of stress granules

To elucidate the molecular mechanism(s) by which CLIC1 acts in vesicular transport, a mass spectrometric analysis was performed to identify putative interactors of immunoprecipitated GFP-CLIC1 and analysed by the Central proteomics facility in Oxford. The mass spectrometry data revealed that most of CLIC1 molecular partners are RNA binding proteins and proteins associated with the stress granule (SG) pathway. Moreover, a large numbers of CLIC1/stress granule-related interacting proteins were also found to co-immunoprecipitate with sedlin, indicating that these proteins could co-operate in the stress granule pathway (Fig 3.12).

Stress granules (SGs) are non-membrane bound aggregates that form in cells upon stress induction to stall mRNA and inhibits translation. In addition to mRNAs and microRNAs, SGs are composed of several RNA binding proteins and components of the CAP-dependent translational machinery but also signalling proteins have been found to co-localize with SG markers. To evaluate whether CLIC1 and sedlin could migrate onto SGs upon stress induction, cellular localization was analysed under conditions that lead to stress granule formation. For the majority of stress studies performed, sodium arsenite, a potent poison broadly accepted to trigger SG formation (Panas et al., 2015), was used. HeLa cells were treated with sodium arsenite for 30 minutes before staining the cells for G3BP (a common marker of SGs), CLIC1, and sedlin. Images clearly show that both CLIC1 and sedlin clearly co-localized on SGs (Fig. 3.13).

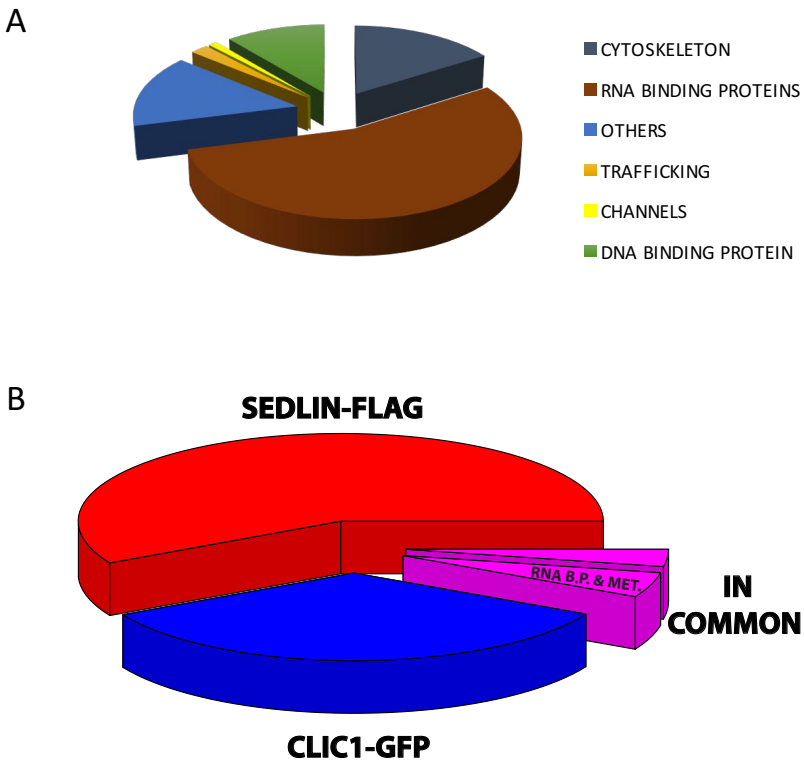

Figure 3.12 CLIC1 and sedlin common interactors are RNA-binding proteins. (A) Cells over-expressing CLIC1-GFP were immunoprecipitated using GFP as bait. CLIC1 interactors were sorted by their summatory of the ions score (probability that observed match between the experimental data and the database sequences is a random event) and grouped for functions. **(B)** Magenta slices of the cake represent sedlin-CLIC1 common interactors. 35 out of 59 CLIC1/Sedlin common interactors are RNA binding

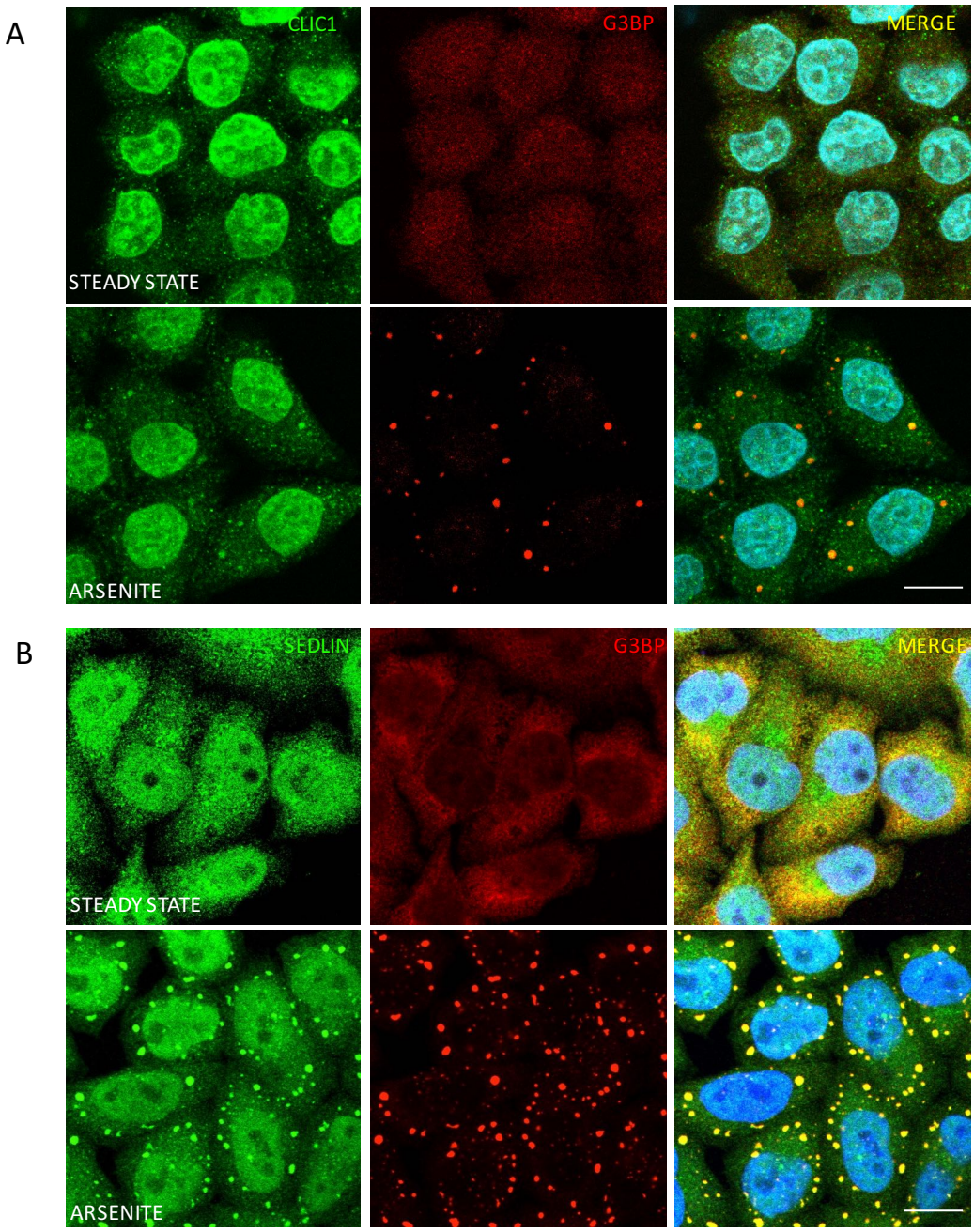

Figure 3.13 CLIC1 and sedlin migrates on stress granules. HeLa cells were treated with sodium arsenite 300µM, 30 min at 37°C and stained for CLIC1 **(A)** and sedlin **(B)** using G3BP as SGs marker. Both CLIC1 and sedlin are recruited onto SGs.

3.6. The TRAPP complex and the COPII inner coat are recruited onto SGs

Since both sedlin and CLIC1 were observed to be components of SGs, I investigated whether other cytosolic membrane trafficking proteins also associate with SGs. Immunofluorescence analysis was used to observe the endogenous behaviour of coil-coiled Golgi proteins (p115, GM130), golgins (Golgin97, GM130), proteins involved in the endocytic machinery (Clathrin, AP2, OCRL), COPI and COPII components in conditions of SG formation. Among the proteins analysed, the TRAPP complex (bet3, sedlin, TRAPPC1/bet5), Sec24C, Sec16 and Sar1a were exclusively recruited onto SGs upon SG induction as shown in figures 3.14-3.15 and schematized in figure 3.15. These analyses indicate that the recruitment of trafficking proteins onto SGs is specific and it selectively involves the ER export machinery.

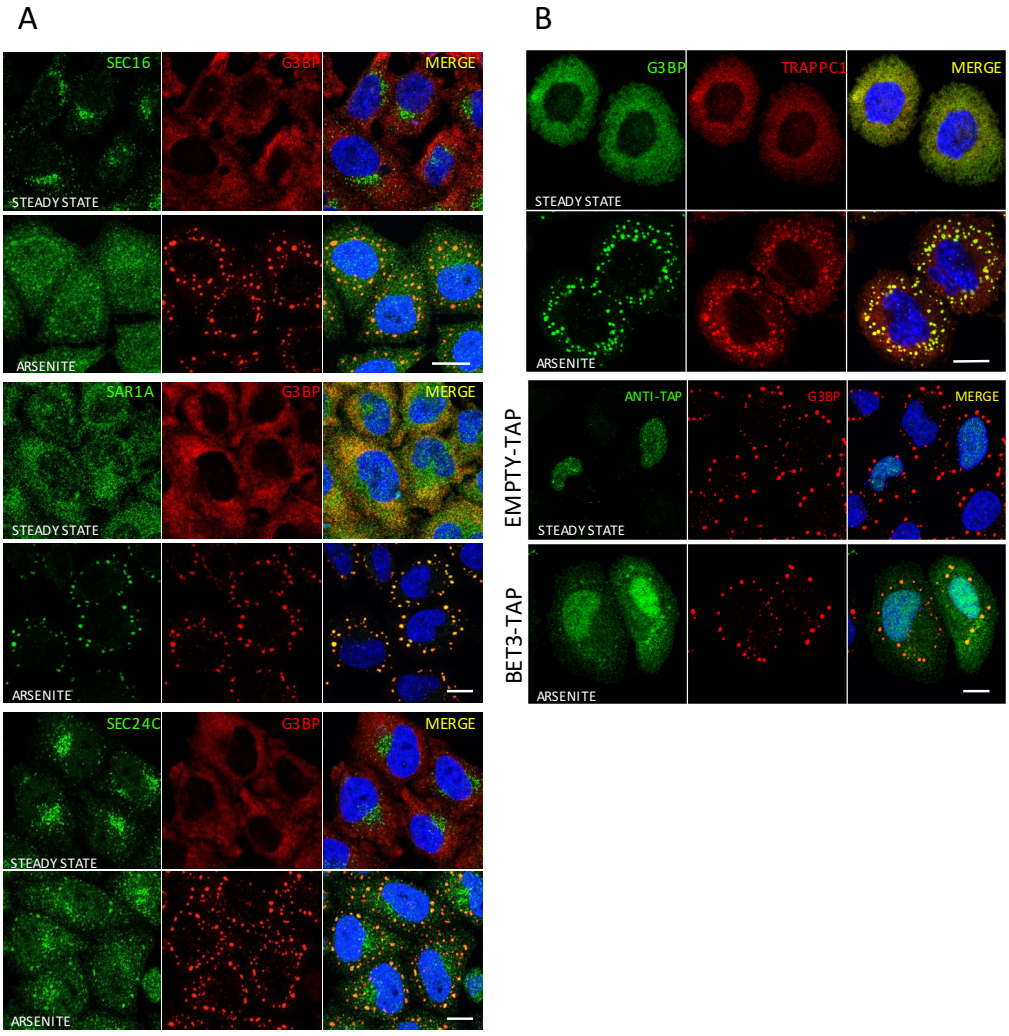

Figure 3.14 TRAPP complex and COPII components preferentially migrate onto SGs Immunofuorescence analysis performed on HeLa cells under arsenite treatment. Endogenous localization of sec16 (A, upper), sar1 (A, middle), sec24 (A, lower) and TRAPPC1 (B, upper) were monitored under stress. (B, lower) TAP-tag control vector and Bet3-TAP-tag plasmid were transfected for 16 hrs. After arsenite treatment, (300µM, 30 min at 37°), cells were stained with anti-TAP (green) and G3BP (red) specific antibodies and imaged by confocal microscopy.

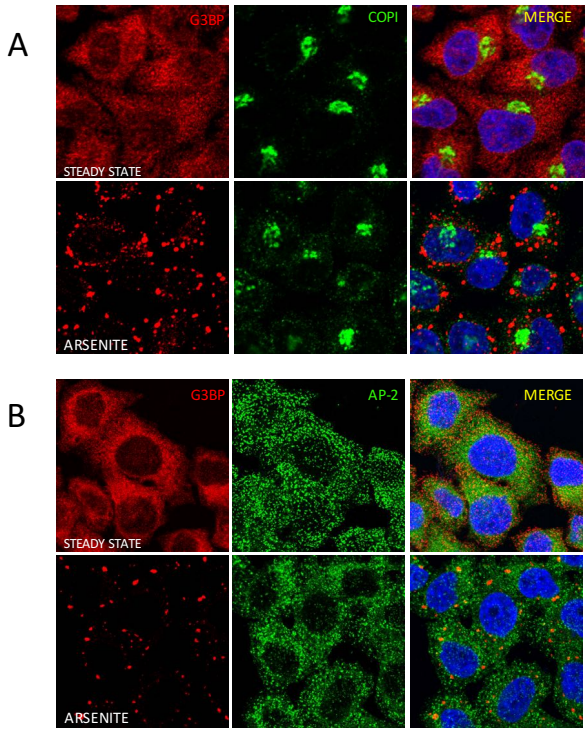

Figure 3.15 COPI and clathrin coated vesicles components do not migrate onto SGs. COPI (A) and AP-2 (B) localization was analyzed under arsenite treatment. Cells were treated with sodium arsenite 300 µM, 30 min at 37°C, stained and imaged by confocal microscopy.

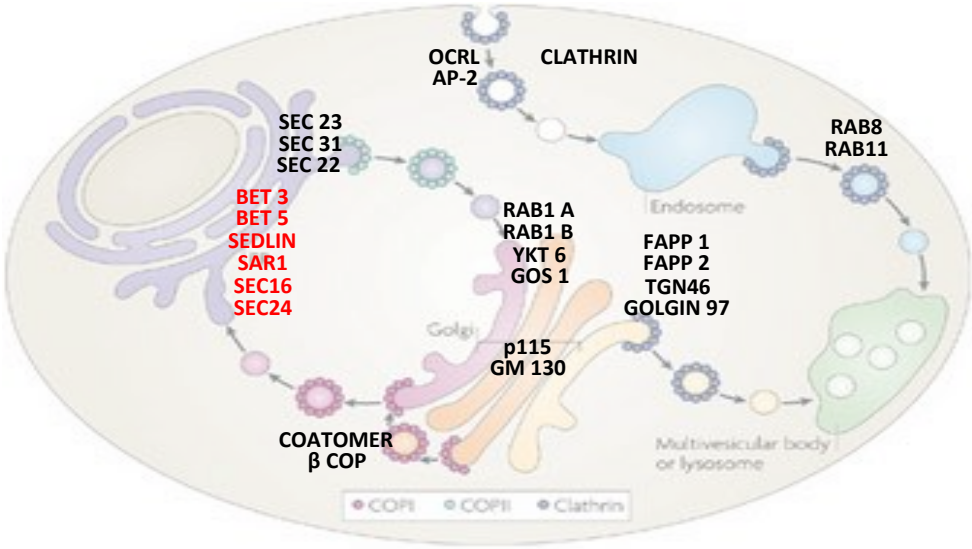

Figure 3.16 Schematic representation of membrane trafficking proteins that re-localize onto SGs. Schematic representation of immuno-based screening performed on HeLa cells under arsenite treatment. The localization of several endogenous membrane trafficking proteins was monitored under stress: bet3, bet5/TRAPPC1, sedlin, sar1A, sec16 and sec24c (in red) are selectively recruited onto SGs. Adapted from VW Hsu et al., 2009.

To test whether the re-localization of membrane transport proteins onto SGs was dependent on the nature of the stress applied to the cells, I treated cells with heat shock that leads to SG aggregation by activating a non-canonical pathway (Grousl et al., 2009). I also overexpressed G3BP that spontaneously forms SGs (Tourrére et al., 2003). In both cases, sedlin and sec24c were able to migrate onto G3BP-positive structures (Fig 3.17; 3.18A).

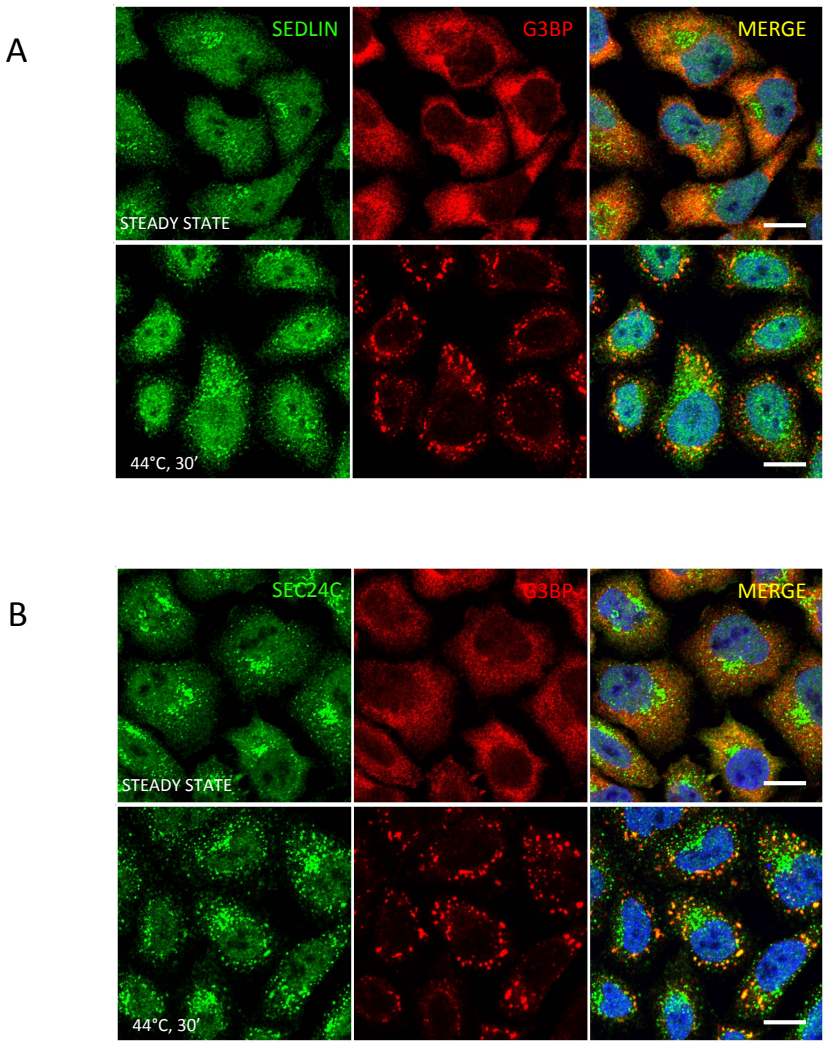

Figure 3.17 TRAPP complex and COPII inner coat recruitment is independent from stress stimuli. HeLa cells were incubated at 44°C for 30', then fixed and stained for sedlin **(A)** and sec24c **(B)** using G3BP as a SGs marker. Both sec24c and sedlin are recruited onto SGs.

In some neurodegenerative disorders (e.g. multi-system proteinopathy (MSP), Frontotemporal Lobar Degeneration (FTLD), Amyotrophyc Lateral Sclerosis (ALS)) mis-folded proteins accumulate over time into cytosolic aggregates that are positive for SG markers (Liu-Yesucevitz et al., 2010). The finding that membrane trafficking proteins can be recruited onto SGs could explain defects in the secretory pathway and Golgi fragmentation observed in ALS and Alzehimer's

disease (Sundaramoorthy et al., 2015). Therefore, I analysed the localization of COPII and TRAPP components while over-expressing WT and mutant forms of TDP-43, a protein associated with ALS. In normal conditions TDP-43 is localized to the nucleus, while a truncated form of the protein (TDP-35 and TDP-25) accumulates in SGs that are also positive for both Sec24c and sedlin (Fig 3.18B). These data clearly demonstrate that the localization of TRAPP complex and COPII components are independent of the stress stimulus, suggesting their involvement is a general mechanism activated under conditions of stress.

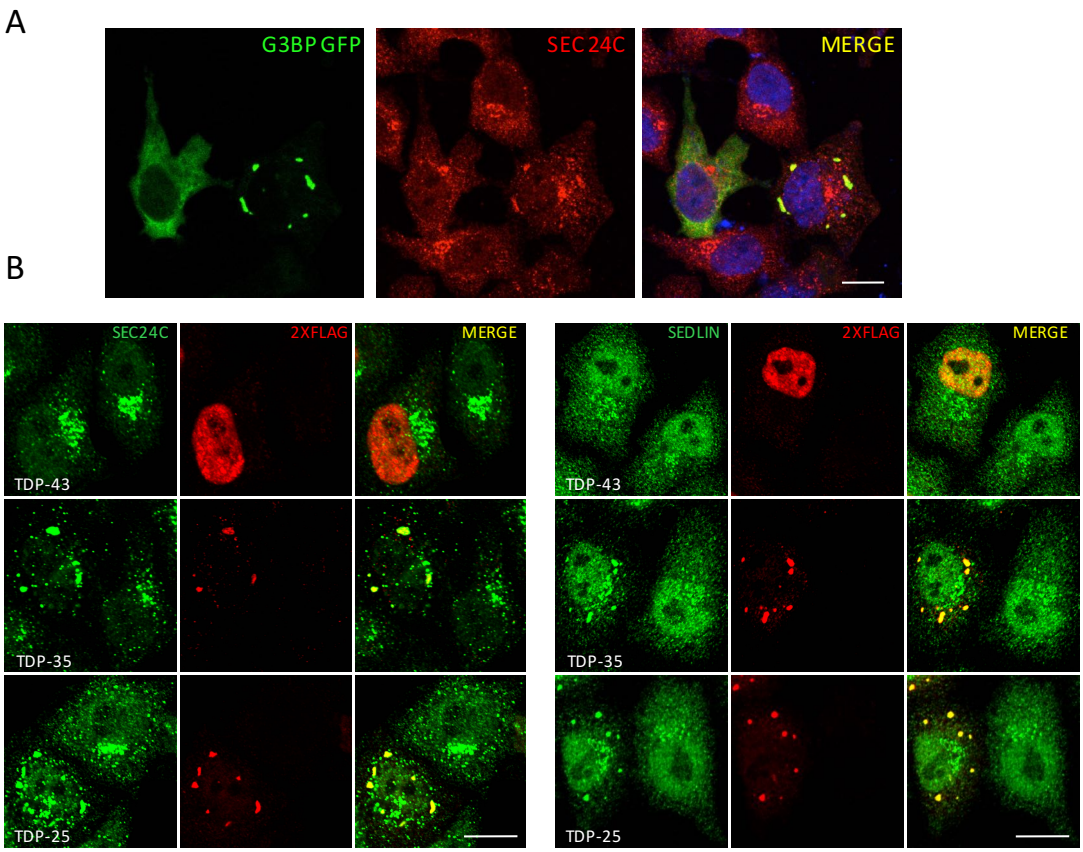

Figure 3.18 TRAPP complex and COPII inner coat recruitment is independent of stress stimuli. (A) HeLa cells were transfected with a plasmid encoding for G3BP-GFP for 16 hours, fixed and stained for sec24c. Scale bar 10 µm. **(B)** HeLa cells were transfected with the construct indicated to the left of each series of panels (wild type TDP-43-3xflag, or mutant TDP35 and 25-3xflag), and fixed at 16 hours post-transfection. Sec24c and sedlin fluorescence is shown in the left panels, and Hoechst nuclei stain is shown in the merge panels. Note the largely nuclear distribution of wildtype and mutant TDP-43-3xflag, and proteins aggregates caused by mutants over-expression. Scale bar 10 µm.

3.7. Trafficking proteins are part of the SG "shell"

Stress granule architecture is divided into two structures: (1) the core, which is detergent resistant and rich in RNAs and RNA-binding proteins, and (2) the shell, which is less stable and composed of specific cytosolic proteins (Jain et al., 2016). SGs begin to form soon after drug treatment (~5-7 minutes) and mature over time. Maturation consists of the docking of a small foci of ribonucleoproteins (RNPs) and the acquisition of proteins that form a second phase in which the foci are embedded (Wheeler et al., 2016). To clarify the sub-localization of trafficking proteins on SGs, SG maturation was followed over time (fig. 3.19). After 7 minutes, G3BP starts to aggregate in the cytosol while ER-export components are still present both in the cytoplasm and on ER-exit sites maintaining their steady state localization. After 15 minutes of arsenite treatment, G3BP foci become larger and a small amount of membrane trafficking proteins appear to be recruited onto the aggregates. After 30 minutes of SG stimulus, the G3BP spots are clearly visible throughout the cytosol and transport proteins are strongly re-localized onto SGs. After one hour of arsenite treatment, the ERES localization of ER export proteins is completely lost and the cytosolic staining is strongly diminished. However, it should be noted that one hour of arsenite treatment is toxic for the cells that become round and start to detach from the coverslip. Thus, for all further experiments (see below), arsenite treatment was for 30 minutes at the concentration of 300 μM.

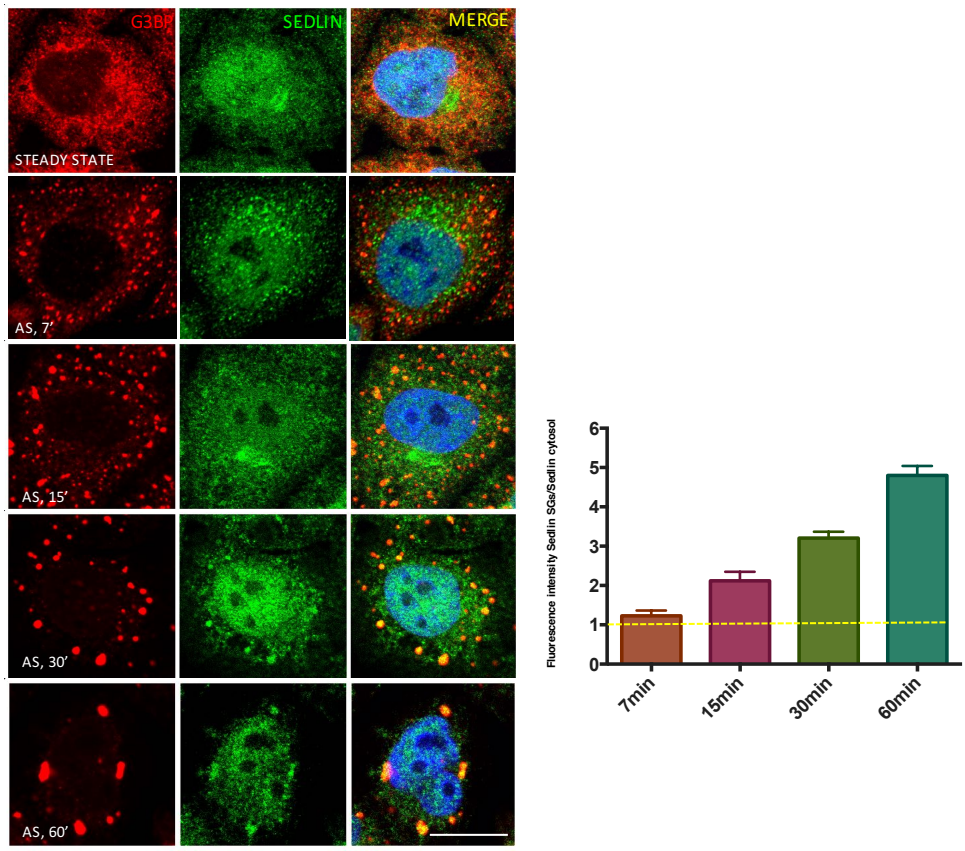

Figure 3.19 Membrane trafficking proteins are recruited on SGs in a time-dependent fashion. HeLa cells were treated with sodium arsenite (300µM, 37°C) for the indicated times, thus fixed and stained for G3BP and sedlin. G3BP spots starts to appear soon after drug treatment while sedlin recruitment occurs after 30' of arsenite stimulus. Graph on the right panel show sedlin mean intensity on G3BP spots with respect to the total. Images were quantified with Columbus software. Scale bar 10 µm.

Furthermore, to visualize the sub-localization of ER export components on SGs, sar1a and sedlin were observed using super resolution microscopy, a technique that has twice the resolution of conventional optical microscopy enabling detailed visualization of minute intracellular structures (Fig. 3.20). Arsenite-induced SGs are around 150-200 nm (Moutaoufik et al., 2014) and can be easily resolved with super resolution microscopy. The images clearly show that both sar1 and sedlin surround the stress granule core marked with G3BP, indicating that trafficking proteins occupy the outer phase of stress granules. Thus, both time-course

experiments and the analysis of membrane trafficking protein sub-localization on G3BP aggregates showed that ER export components are recruited on SGs after nucleation of RNA foci suggesting that membrane transport proteins are part of the stress granule "shell".

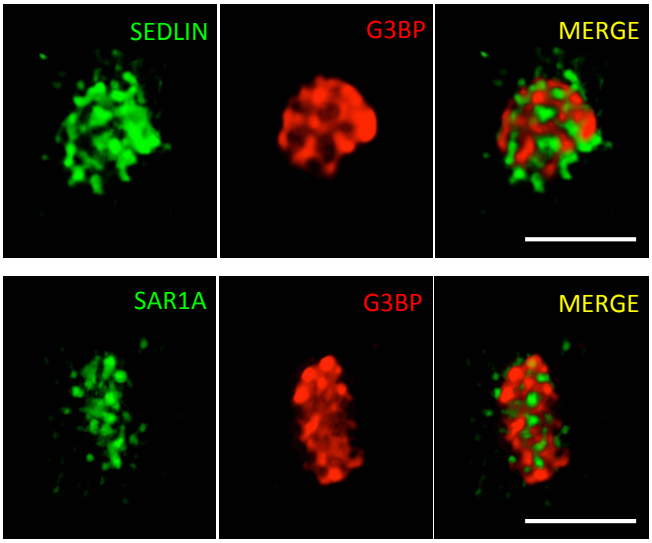

Figure 3.20 COPII components and the TRAPP complex are not part of SGs core. HeLa cells were treated with sodium arsenite, 300μM for 30', fixed and stained for G3BP (localized on SGs core), sar1a and sedlin, respectevely. A stress granule was observed by super resolution microscopy (SIM). Both sar1 and Sedlin appear interpersed into G3BP-positive domains on the stress granules suggesting that membrane trafficking proteins are part of SGs shell. Scale bar 200nM.

3.8. Consequences and role of the recruitment of components of the membrane trafficking machinery to stress granules

3.8.1 Impact on ER-Golgi trafficking

Due to the localization of Sar1, Sec16, Sec24 and TRAPP complex components under stress, I speculated that their changes in cellular localization could lead to alterations in the efficiency of cargo exit from the ER. To test this hypothesis, both PCI and PCII transport assay was performed on rat chondrocytes and human fibroblasts pre-treated with sodium arsenite 30 minutes before a temperature shift. The images show that procollagen is blocked from exiting the ER during SG formation (Fig 3.21).

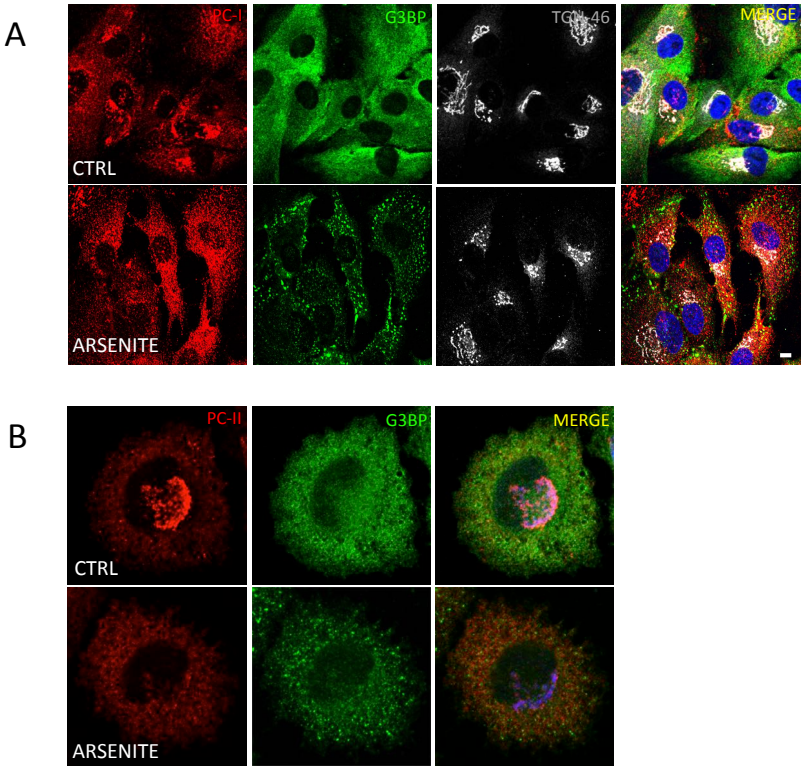

Figure 3.21 Procollagen secretion is blocked upon arsenite treatment. (A) Human fibroblasts were incubated for 3 hrs at 40°C. 30' before temperature shift cells were treted with sodium arsenite, thus samples were incubated at 32°C for 15' fixed and processed for immunofluorescence analysis. Scale bar 10 μm. **(B)** Rat chondrosarcoma chondrocytes were treated as described above and stained for PC-II and G3BP. Images show that procollagens are retained into the ER in arsenite treated cells.

As collagens need an efficient export machinery, I considered whether the defect on membrane trafficking was universal to all cargoes or if it was the consequence of a decrease in the kinetics of the machinery that affects only the transport of large cargoes. I performed a VSV-G transport assay in HeLa cells treated with arsenite or heat stress (44°C). After 15 minutes at the permissive temperature (32°C), VSV-G remained blocked in the ER revealing a general inhibition of the ER-to-Golgi pathway (Fig. 3.22).

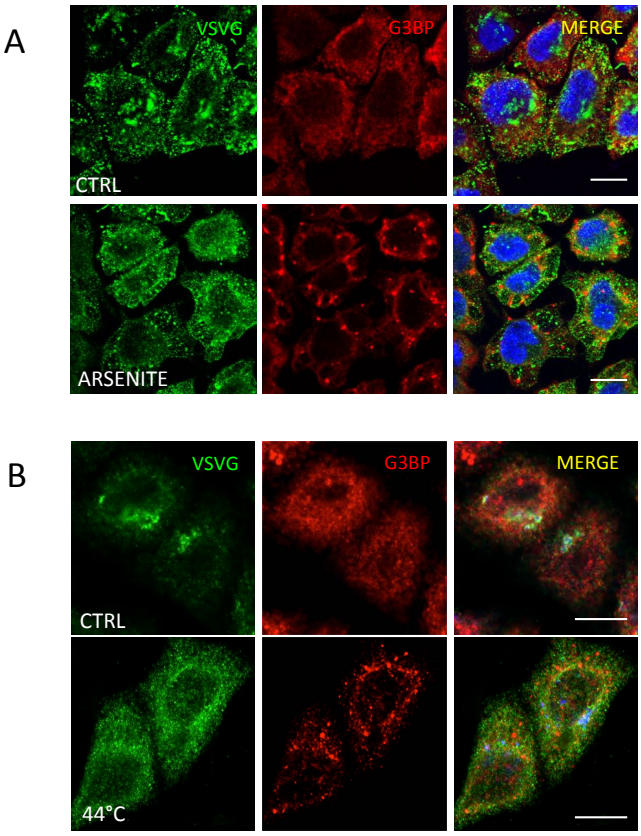

Figure 3.22 Anterograde trafficking is inhibited upon SGs induction. (A) HeLa cells were infected with VSV for 1hr at 32°C, thus incubated at 40°C for 3 hrs. 30' before temperature shift samples were either treated with sodium arsenite **(A)**, or incubated at 44°C **(B)**. Finally, cells were shifted at 32°C and fixed after 15' at permessive temperature. VSV-G is blocked into the ER in condition that trigger SGs formation. Scale bar 10 μm.

Thus, stresses that trigger stress granule formation also seem to inhibit membrane trafficking. This effect could be due to:

a) stress granules are toxic for cells resulting in global cellular dysfunction

   or

b) stress granules sequester specific components of the ER-to-Golgi trafficking machinery impairing the first step of the secretory pathway.

To investigate the first hypothesis, both PCII and VSV-G trafficking were measured in conditions of arsenite concentration titration. Cells treated with lower doses of arsenite (100 µM) form G3BP aggregates that are indistinguishable from those seen at higher concentrations of arsenite (from 300 µM to 500 µM). However, membrane trafficking protein recruitment onto SGs is strictly dependent on the concentration (fig.3.23).

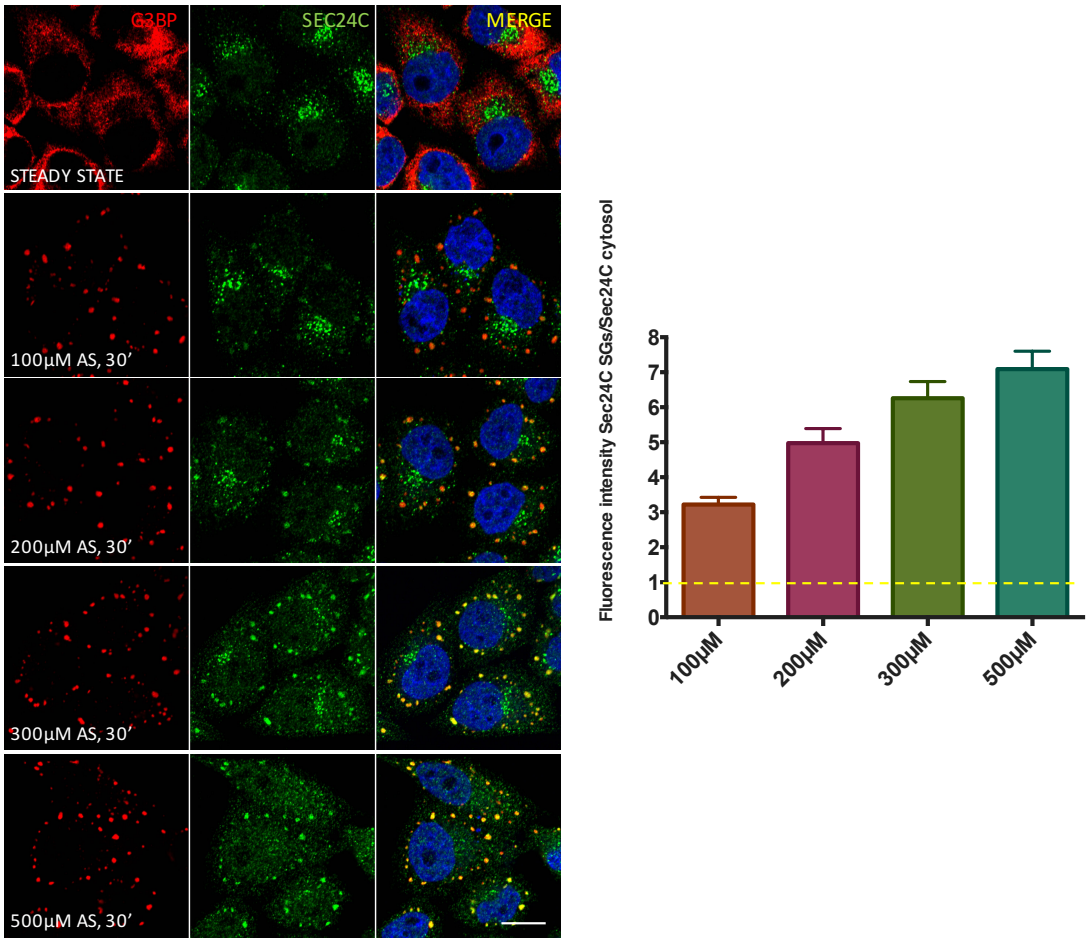

Figure 3.23 Membrane trafficking proteins recruitment onto SGs increase with arsenite concentration. HeLa cells were treated with 100, 200, 300 and 500µM sodium arsenite for 30 minutes at 37°C. G3BP antibody was used to mark SGs and sec24c to stain the ER-export machinery. Sec24c is proportional to arsenite concentration. Graph on the right panel show sec24c mean intensity on G3BP spots with respect to the cytoplasm. Images were quantified with Imagej software. Dashed red light indicates the steady state condition. Scale bar 10 µm.

I therefore, treated both HeLa and RCS cells with lower concentrations of arsenite that still allow stress granule aggregation without recruitment of membrane trafficking proteins. Under these conditions, cargoes are able to reach the Golgi (fig. 3.24).

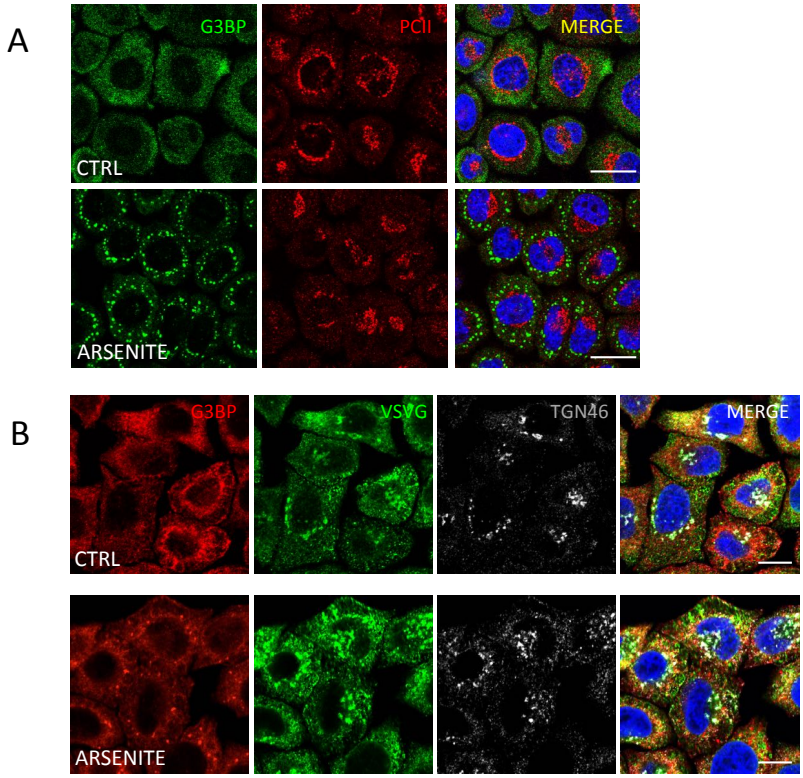

Figure 3.24 Membrane transport inhibition depends on SGs recruitment of membrane trafficking proteins. (A) RCS cells were incubated for 3 hrs at 40°C to synchronize PCII in the endoplasmic reticulum. 30' before temperature shift cells were treated with 100µM arsenite for 30' minutes and then fixed after 15' at permissive temperature. Scale bar 10 µm **(B)** HeLa cells were infected with VSV for 1hr at 32°C, thus incubated at 40°C for 3 hrs. 30' before temperature shift samples were treated with 100µM sodium arsenite. Finally, cells were shifted at 32°C and fixed after 15' at permessive temperature. Cargoes transport is not altered under these conditions. Scale bar 10 µm

To investigate the specificity of the effect, I also monitored VSV-G transport from the Golgi to the PM upon stress condition in which inhibition of ER-to-Golgi trafficking was observed. Thus, cells were infected with VSV-G, incubated for 2 hours at 20°C to allow accumulation of the cargo in the Golgi complex and then shifted to 32°C in the presence of arsenite. Under these conditions no significant differences in the arrival of VSV-G to the PM were observed (Fig 3.25) demonstrating that inhibition of membrane trafficking is due to a specific recruitment of membrane trafficking proteins on SGs that results in the inhibition of anterograde trafficking at the ER.

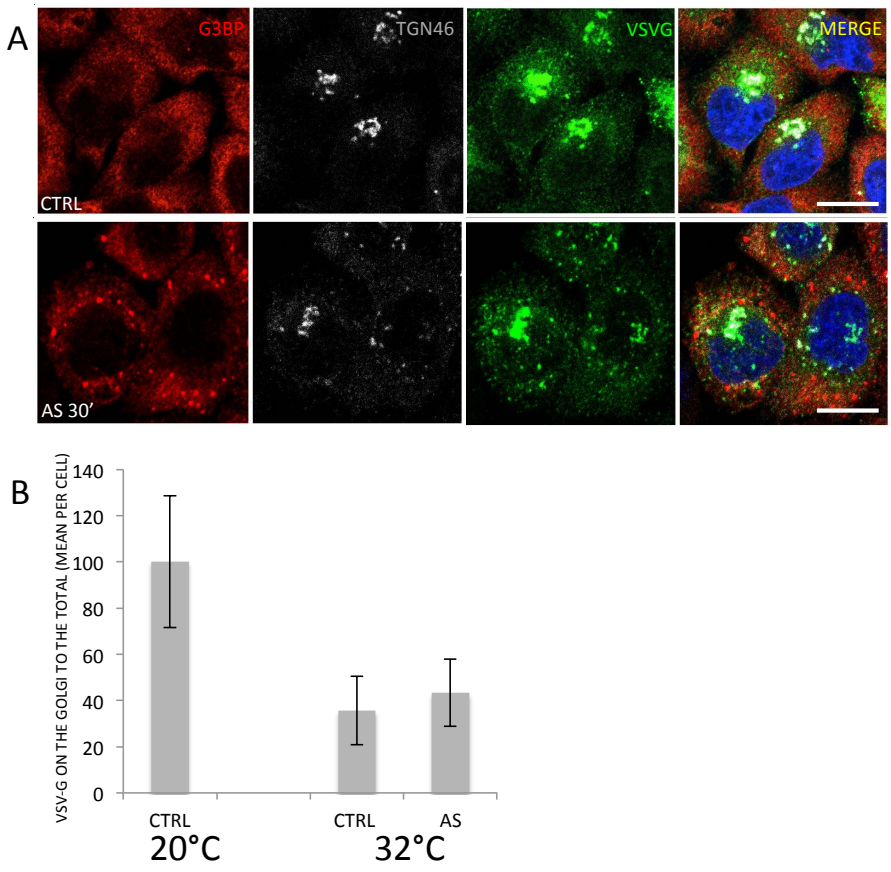

Figure 3.25 SGs specifically inhibits ER-to-Golgi trafficking. (A) HeLa cells were infected vith VSV for 1 hr at 32°C and incubated for 3hrs at 40°C. Subsequently, samples were incubated at 20°C for 2 hrs to synchronize the viral cargo in the Golgi complex. Thus, cells were shifted at 32°C and treated with sodium arsenite, 300 µM. Scale bar 10µm. **(B)** VSV-G trafficking was measured by evaluating the ratio between VSV-G in the Golgi area and the total amount of the viral protein. The data are expressed as % of cells with VSVG at the PM. Columbus was used as software to quantity images.

3.8.2 Consequences of stress granule formation on the secretory pathway

As previously discussed, COPII carriers are composed of an inner (Sec23/Sec24) and an outer cage (Sec13/Sec31) that rapidly cycle between membranes and cytosol. Formation of carriers is initiated by GTP-Sar1 that inserts into the membrane at ERES, Sec23/24 subsequently bind sar1, and, ultimately the heterodimer Sec13/31 binds at ERES membranes. Sec23/24 depletion or loss-of-function blunts the capability of Sec13/31 to bind to membranes leading to redistribution of the proteins to the cytosol. Thus, the recruitment of Sec24 onto SGs should impact on Sec13/31 localization leading to redistribution of the protein throughout the cytosol. To test this hypothesis, I therefore analysed Sec31 cellular localization under conditions in which Sec24C localizes to stress aggregates and, indeed, Sec31 becomes cytosolic under stress suggesting that COPII carriers are unable to bud from the ERES (Fig. 3.26A).

The TRAPP complex acts as a GEF for the small GTPase RAB1. RAB1 cycles from the cytosol (GDP-bound) and the Golgi (GTP-bound), which ultimately dictates the efficiency of anterograde trafficking. Alterations in RAB1 activity (KD, expression of GDP-locked or GTP-locked mutants) block cargo from exiting the ER (Tisdale EJ et al., 1992). Under conditions of SG formation, RAB1 loses its ability to bind to the Golgi (Fig. 3.26B) and redistributes to the cytosol, further suggesting that the GEF activity of the TRAPP complex is impaired and this could negatively affect ER-to-Golgi trafficking.

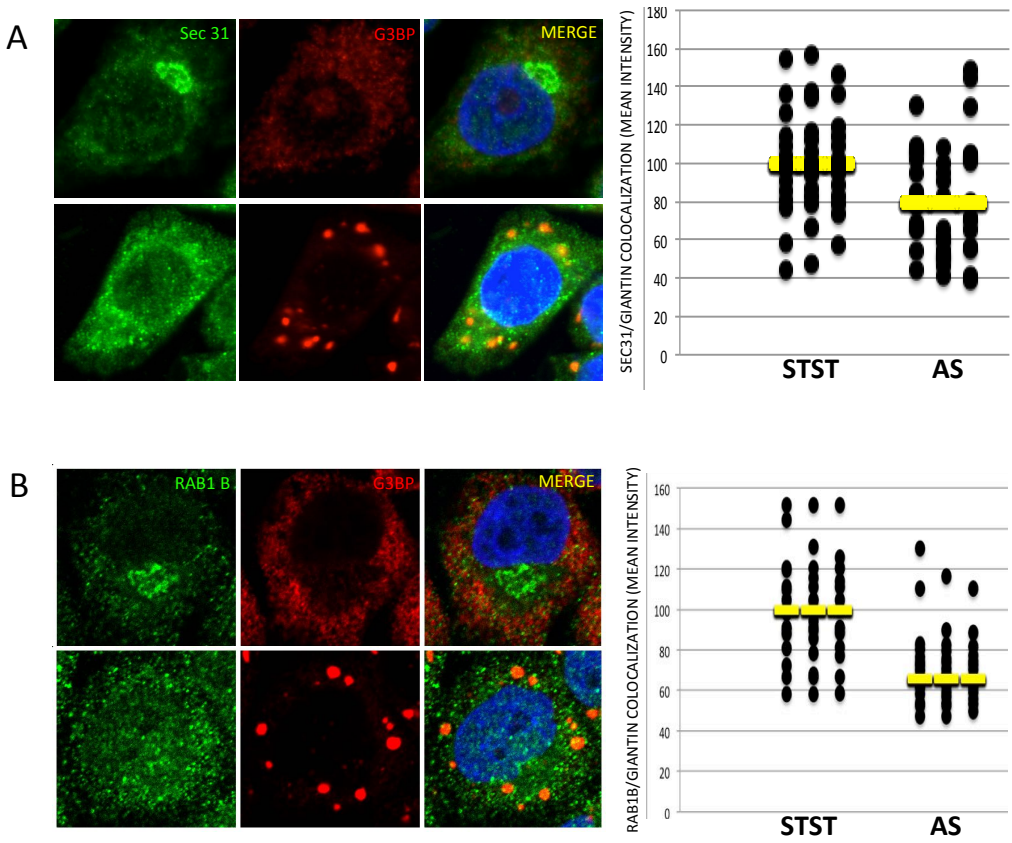

Figure 3.26 COPII outer coat and the TRAPP complex effector rab1 disperse into the cytoplasm upon SGs induction. HeLa cells were treated with sodium arsenite (300 µM, 30' at 37°C), fixed and stained for sec31 **(A)** and rab1B **(B)**, respectively. Graphs on the right panel express % of the proteins (sec31 and rab1 respectively) that co-localize with a Golgi marker (Giantin) with respect to the total proteins amount. Images were taken with confocal microscope Zeiss LSM-700 and quantified with ImageJ software.

Furthermore, Rab1 inactivation promotes Golgi fragmentation (Wilson BS et al., 1994). Thus, to assess whether stress granules lead to Rab1 inactivation, I monitored Golgi structure under arsenite treatment. Stress granule formation fragments the Golgi and Golgi morphology is rescued by over-expression of RAB1 (3.27) demonstrating that under acute stress response stress granules inactivate rab1 by recruiting its GEF TRAPP leading to fragmentation of the Golgi complex.

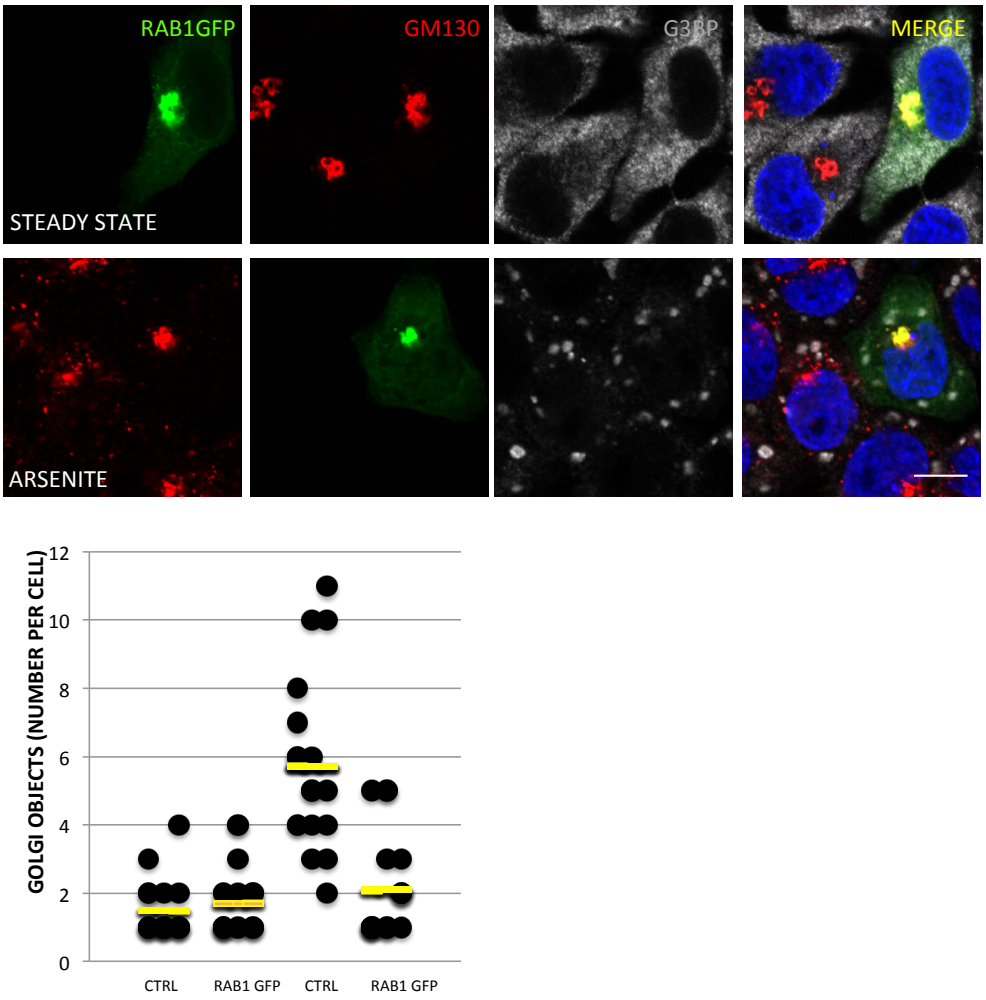

Figure 3.27 Stress granules fragments the Golgi complex by inactivating Rab1 (A) HeLa cells were transfected with rab1B for 16 hrs, thus treated with sodium arsenite (300 µM, 60' at 37°C), fixed and stained for GM130. Scale bar 10 µM. **(B)** Images were quantified counting Golgi particles per cells by imagej software (n=30).

3.8.3 Role of TRAPP in the biogenesis and function of stress granules

Migration of trafficking proteins onto SGs could result from a passive recruitment or an active process that requires the TRAPP complex. To address this point, I analyzed stress granule formation in HeLa cells depleted for the TRAPP complex. I silenced the whole TRAPP complex by depleting Bet3 (Bet3 KD destabilizes the TRAPP complex (Venditti et al., 2012)) or just sedlin and then treated cells with arsenite. TRAPP depletion but also sedlin KD showed a delay in SG aggregation and once formed SGs appear significantly smaller suggesting that TRAPP has a structural role on SGs (Fig. 3.28).

In order to assess if the defect in SG size was a direct effect due to the lack of TRAPP, I microinjected a blocking antibody against Bet3 in live cells. An acute block of Bet3 leads to an inhibition in ER-to-Golgi trafficking and Golgi fragmentation (Loh et al., 2005). Cells were imaged after 30' of arsenite treatment and stained for both Golgi and SGs using specific markers. A significant reduction in SG size compared to cells microinjected with pre-immune IgG were observed demonstrating that TRAPP function is required for SG docking and maturation (fig. 3.28).

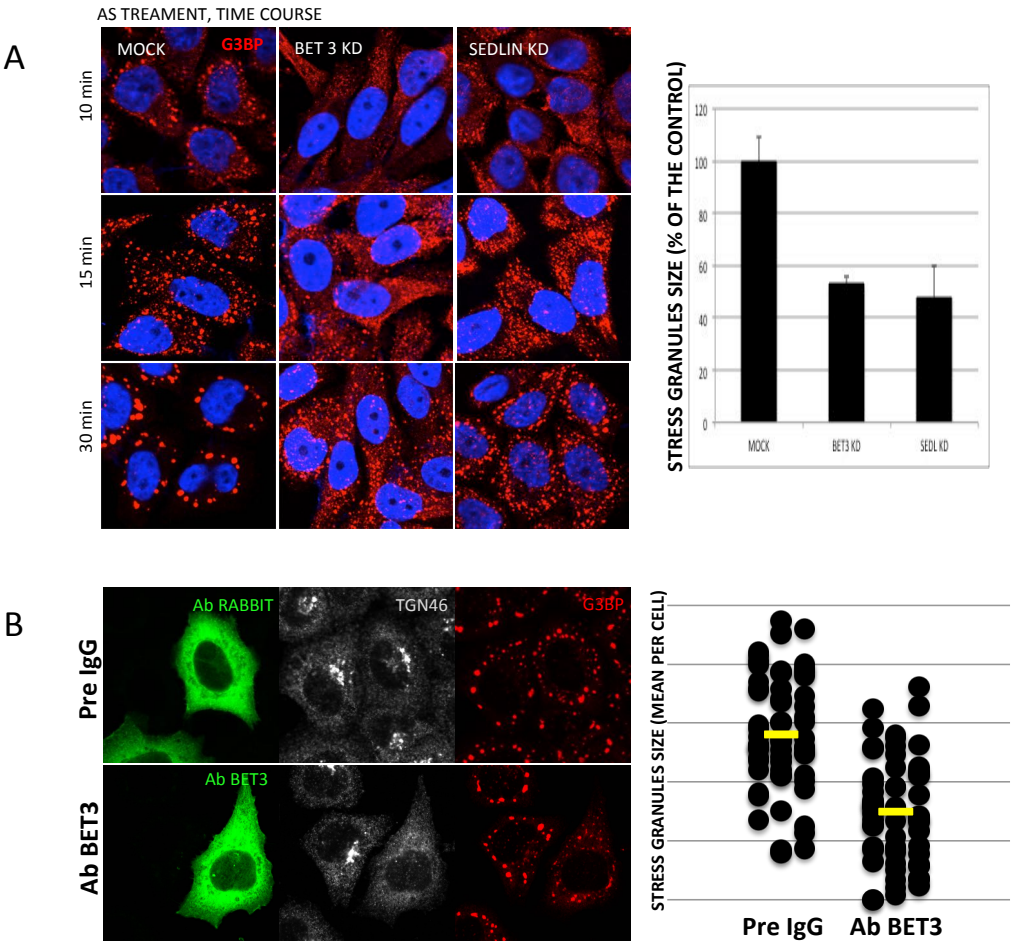

Figure 3.28 TRAPP depletion led to a defect in SGs formation. **(A)** HeLa cells were treated with small interfering RNA (siRNA) against Bet3 and Sedlin. Stress was induced by AS treatment (300µM, 30'). The graph on the right express SGs size quantified with Columbus software. **(B)** HeLa cells were microinjected with pre-immunized IgG and specific antibody against bet3. Quantification of one of three independent experiment on the right side of the panel show SGs numbers per cells in control (pre-IgG) and treated samples. Images show that TRAPP depletion/inactivation affects SGs size.

Stress granules are a defence mechanism used from stressed cells to shut down translation, a process that guarantees cell survival (Arimoto et al., 2008; Thedieck et al., 2013). I first wondered whether defects in SG size induced by arsenite were due to an alteration of the signalling triggered by sodium arsenite. Sodium arsenite activates the kinase HRI that in turn phosphorylates and thus inactivates eIF2alpha

(McEwen et al., 2005). To this aim, I checked phosphorylation of eIF2alpha in both control (mock) and sedlin KD cells treated with arsenite for different times. Western blot analysis revealed no differences in the rate of eIF2alpha inactivation compared to control cells. Furthermore, defects in SG size were also observed after heat shock, a stimulus independent of eIF2alpha inactivation but related to the inhibition of eIF4E, a component of the pre-initiation complex (Emara et al., 2012) (Fig 3.29).

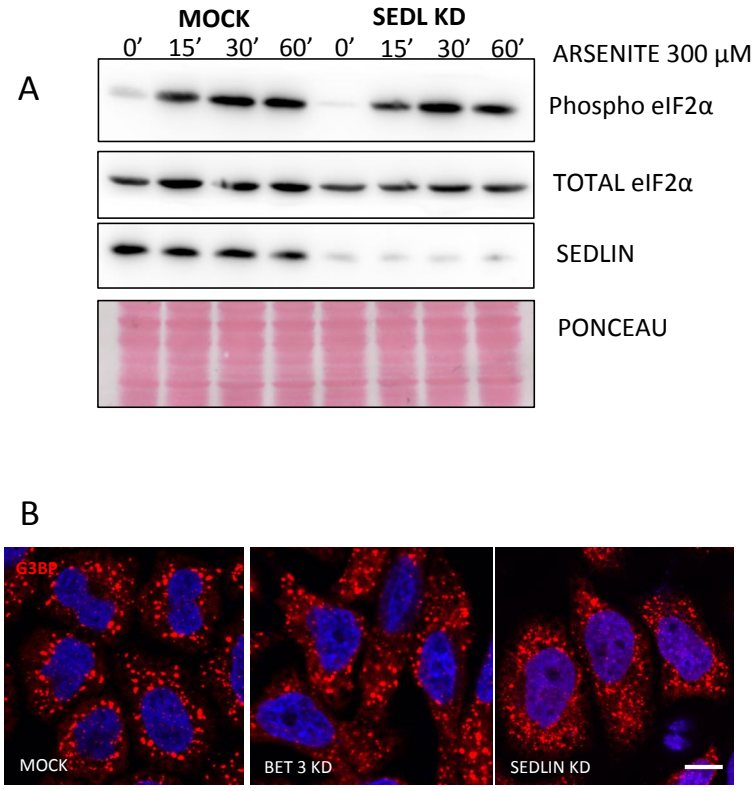

Figure 3.29 SGs defects are independent from stress stimuli. **(A)** HeLa cells were treated with small interfering RNA (siRNA) against Sedlin. Stress was induced by AS treatment for indicated times. Samples were lysed and processed for western blot analysis. Immunoblot with sedlin antibody was used to evaluate the efficiency of the KD. Phosphorylation of eIF2α monitored with a specific antibody showed no significant differences in CTRL (mock) and sedlin KD cells. Ponceau was used as loading control. **(B)** Ctrl (mock) bet3 and sedlin KD cells were incubated at 44°C for 30’ fixed and stained with G3BP as SGs marker. Images showed reduction in SGs size in TRAPP depleted cells.

To assess whether inhibition of protein synthesis occurs in TRAPP-depleted cells as in control cells under stress conditions, I performed a puromycin assay, a quantification method to monitor translating ribosome (David et al., 2012). Control (mock), Bet3 and sedlin KD cells where treated with arsenite and assayed for PMY incorporation (see methods). Western blot analysis showed that knock down cells were comparable to control samples in blocking translation upon stress (Fig. 3.30).

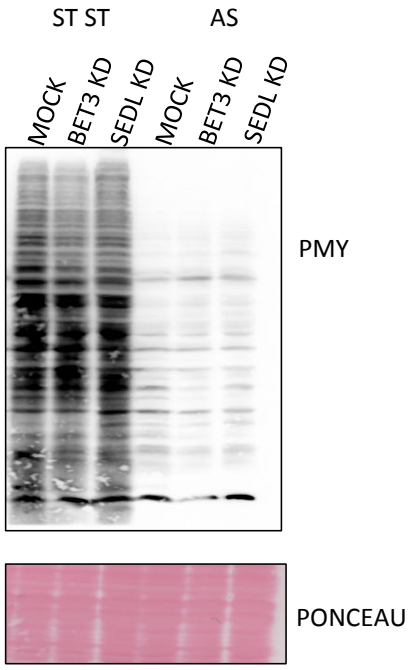

Figure 3.30 TRAPP depletion does not alters inhibition of translation induced by SGs. HeLa cells were treated with small interfering RNA (siRNA) against both Bet3 and Sedlin. Cells were treated with sodium arsenite (300μM, 30') and samples were incubated with DMEM supplemented with 91μM PMY for 5' min at 37°C. Cells lysates were then lysates and samples separated by SDS-page. Immuno-blot with PMY revealed the significant reduction of translating ribosome in AS treated cells independently from depletion of the TRAPP complex.

The granules start aggregating on disassembled ribosomes, then they dock with each other, becoming bigger and acquiring the “shell” (Wheeler et al., 2016). The shell is very heterogeneous in composition and so far a variety of proteins have been identified (Jain et al., 2016). Of these the kinase RACK1 has been described to be sequestered onto SGs and to block apoptotic signalling upstream MAPKs (Kim et al., 2012). Thus, I checked migration of RACK1 onto SGs in Bet3 and sedlin KD cells as a read out for defects in shell composition and found a severe reduction in RACK1 recruitment in TRAPP-depleted and sedlin-depleted cells compared to control suggesting that TRAPP migration onto aggregates is essential for correct signalling from SGs (Fig. 3.31). Taken together these results suggest that the recruitment of the TRAPP complex onto SGs is a tuned process with two main roles: one that acts on ER Exit Sites with consequences on membrane trafficking and another that affects SG secondary functions and leads to a mis-regulation of anti-apoptotic pathways.

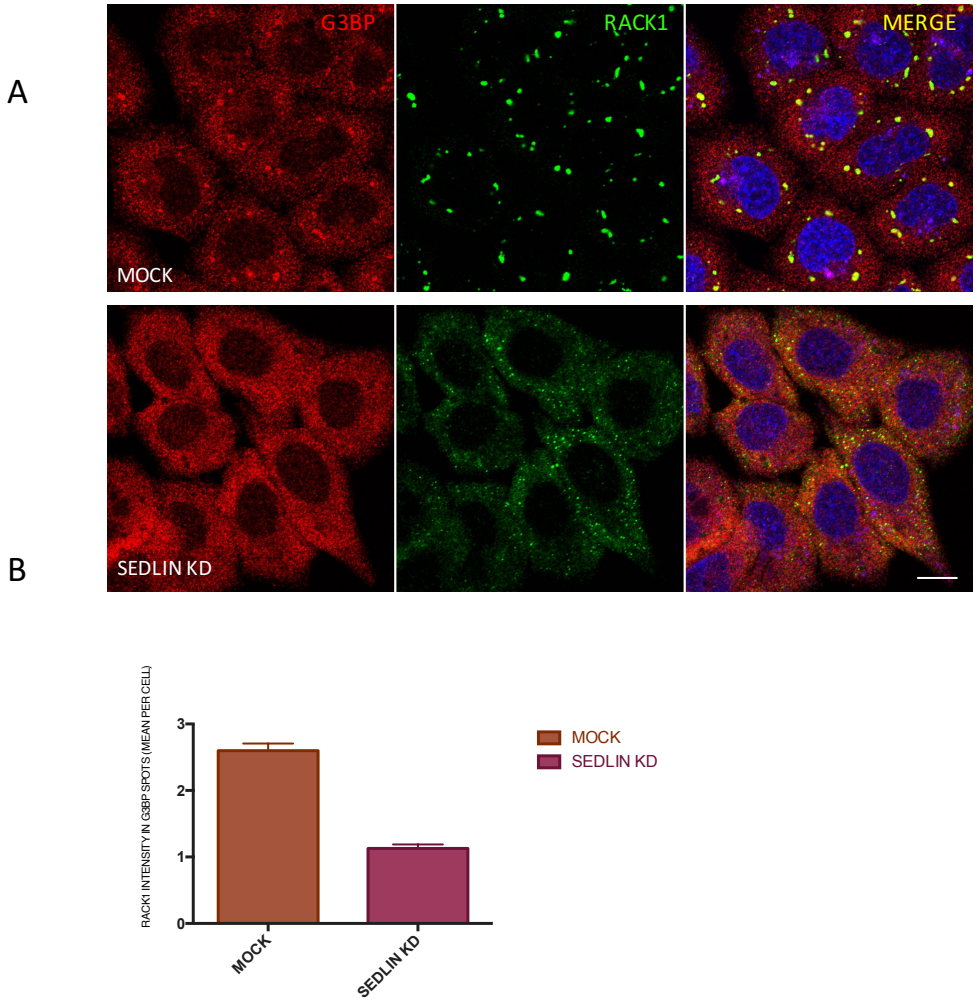

Figure 3.31 TRAPP depletion does affect SGs signaling. **(A)** HeLa cells were treated with small interfering RNA (siRNA) against Sedlin. Cells were treated with sodium arsenite (300 µM, 30') and samples were fixed and stained with RACK1. RACK1 migration onto SGs is severely reduced in sedlin KD cells. **(B)** Graph indicates RACK1 fluorescence intensty onto SGs on total fluorescence per cell. Images were taken at Zeiss LSM-710 and quantified with Columbus software.

3.9 Medaka as an animal model to study SEDT

To study the effect of sedlin depletion in a whole organism and to try to gain insights into the pathogenesis of SEDT I choose Medaka fish (*Oryzias latipes*), a particularly amenable model system to carry out gene functional studies.

3.9.1 Sedlin expression during medaka development

Firstly, in silico analysis to search for a sedlin gene in medaka were performed by Rossella Venditti in Antonella De Matteis's lab (Fig. 3.32, panel A). Sedlin is highly conserved in the medaka genome and importantly it is present as a single gene. This is noteworthy since sedlin possesses a very complex genomic organization in mammals, with the presence of several additional pseudogenes (Gecz et al., 2003).

I then monitored by qPCR sedlin, Bet3 and PCII expression during embryonic development and observed that there is significant co-expression of the 3 genes (Fig. 3.28). The maximum peak of expression was observed at stage 35 when the mineralization process starts (Hynohaya et al., 2007), further corroborating that TRAPP, through sedlin, is required for collagen function. Next, I analyzed sedlin expression in whole mounts using in situ hybridization. Although the signal was very weak, a specific staining in the centrum on vertebrae was detected indicating sedlin is preferentially, but not exclusively, expressed in vertebrae (Fig. 3.32, panel B, C).

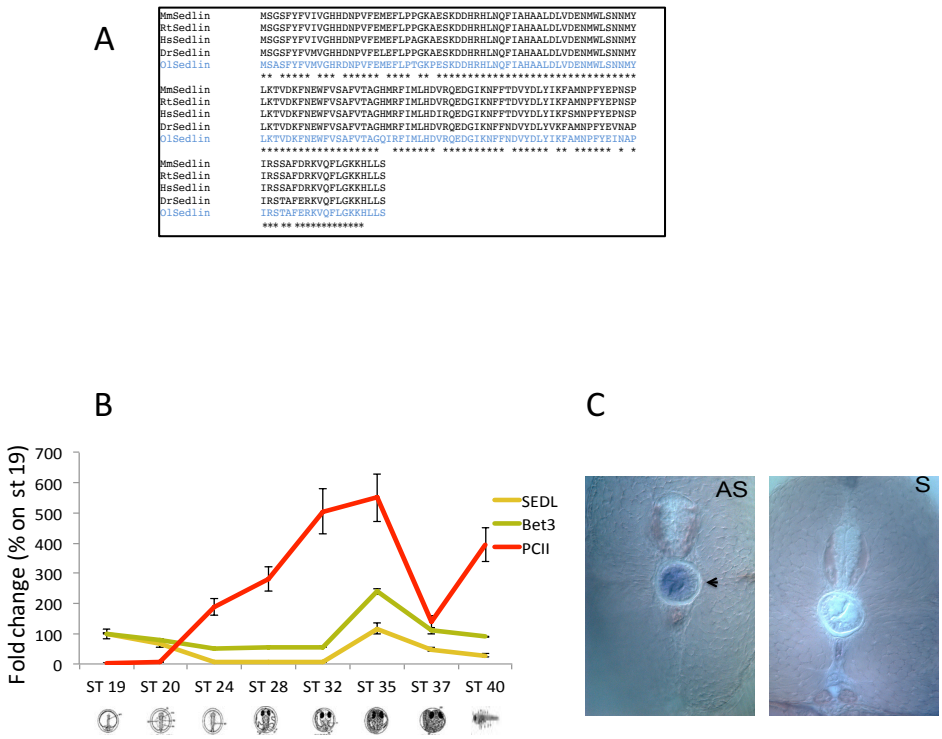

Figure 3.32 Medaka is a suitable model to study SEDT. **(A)** Blast analysis comparing TRAPPC2 gene during evolution **(B)** Sedl, Bet3 and PC-II expression during development. **(C)** RNA *in situ* hybridization of frontal section of WT larvae at stage 40. Sedlin is preferentially expressed in the *centrum* of body vertebrae.

3.10 Generation of a medaka SEDT model

I adopted different approaches to deplete sedlin in medaka:

- transient knock down by morpholino (MO) injection
- genetic ablation by TALEN technology

Morpholino injection is a very fast and cheap method able to generate a transient KD in a whole organism. Some MOs work extremely well and there are many MO phenotypes that efficiently mimic mutant phenotypes without any noticeable side

effects. However, MOs can lead to artefacts and for many MOs the phenotypes caused by specific binding to the intended target RNA are difficult to separate from those caused by the non-specific binding to unintended targets. Furthermore, the phenotype can be very heterogeneous due to the manual injection of a morpholino solution and the molecule starts to be ineffective 72-96 hours post-injection since MOs undergo dilution effects due to embryo development. This process is particularly relevant for the study of late onset phenotypes such as skeletal development that starts five days post-fertilization.

In recent years the morpholino technique has been overtaken by genome editing using CRISPr or TALEN technology. TALENs and CRISPr are very powerful tools to generate stable KO lines. However, analysis of the phenotype is not as immediate as when morpholino injection since these nuclease-injected embryos are most likely to be mosaic for the resulting genomic lesions and genetic screening to obtain pure KO lines can take time. In addition, the designed TALEN/CRISPr may be not effective or cleave off-target loci that mostly occur using CRISPr (Chhabra, 2014).

For the above reasons, I decided to use both morpholino and TALEN strategy to perform my studies.

3.10.1 Morpholino-mediated KO of sedlin

The MO antisense technology is based on nucleic acid bases that are linked to morpholine rings and a non-charged phosphorodiamidate backbone. The rationale for this design was that MOs would not bind electrostatically to proteins, hence causing less toxicity, while at the same time being resistant to nucleases. MOs are injected into early or medaka embryos using standard techniques. Commonly, they

are ~25-mers designed to be an exact antisense match against the region surrounding the first translated ATG (to block translation) or against a splice donor or acceptor site (to interfere with precursor mRNA splicing). To evaluate the effect of sedlin KD in medaka, a specific morpholino against medaka sedlin were designed as described in methods.

The morpholino were injected into a one-cell stage embryo and the phenotype was analysed after hatching. Injected larvae appeared smaller and showed a severe defect in skeletal development. Furthermore, vertebrae appeared flatter and smaller compared to control injected larvae recapitulating the platyspondily documented in SEDT patients and thus suggesting that medaka is a suitable model to study SEDT *in vivo* (Fig. 3.33).

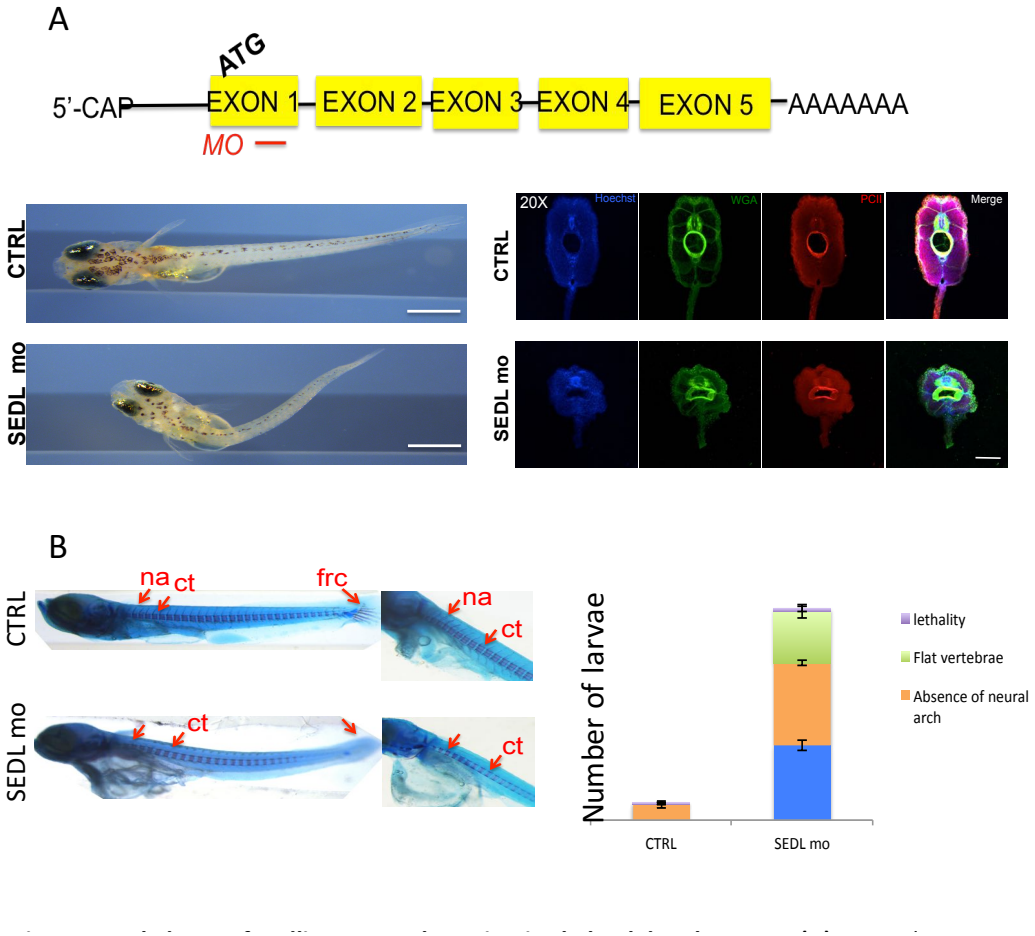

Figure 3.33 Knock down of sedlin causes alteration in skeletal development. (A) Control-mo and a specific morpholino against sedl ATG was injected in one cell stage embryos. (Left) Sedlin-mo larvae present macroscopic defects of the skeleton. Scale bar 0.5 mm. (right) Immunofluorescence analysis of frontal vertebra section show a significant alteration in vertebrae size and morphology. Scale bar 100 µm. (B) Alizarin red staining marking mineralized tissue revealed reduction in vertebrae (ct) number, platyspondyly, absence of caudal fin (frc) and neural arch (na). Quantification of phenotypes observed is shown in the right panel.

3.10.2 TALEN-mediated KO of sedlin

Transcription activator-like effector nucleases (TALENs) are a powerful tool widely used in biological research to edit genome. These chimeric nucleases are composed of programmable, sequence-specific DNA-binding modules linked to a

nonspecific DNA cleavage domain. TALENs enable a broad range of genetic modifications by inducing DNA double-strand breaks that stimulate error-prone non-homologous end joining or homology-directed repair at specific genomic locations. TALEN are composed of a series of 33–35-amino-acid repeat domains that each recognizes a single base pair. TALEN specificity is determined by two hypervariable amino acids that are known as the repeat-variable di-residues (RVDs). Each TALEN is fused to an endonuclease, Fok1, that works in a dimeric fashion, and thus a pair of TALENs is needed to make a cut at a particular site of the genome. The pair of designed TALENs binds to their target DNA sequences flanking a spacer DNA (usually 14-18 bp), which facilitates the Fok I heterodimerization.

mRNAs encoding left and right TALEN were synthetized and injected at about the one-cell stage and a G0 mosaic population was obtained (Fig. 3.34). To evaluate the presence of TALEN-induced mutations, I analysed the target region in medaka larvae deriving from injected embryos.

TALEN-induced mutations were found in 4/24 (~16.7%) larvae from sedlin TALEN-injected embryos. As expected, I observed multiple mutations in a mosaic fashion in the spacer sequence (Fig. 3.30).

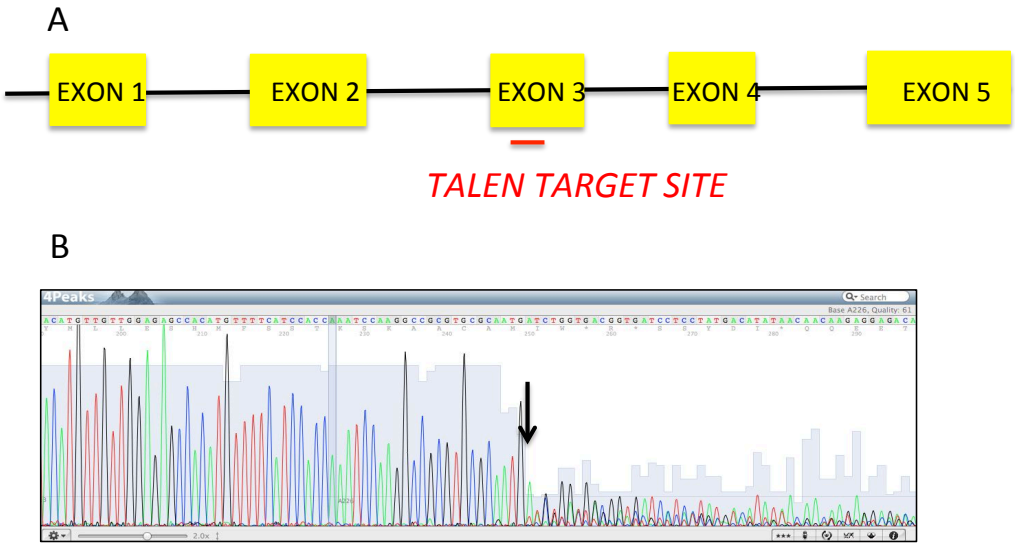

Figure 3.34 TALEN induced mutation in sedlin gene. **(A)** Schematic representation on TALEN target site on exon 3. (**B**) Starting from nucleotide position 101 of *Sedlin* gene, the presence of multiple peaks underneath the predominant wt sequence (black arrow) suggests TALEN-induced mosaicism.

Germline transmission was not detected in 1/4 of the G0 fish derived from TALEN-injected embryos. For fish showing germline transmission, the percentage of the offspring carrying mutations in the sedlin gene ranged from 5% to 40%.

The analysis of sedlin target sequences from G1 heterozygous fish revealed 4 different TALEN-induced mutations. There was only one in-frame mutation, whereas the others were frameshift insertions or deletions (Fig. 3.35). Fish heterozygous for each mutation were mated to obtain 4 different sedlin KO lines.

A

MEDAKA SEDLIN MUTATIONS
r.111_118 del GAACCAGT
r.166 del A
r.111_119 del GAACCAGTT
r.117_121 dup CCAG
r.113_116 del ACCA

B

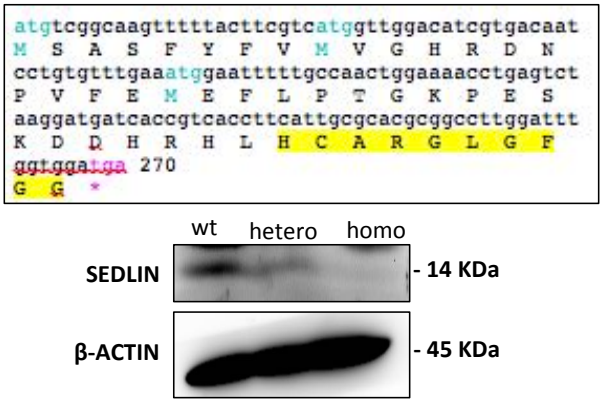

Figure 3.35 Generation of Sedl-/- line (A) (indels) detected in larvae by targeting the exon 4 of the *sedlin* medaka gene. **(B) (upper)** Sedlin r.111_118 del GAACCAGT protein product. Starting from amino acid 38 in the Sedlin r.111_118 del mutant ten base pairs substitutions (in yellow) precede a stop codon (magenta). **(Lower)** WT, hetero and homozigous Sedlin r.111_118 del were lysated and processed for Western blot analysis. Sedlin r.111_118 are functional KO and hereafter called *sedl-/-.*

3.10.2.1 Characterization of sedlin KO

I focused my attention on the sedl$^{del101\text{-}109/\ del101\text{-}109}$ line, a nonsense deletion that results in the absence of the sedlin gene product (fig. 3.35B) . Homozygous sedlin-/- embryos were monitored over the time and no macroscopic abnormalities such as defects in somatogenesis were observed during embryogeneis. However, larvae had a delayed mean hatching time suggesting severe reduction of prenatal motility. Furthermore, KO larvae showed dramatically reduced movement and they died in the first hours after hatching. Sedl-/- larvae showed abnormalities in cranio-facial

development, a region rich in chondrocytes, while alizarin red staining revealed a dramatic alteration in osteogenesis (Fig. 3.36)

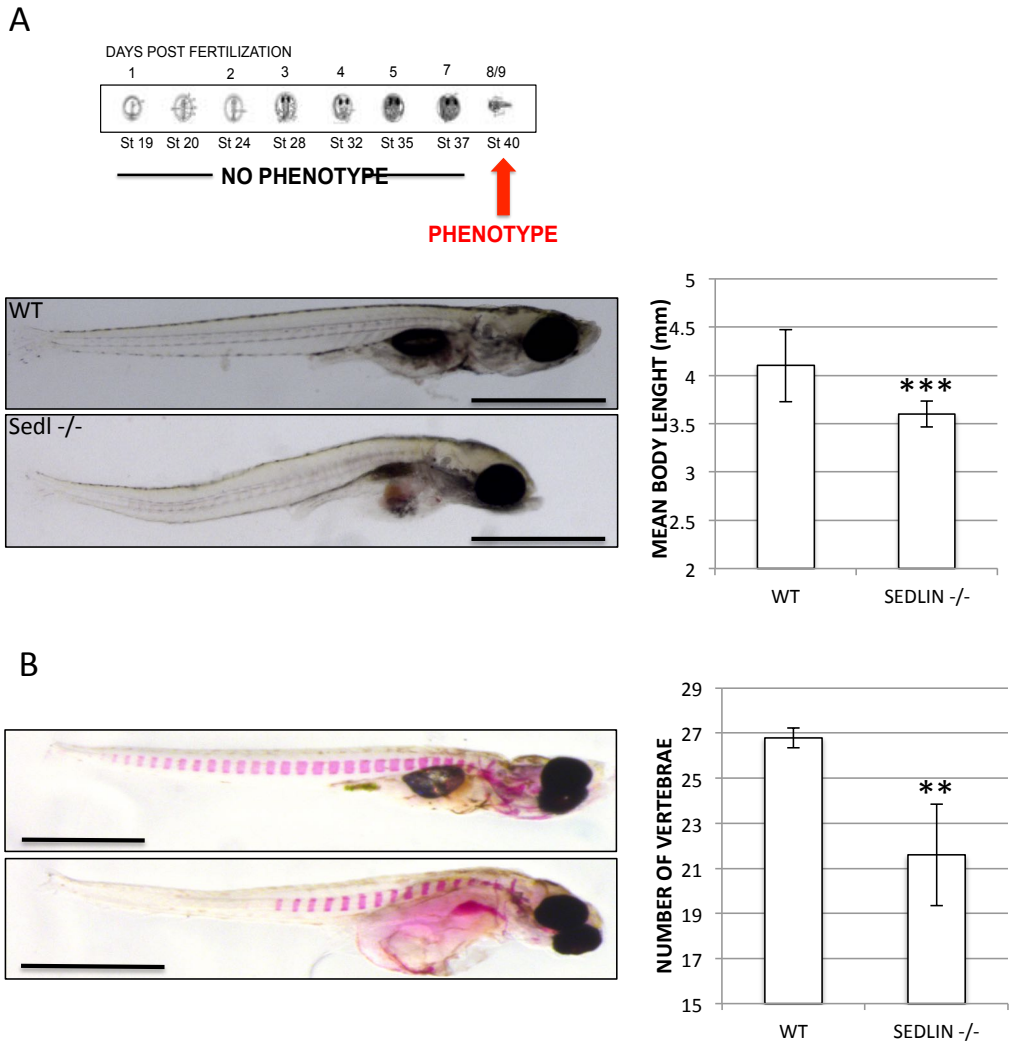

Figure 3.36 Analysis of Sedl-/- skeletal phenotype. (A) WT and KO larvae were monitored day by day during development. No macroscopic differences are appreciable in the first days of development. WT and sedl-/- larvae at stage 40. Sedl-/- are shorter and present facial abnormalities. Scale bar 1mm. Quantification in right part of the panel. ***p<0.002. **(B) (left)** Alizarin red staining of WT and sedl -/- larvae show defect in vertebrae mineralization and morphology. **(Right)** Quantification of number of vertebrae in KO larvae compared to the WT. Scale bar WT 1mm; KO 1.3 mm. **p<0.005.

3.10.2.2 *Gene expression profiling of sedlin-/- homozygous larvae*

I performed a gene expression profile on whole larvae using NGS technology. Three different pools for a total of 31 WT and 31 KO were analysed. Eggs were collected from *sedlin+/-* in-breeding. Embryos were sacrificed eight days post fertilization, a time at which ~50% of the eggs had hatched. Genomic DNA was extracted from the organic phase and then samples selected and pooled (fig.3.37).

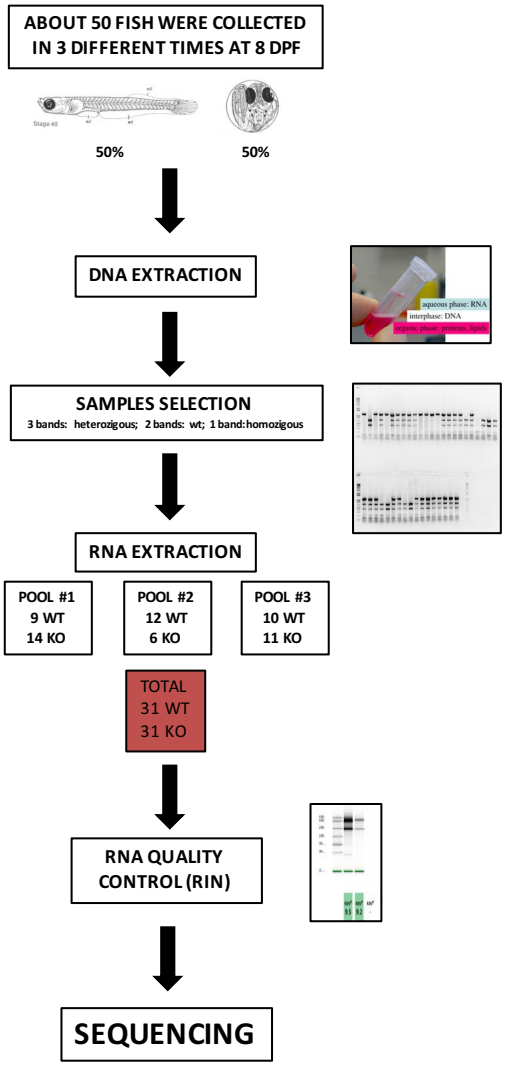

Figure 3.37 Next generation sequencing of sedl-/- larvae. Experimental pipeline. In brief: Embryos were collected 8 d.p.f., lysed in quiazol and extracted with chloroform. Genomic DNA was purified from the interphase. After genotyping larvae WT and KO were pulled, respectevely and samples were processed for RNA extraction. 3 different pools were analysed by NGS.

Transcriptomic data were analysed by the bioinformatics core at TIGEM in collaboration with Mario Failli (a Ph.D. student in De Matteis' lab). The gene expression profile analysis revealed two important aspects:

- sedlin-/- larvae show a significant reduction in the expression of genes encoding extracellular matrix proteins
- Sedlin acts upstream of a cluster of genes involved in eye development (Fig. 3.38)

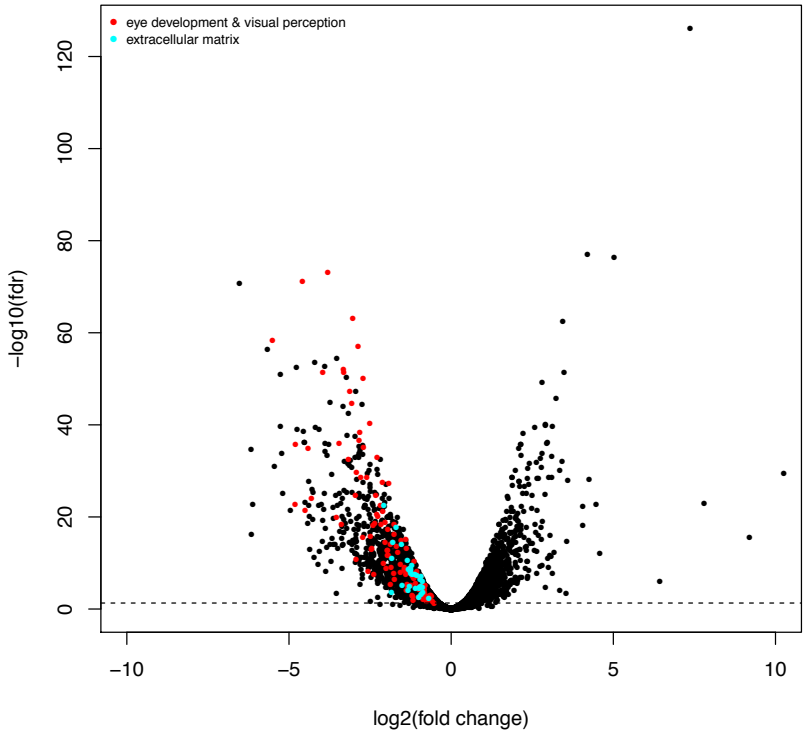

Figure 3.38 Sedlin -/- gene expression profile. Volcano plot of sedl-/- gene expression data. Horizontal black line: -log10 of FDR (False Discovery Rate, significance threshold 0.05). 1410 genes up-regulated above and 1747 genes down-regulated above. Red dots indicate 128 down-regulated genes belong to eye development and visual perception pathways; blue light dots indicate 33 genes involved in extracellular matrix deposition.

First, I confirmed by immunofluorescence and by Western blot that there was a reduction in the levels of the PCII protein (Fig. 3.38A). I checked whether the reduction in the expression of ECM genes was a direct mechanism or if it was an epistatic effect due to skeletal defects. To this end the expression of ECM genes was monitored during medaka development. qPCR analysis revealed an increase in the expression of procollagens in the early stages of development that drops at stage 40, as highlighted by the sequencing data. These lines of evidence suggest that sedlin does not directly regulate expression of extracellular matrix genes (Fig. 3.39).

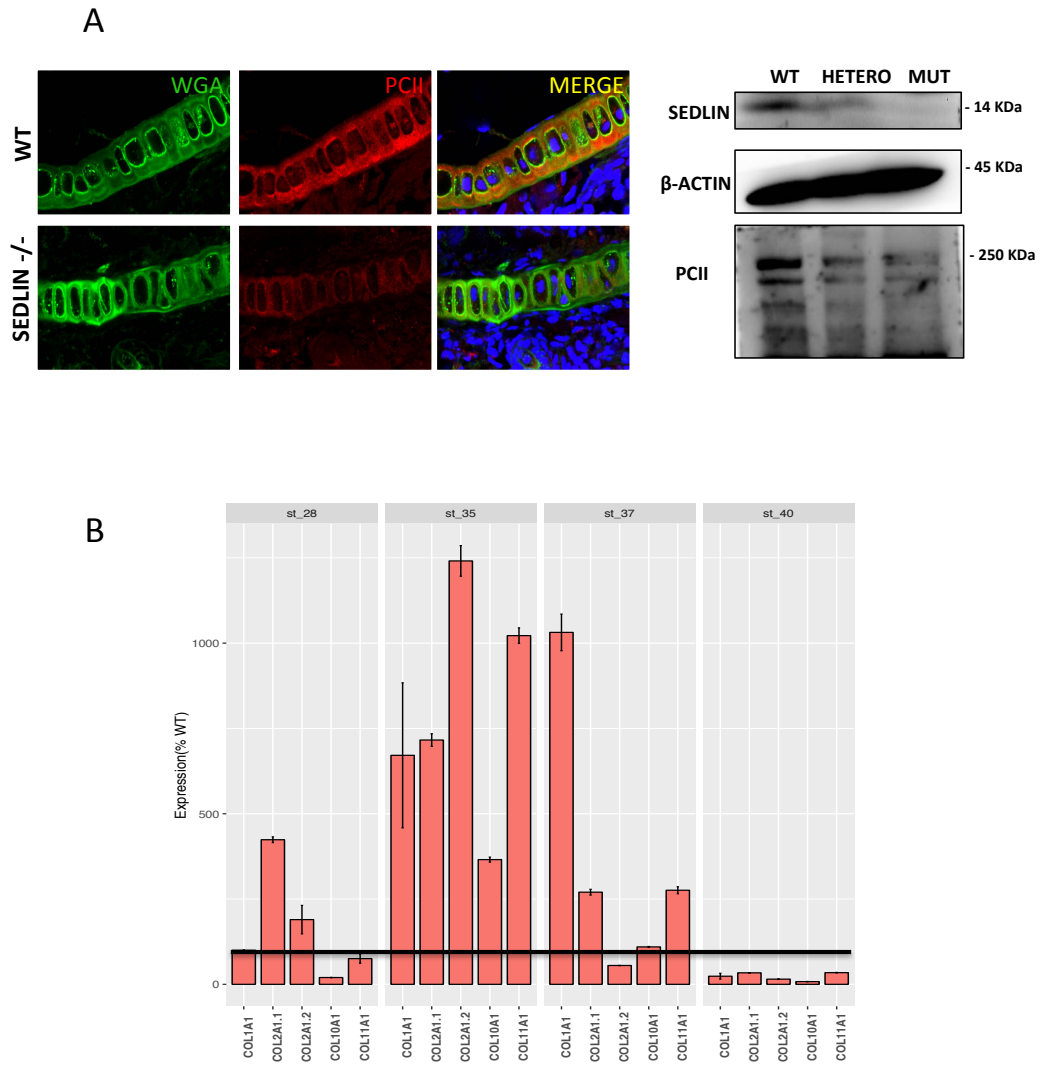

Figure 3.39 Procollagens are down-regulated in sedl -/- larvae. (A) (left) Meckel's cartilage was stained with WGA and α-PCII. PCII fluorescence intensity was significantly lower compared to the WT. **(Right)** WT, sedl+/- and sedl-/- were lysed and processed for western blot analysis. PCII was down-regulated in KO larvae. **(B)** Procollagens expression during development. % of the WT.

3.11 Sedlin in eye development

The analysis of the data from the gene expression profiling of sedlin KO larvae suggested that sedlin might act upstream of genes involved in eye development. To

explore the eye phenotype in sedlin-/- homozygous larvae I started to collaborate with Ivan Conte at TIGEM. The immunofluorescence analysis performed on eye sections stained for rods and cones showed a severe alteration of sedlin-/- photoreceptors (Fig. 3.40). Rhodopsin, the most highly expressed protein in photoreceptors, is a prototypic G-coupled receptor exclusively expressed in rods that enters the secretory pathway and localized on photoreceptor disks. Mutations in rhodopsin cause autosomal dominant retinitis pigmentosa. A subset of rhodopsin mutations accounts for protein mis-trafficking through the secretory pathway. Thus I wondered whether retinal degeneration observed in sedlin-/- larvae could be ascribed to a defect in rhodopsin trafficking. To evaluate trafficking *in vitro,* I transiently overexpressed WT-Rhodopsin in both mock and sedlin-KD HeLa cells in the presence of cycloheximide to synchronize protein transport out of the endoplasmic reticulum. Rhodopsin localization was analysed 2 hours after the removal of cycloheximide. In control (mock) cells rhodopsin is able to reach the plasma membrane while rhodopsin accumulates in the Golgi complex in sedlin-KD cells (Fig. 3.40) suggesting that sedlin can affect rhodopsin trafficking to the plasma membrane and thus lead to photoreceptor degeneration *in vivo.*

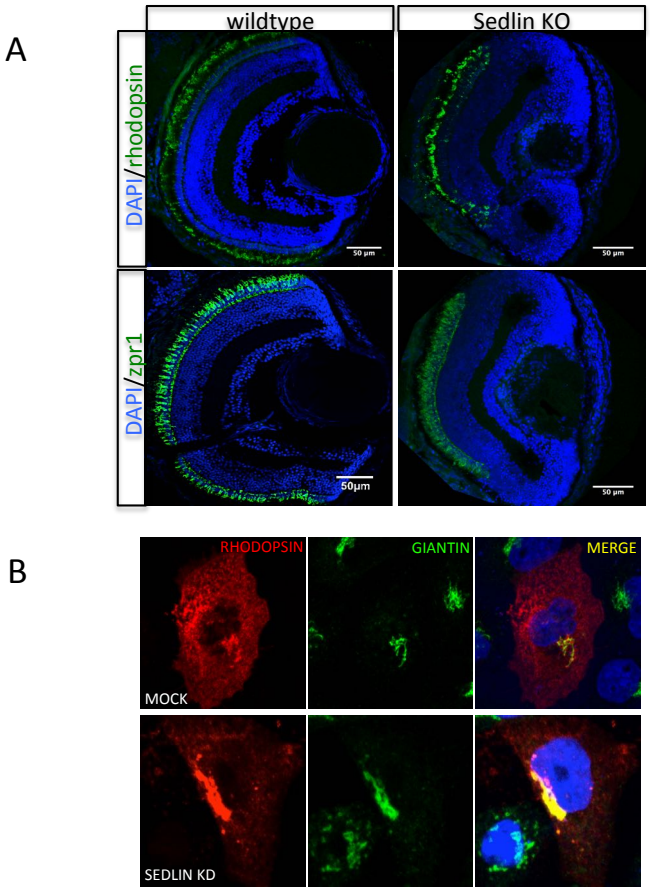

Figure 3.40 Knock out of sedl -/- results in an alteration of photoreceptors. (A) Immunofluorescence analysis of frontal eye sections stained for Rhodopsin (rods) and zpr1 (cones) revealed photoreceptors degeneration of in sedl-/- animals. Scale bar 50µm. **(B)** HeLa ctrl (mock) and sedlin KD were transiently transfected with Rhodopsin-WT for 16 hrs in presence of cycloeximide (CXM) to synchronize rhodopsin expression. CXM was washed out and cells fixed after 2hrs. In mock cells rhodopsin reach the PM while in sedlin KO the cargo is blocked in the Golgi complex.

Chapter 4

Discussion

4.1 CLIC1 dictates export from the ER

CLIC's were first identified as a family of chloride intracellular channels but a series of emerging functions for these proteins has been described recently (see introduction). Using RNAi and a CLIC1 specific inhibitor, this thesis work provides evidence that CLIC1 is specifically required for ER-to-Golgi anterograde trafficking and for Golgi structure maintenance. Moreover, starting from protein-protein interaction studies, I found that CLIC1 is intimately connected to mRNA metabolism processes suggesting the existence of a strong cross-talk between translational and post-translational events. Previous immunofluorescence-based studies revealed multiple localizations of CLIC1 (plasma membrane, endoplasmic reticulum, cytosol, nucleus and nuclear envelope). However, I found that CLIC1 is mainly nuclear and cytosolic at steady state in HeLa cells while it localizes to cytosolic aggregates under stress conditions indicating that the ER-to-Golgi transport pathway is implicated (or controlled?) in the stress response.

However, further studies are needed to elucidate whether the channel activity of CLIC1 is required for ER export or whether CLIC1 can function as an adaptor and directly impact the COPII machinery.

4.2 Sedlin is a player of the integrated stress response

Cells rapidly counteract perturbations under stress conditions by activating numerous pro-survival mechanisms. To save energy and decrease metabolism, cells shut down translation by sequestering mRNAs and ribonucleoproteins into stress granules. mRNA recruitment is selective since mRNAs that contain internal

ribosome entry sites (IRESs), which recruit translation factors and the ribosome in a cap-independent manner, are often preferentially translated during stress (Spriggs et al., 2008).

Interestingly, ER-associated mRNAs escape from stress granule sequestration suggesting that proteins that enter the secretory pathway are still transcribed (Unsworth et al., 2010). Thus, another level of control may be required to transiently keep newly-synthetized proteins in the endoplasmic reticulum. This thesis project provides evidence that cells use stress granules to selectively recruit key players of the ER-export machinery. COPII members (Sar1, Sec24), Sec16 and the TRAPP complex translocation onto stress granules is independent of the stimulus indicating that the early secretory pathway is implicated in (or controlled by?) a more general stress response. Moreover, migration of membrane trafficking proteins from ERES to cytosolic aggregates is time and dose dependent suggesting that these proteins do not take part to the initial step of RNP aggregation. SGs *per se* do not inhibit cargo transport indicating that the effect on membrane trafficking is not an epistatic effect due to SG aggregation but a direct consequence of ERES remodeling. (fig.4.1).

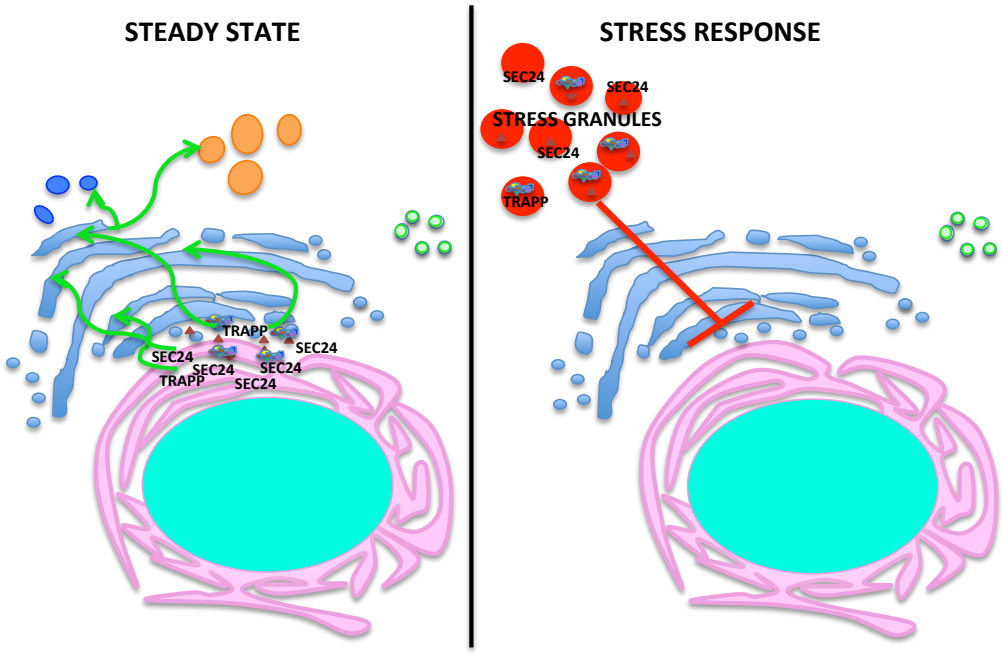

Figure 4.1 Working model. At steady state conditions proteins that enter the secretory pathway exit the ER via COPII vesicles, thus reach the Golgi and after undergoing post-translational modification they are sorted to their final destination. Under stimuli that perturb cell homeostasis, cells counteract stress activating the "integrated stress response" and triggering SGs formation. SGs aggregation is a mechanism with two main purposes: protein synthesis shut down and recruitment of key components ER-to-Golgi membrane trafficking to inhibit anterograde trafficking.

TDP-43 is a DNA- and RNA- binding protein that normally localizes to the nucleus where it regulates splicing and mRNA stability. TDP-43 is mutated and accumulates in large cytoplasmic aggregates in degenerating neurons and glia of ALS patients. TDP-43 is not the only protein involved in the pathogenesis of ALS since mutations of FUS, another component of SGs that form stress granules, were identified in familial and sporadic ALS patients (Liu-Yesucevitz et al., 2010). I found that both the TRAPP complex and COPII inner coat co-localize with SGs derived from transient overexpression of TDP-43 mutants.

Of note, fragmentation of the Golgi is a common feature in ALS patients. Compared to healthy subjects, the Golgi in ALS patients is reduced in size and fragmented,

appearing as disconnected punctate structures similar to the Golgi morphology in cells treated with microtubule depolymerisation agents (Mourelatos et al., 1990). Interestingly, Golgi fragmentation is more prominent in larger human motor neurons, such as those in the cerebral cortex (Fujita et al., 1999) and anterior horn (Fujita et al., 2000), suggesting they are specifically vulnerable to disturbances in Golgi function. The organization of the Golgi depends on efficient bidirectional vesicular transport with the ER. The formation of Golgi stacks requires continuous recycling of Golgi proteins to/from the ER (Lippincott-Schwartz et al., 2000). Inhibition of protein export from the ER disrupts Golgi organization (Storrie et al., 1998), resulting in the formation of tubulovesicular Golgi clusters, some of which fuse with the ER (Puri and Linstedt, 2003). Moreover, the Golgi complex is the main hub of cellular trafficking and alterations in its function lead to impairment of other vesicular transport pathways such as endocytosis, COPI-mediated retrograde trafficking and autophagy. Recently, it has been demonstrated that mutant forms of both FUS and TDP-43 impair the incorporation of secretory cargo into COPII vesicles, impeding protein export from the ER (Soo et al., 2015). I observed that treatment with arsenite (a SG inducer) triggers Golgi fragmentation (fig. 3.23). Thus, it is tempting to interpret these findings by speculating that the pathogenesis of ALS and related neurodegenerative disorders is an event cascade that, starting from stress granule aggregation, leads to mis-localization of ER-to-Golgi proteins with subsequent impairment in anterograde trafficking that results in Golgi fragmentation.

Furthermore, TRAPP depletion leads to defective SGs that lose their capability to capture cytosolic signalling molecules indicating that TRAPP is necessary for functional stress granules.

Starting from the study of sedlin and the TRAPP complex, this project thesis described a more general mechanism in which the ER-export machinery is involved. Further studies are needed to understand whether sedlin is upstream of the recruitment of membrane trafficking components onto SGs or whether proteins translocate independently. SG components can aggregate through low-complexity domains that allow protein interactions or alternatively as a response to specific signalling that mediates post-translational modifications. Whether the membrane trafficking components involved in this process are passively sequestered from the cytosolic bulk flow or if they acquire specific features that direct their localization remains to be addressed.

4.3 Sedlin controls bone and eye development in vivo

Sedlin is highly conserved during evolution and is an essential gene in yeast. However, sedlin mutations in humans cause a cartilage-restricted phenotype probably due to the expression of a sedlin protein codified by a pseudo-gene on chromosome 19 that can compensate loss-of-function of the gene product. This thesis work provides evidence that sedlin is expressed as a single copy in lower vertebrates and that genetic ablation of sedlin gene in vertebrates causes skeletal abnormalities that resemble the human defect. However, medaka sedl-/- larvae die at birth and present severe defects in photoreceptor development, raising the possibility that sedlin can exert functions also in eye development. Rhodopsin is a typical G-coupled receptor domain that traffics from the ER to the rod disks. It represents the most expressed protein in photoreceptors and its trafficking needs to be finely tuned to produce a perfectly functional rhodopsin (Nemet et al., 2015). Rhodopsin mis-localization or loss of function are causative of retinitis pigmentosa, an inherited degenerative eye disease that causes vision impairment due to the progressive degeneration of rods. I found that rhodopsin is retained in the Golgi complex in sedlin-depleted cells indicating that sedlin can also impact rhodopsin trafficking. Moreover, analysis of medaka eye sections revealed a hyperproliferation in the ciliary marginal zone (CMZ) (Fig. 4.2), a region of the eye where cells proliferate before exiting the cell cycle to differentiate into photoreceptors. It has been described that cell differentiation in the CMZ is orchestrated by inactivation of both Notch and Wnt signalling since mutations in SFRP1 and 2, that sequester the signalling molecule Wnt, negatively modulate ADAM10 (a Notch activator) to regulate retinal neurogenesis (Esteve et al., 2011) (fig. 4.2). Moreover, it has been broadly described that both Wnt and Notch have a

pivotal role in skeletal development (Baldridge et al., 2010). As a result, SFRP1 and 2 knock-out mice show severe defects in skeletogenesis (Satoh et al., 2008). Interestingly, the gene expression profile obtained from sedl-/- larvae show significant down-regulation of SFRP1 and 2 raising the possibility that sedlin can directly or indirectly control Notch signalling, and that bone and eye phenotypes underlie a common cause. However, further studies are needed to refute or prove this hypothesis.

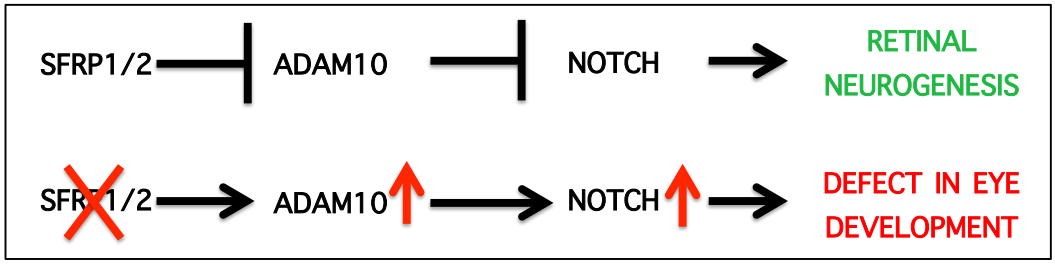

Figure 4.2 Wnt and Notch signaling in eye development. Notch signalling is required for retinal neurogenesis. SFRP1 and 2 bind and downregulate ADAM10, the metalloprotease responsible for the second cleavage of Notch, which is required for its activation. In retinas from Sfrp1-/-; Sfrp2-/- embryos, Notch signaling is transiently upregulated causing an impairment in retinal neurogenesis.

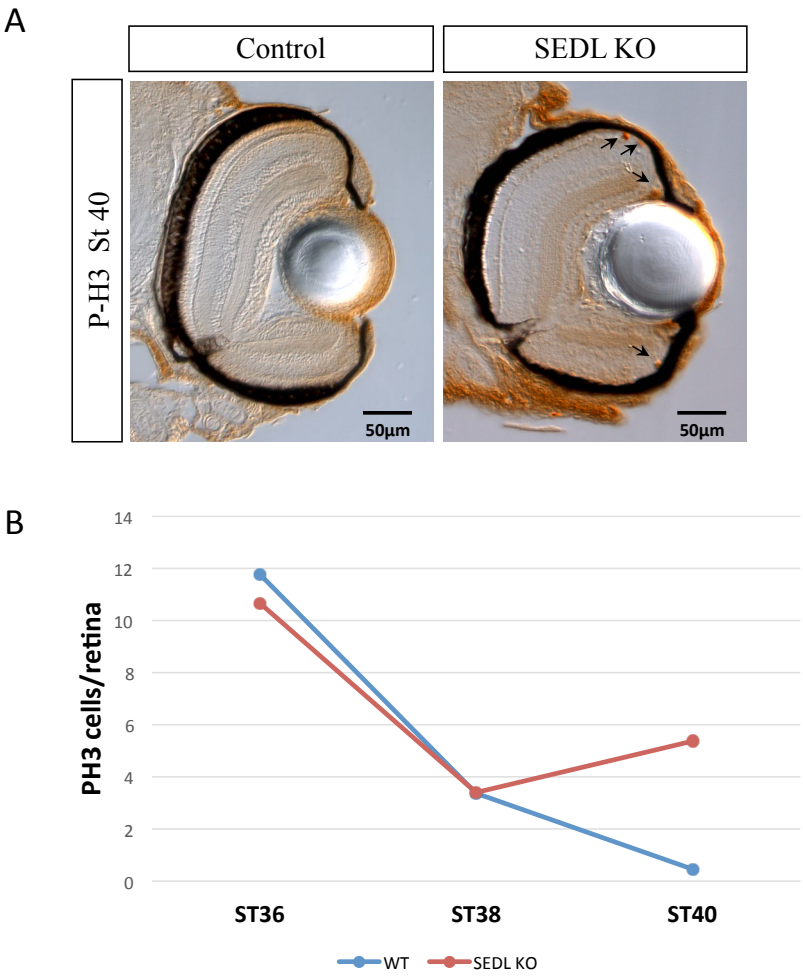

Figure 4.3 Sedlin KO show iperproliferation of the CMZ. (A) Frontal vibratome sections of St40 control and SEDL KO medaka embryos immunostained with antiphospho-histone H3 (P-H3) antibodies. Scale bar 50µm. **(B)** Quantification of PH3-positive cells in the retina of control and SEDL KO embryos at different embryonic stages, as indicated. No significant differences were detected between control and SEDL KO embryos at St36 and St38. In contrast, a significant increase was detected in St40 KO eyes compared with controls. Red arrows, P-H3-positive cells.

List of abbreviations

ALS amyotrophic lateral sclerosis

AS arsenite

BSA bovine serum albumin

cDNA complementary DNA

CGN Cis-Golgi network

Cas9 crisp associated protein 9

CME clathrin-mediated endocytosis

CMZ ciliary marginal zone

COPI/COPII coat protein I/II or coatomer

CPM count per milion

CPY carboxypeptidase Y

CRISPr Clustered Regularly Interspaced Short Palindromic repeats

DMEM Dulbecco's Modified minimal Essential Medium

DNA deoxyribonucleasic acid

EDTA ethylenediamine tetraacetic acid

eIF eukaryotic Initiation factor

EM Electron Microscopy

ER Endoplasmic Reticulum

ERES Endoplasmic Reticulum Exit Sites

ERGIC ER-Golgi Intermediate Compartment

FCS Fetal Calf Serum

FMRP fragile X-mental retardation protein

FTLD frontotemporal lobar degeneration

GAP Guanine Activating Protein

GEF Guanine Exchange Factor

GFP Green Fluorescence Protein

GTP guanosine triphosphate

GTPase guanosine triphosphatase

G3BP Ras GTPase-activating **protein-binding protein** 1

HeLa cells Henrietta Lacks cells

HEPES N-2-hydroxyethylpiperazine-N-2-ethanesulfonic acid

HF human fibroblasts

HRP horseradish peroxidase

IF immunofluorescence

IgG Immunoglobuline G

IP immunoprecipitation

KD Knock Down

kDa kilo Dalton

KO Knock Out

LB Luria Broth

Mo morpholino

mTRAPP mammalian transport protein particle

MW Molecular Weight

PAGE Polyacrylamide Gel Electrophoresis

PAS Pre-autophagosomal Structure

PBS phosphate buffered saline

PCI procollagen type I

PCII procollagen type II

PCR polymerase chain reaction

PFA paraformaldehyde

pIRES internal ribosomal entry sites

PM plasma membrane

PTW PBS 0.1% tween

qPCR quantitative polymerase chain reaction

RBP ribonucleoparticle

RNA ribonucleic acid

rpm revolution per minute

SDS Sodium dodecyl sulfate

SEDL spondyloepiphyseal dysplasia late

SFRP secreted frizzled related protein

SNARE N-ethylmaleimide-sensitive fusion attachment protein receptor

SGs stress granules

SRP signal recognition particle

TALEN transcription activator like-effector nucleases

TBS 150 mM NaCl, 50 mM Tris-HCl pH 7.5

TDP-43 transactive response DNA binding protein 43 kDa

Trs transport subunits

TGN trans-Golgi network

TEMED tetrametylethylenediammine

TMM trimmed mean of M-values

TF transferrin

TRIS tris(hydroxymethyl)aminomethane

TRAPP Transport Protein Particles

TTBS 0.05% Tween 20, 150 mM NaCl, 50 mM Tris-HCl pH 7.5

UPR unfolded protein response

VSV vesicular stomatitis virus

VSV-G vesicular stomatitis virus G protein **VTC** vesicular-tubular cluster

WARBM Warburg–Sjo–Fledelius syndrome

WGA wheat germ agglutinin

WT wild type

w/v weight/volume

ZFNs Zinc Finger Nucleases

Bibliography

Al Khamici, H., Brown, L.J., Hossain, K.R., Hudson, A.L., Sinclair-Burton, A.A., Ng, J.P.M., Daniel, E.L., Hare, J.E., Cornell, B.A., Curmi, P.M.G., et al. (2015). Members of the chloride intracellular ion channel protein family demonstrate glutaredoxin-like enzymatic activity. PloS One *10*, e115699.

Amodio, G., Venditti, R., De Matteis, M.A., Moltedo, O., Pignataro, P., and Remondelli, P. (2013). Endoplasmic reticulum stress reduces COPII vesicle formation and modifies Sec23a cycling at ERESs. FEBS Lett. *587*, 3261–3266.

Ansai, S., and Kinoshita, M. (2014). Targeted mutagenesis using CRISPR/Cas system in medaka. Biol. Open *3*, 362–371.

Ansai, S., Ochiai, H., Kanie, Y., Kamei, Y., Gou, Y., Kitano, T., Yamamoto, T., and Kinoshita, M. (2012). Targeted disruption of exogenous EGFP gene in medaka using zinc-finger nucleases. Dev. Growth Differ. *54*, 546–556.

Ansai, S., Sakuma, T., Yamamoto, T., Ariga, H., Uemura, N., Takahashi, R., and Kinoshita, M. (2013). Efficient targeted mutagenesis in medaka using custom-designed transcription activator-like effector nucleases. Genetics *193*, 739–749.

Antonny, B., Madden, D., Hamamoto, S., Orci, L., and Schekman, R. (2001). Dynamics of the COPII coat with GTP and stable analogues. Nat. Cell Biol. *3*, 531–537.

Arimoto, K., Fukuda, H., Imajoh-Ohmi, S., Saito, H., and Takekawa, M. (2008a). Formation of stress granules inhibits apoptosis by suppressing stress-responsive MAPK pathways. Nat. Cell Biol. *10*, 1324–1332.

Arimoto, K., Fukuda, H., Imajoh-Ohmi, S., Saito, H., and Takekawa, M. (2008b). Formation of stress granules inhibits apoptosis by suppressing stress-responsive MAPK pathways. Nat. Cell Biol. *10*, 1324–1332.

Aulas, A., and Vande Velde, C. (2015). Alterations in stress granule dynamics driven by TDP-43 and FUS: a link to pathological inclusions in ALS? Front. Cell. Neurosci. *9*, 423.

Averaimo, S., Milton, R.H., Duchen, M.R., and Mazzanti, M. (2010). Chloride intracellular channel 1 (CLIC1): Sensor and effector during oxidative stress. FEBS Lett. *584*, 2076–2084.

Baldridge, D., Shchelochkov, O., Kelley, B., and Lee, B. (2010). Signaling pathways in human skeletal dysplasias. Annu. Rev. Genomics Hum. Genet. *11*, 189–217.

Barlowe, C., and Helenius, A. (2016). Cargo Capture and Bulk Flow in the Early Secretory Pathway. Annu. Rev. Cell Dev. Biol. *32*, 197–222.

Barlowe, C., Orci, L., Yeung, T., Hosobuchi, M., Hamamoto, S., Salama, N., Rexach, M.F., Ravazzola, M., Amherdt, M., and Schekman, R. (1994). COPII: a membrane coat formed by Sec proteins that drive vesicle budding from the endoplasmic reticulum. Cell *77*, 895–907.

Barr, F., and Lambright, D.G. (2010). Rab GEFs and GAPs. Curr. Opin. Cell Biol. *22*, 461–470.

Barrowman, J., Sacher, M., and Ferro-Novick, S. (2000). TRAPP stably associates with the Golgi and is required for vesicle docking. EMBO J. *19*, 862–869.

Barrowman, J., Bhandari, D., Reinisch, K., and Ferro-Novick, S. (2010). TRAPP complexes in membrane traffic: convergence through a common Rab. Nat. Rev. Mol. Cell Biol. *11*, 759–763.

Bassik, M.C., Kampmann, M., Lebbink, R.J., Wang, S., Hein, M.Y., Poser, I., Weibezahn, J., Horlbeck, M.A., Chen, S., Mann, M., et al. (2013). A systematic mammalian genetic interaction map reveals pathways underlying ricin susceptibility. Cell *152*, 909–922.

Bentmann, E., Haass, C., and Dormann, D. (2013). Stress granules in neurodegeneration--lessons learnt from TAR DNA binding protein of 43 kDa and fused in sarcoma. FEBS J. *280*, 4348–4370.

Bi, X., Corpina, R.A., and Goldberg, J. (2002). Structure of the Sec23/24-Sar1 pre-budding complex of the COPII vesicle coat. Nature *419*, 271–277.

Bögershausen, N., Shahrzad, N., Chong, J.X., von Kleist-Retzow, J.-C., Stanga, D., Li, Y., Bernier, F.P., Loucks, C.M., Wirth, R., Puffenberger, E.G., et al. (2013). Recessive TRAPPC11 mutations cause a disease spectrum of limb girdle muscular dystrophy and myopathy with movement disorder and intellectual disability. Am. J. Hum. Genet. *93*, 181–190.

Braakman, I., and Bulleid, N.J. (2011). Protein folding and modification in the mammalian endoplasmic reticulum. Annu. Rev. Biochem. *80*, 71–99.

Brunet, S., Shahrzad, N., Saint-Dic, D., Dutczak, H., and Sacher, M. (2013). A trs20 mutation that mimics an SEDT-causing mutation blocks selective and non-selective autophagy: a model for TRAPP III organization. Traffic Cph. Den. *14*, 1091–1104.

Cai, H., Zhang, Y., Pypaert, M., Walker, L., and Ferro-Novick, S. (2005). Mutants in trs120 disrupt traffic from the early endosome to the late Golgi. J. Cell Biol. *171*, 823–833.

Cai, H., Yu, S., Menon, S., Cai, Y., Lazarova, D., Fu, C., Reinisch, K., Hay, J.C., and Ferro-Novick, S. (2007). TRAPPI tethers COPII vesicles by binding the coat subunit Sec23. Nature *445*, 941–944.

Cong, L., Ran, F.A., Cox, D., Lin, S., Barretto, R., Habib, N., Hsu, P.D., Wu, X., Jiang, W., Marraffini, L.A., et al. (2013). Multiplex genome engineering using CRISPR/Cas systems. Science *339*, 819–823.

David, A., Dolan, B.P., Hickman, H.D., Knowlton, J.J., Clavarino, G., Pierre, P., Bennink, J.R., and Yewdell, J.W. (2012). Nuclear translation visualized by ribosome-bound nascent chain puromycylation. J. Cell Biol. *197*, 45–57.

Davis, S., Wang, J., Zhu, M., Stahmer, K., Lakshminarayan, R., Ghassemian, M., Jiang, Y., Miller, E.A., and Ferro-Novick, S. (2016). Sec24 phosphorylation regulates autophagosome abundance during nutrient deprivation. ELife *5*.

Elkin, S.R., Lakoduk, A.M., and Schmid, S.L. (2016). Endocytic pathways and endosomal trafficking: a primer. Wien. Med. Wochenschr. 1946 *166*, 196–204.

Emara, M.M., Fujimura, K., Sciaranghella, D., Ivanova, V., Ivanov, P., and Anderson, P. (2012). Hydrogen peroxide induces stress granule formation independent of eIF2α phosphorylation. Biochem. Biophys. Res. Commun. *423*, 763–769.

Forster, R., Weiss, M., Zimmermann, T., Reynaud, E.G., Verissimo, F., Stephens, D.J., and Pepperkok, R. (2006). Secretory cargo regulates the turnover of COPII subunits at single ER exit sites. Curr. Biol. CB *16*, 173–179.

Fujita, Y., Okamoto, K., Sakurai, A., Amari, M., Nakazato, Y., and Gonatas, N.K. (1999). Fragmentation of the Golgi apparatus of Betz cells in patients with amyotrophic lateral sclerosis. J. Neurol. Sci. *163*, 81–85.

Fujita, Y., Okamoto, K., Sakurai, A., Gonatas, N.K., and Hirano, A. (2000). Fragmentation of the Golgi apparatus of the anterior horn cells in patients with familial amyotrophic lateral sclerosis with SOD1 mutations and posterior column involvement. J. Neurol. Sci. *174*, 137–140.

Furutani-Seiki, M., and Wittbrodt, J. (2004). Medaka and zebrafish, an evolutionary twin study. Mech. Dev. *121*, 629–637.

Gallione, C.J., and Rose, J.K. (1985). A single amino acid substitution in a hydrophobic domain causes temperature-sensitive cell-surface transport of a mutant viral glycoprotein. J. Virol. *54*, 374–382.

Gécz, J., Hillman, M.A., Gedeon, A.K., Cox, T.C., Baker, E., and Mulley, J.C. (2000). Gene structure and expression study of the SEDL gene for spondyloepiphyseal dysplasia tarda. Genomics *69*, 242–251.

Gécz, J., Shaw, M.A., Bellon, J.R., and de Barros Lopes, M. (2003). Human wild-type SEDL protein functionally complements yeast Trs20p but some naturally occurring SEDL mutants do not. Gene *320*, 137–144.

Gedeon, A.K., Tiller, G.E., Le Merrer, M., Heuertz, S., Tranebjaerg, L., Chitayat, D., Robertson, S., Glass, I.A., Savarirayan, R., Cole, W.G., et al. (2001). The molecular basis of X-linked spondyloepiphyseal dysplasia tarda. Am. J. Hum. Genet. *68*, 1386–1397.

Gilks, N., Kedersha, N., Ayodele, M., Shen, L., Stoecklin, G., Dember, L.M., and Anderson, P. (2004). Stress granule assembly is mediated by prion-like aggregation of TIA-1. Mol. Biol. Cell *15*, 5383–5398.

Grousl, T., Ivanov, P., Frýdlová, I., Vasicová, P., Janda, F., Vojtová, J., Malínská, K., Malcová, I., Nováková, L., Janosková, D., et al. (2009). Robust heat shock induces eIF2alpha-phosphorylation-independent assembly of stress granules containing eIF3 and 40S ribosomal subunits in budding yeast, Saccharomyces cerevisiae. J. Cell Sci. *122*, 2078–2088.

Imai, K., Hao, F., Fujita, N., Tsuji, Y., Oe, Y., Araki, Y., Hamasaki, M., Noda, T., and Yoshimori, T. (2016). Atg9A trafficking through the recycling endosomes is required for autophagosome formation. J. Cell Sci. *129*, 3781–3791.

Inohaya, K., Takano, Y., and Kudo, A. (2007). The teleost intervertebral region acts as a growth center of the centrum: in vivo visualization of osteoblasts and their progenitors in transgenic fish. Dev. Dyn. Off. Publ. Am. Assoc. Anat. *236*, 3031–3046.

Ishikawa, Y. (2000). Medakafish as a model system for vertebrate developmental genetics. BioEssays News Rev. Mol. Cell. Dev. Biol. *22*, 487–495.

Iwamatsu, T. (2004). Stages of normal development in the medaka Oryzias latipes. Mech. Dev. *121*, 605–618.

Jain, S., Wheeler, J.R., Walters, R.W., Agrawal, A., Barsic, A., and Parker, R. (2016). ATPase-Modulated Stress Granules Contain a Diverse Proteome and Substructure. Cell *164*, 487–498.

Jayabalan, A.K., Sanchez, A., Park, R.Y., Yoon, S.P., Kang, G.-Y., Baek, J.-H., Anderson, P., Kee, Y., and Ohn, T. (2016). NEDDylation promotes stress granule assembly. Nat. Commun. *7*, 12125.

Jones, S., Newman, C., Liu, F., and Segev, N. (2000). The TRAPP complex is a nucleotide exchanger for Ypt1 and Ypt31/32. Mol. Biol. Cell *11*, 4403–4411.

Jongjitwimol, J., Baldock, R.A., Morley, S.J., and Watts, F.Z. (2016). Sumoylation of eIF4A2 affects stress granule formation. J. Cell Sci. *129*, 2407–2415.

Kakuta, S., Yamamoto, H., Negishi, L., Kondo-Kakuta, C., Hayashi, N., and Ohsumi, Y. (2012). Atg9 vesicles recruit vesicle-tethering proteins Trs85 and Ypt1 to the autophagosome formation site. J. Biol. Chem. *287*, 44261–44269.

Kim, J.J., Lipatova, Z., and Segev, N. (2016). TRAPP Complexes in Secretion and Autophagy. Front. Cell Dev. Biol. *4*, 20.

Kim, W.J., Back, S.H., Kim, V., Ryu, I., and Jang, S.K. (2005). Sequestration of TRAF2 into stress granules interrupts tumor necrosis factor signaling under stress conditions. Mol. Cell. Biol. *25*, 2450–2462.

Kim, Y.-G., Raunser, S., Munger, C., Wagner, J., Song, Y.-L., Cygler, M., Walz, T., Oh, B.-H., and Sacher, M. (2006). The architecture of the multisubunit TRAPP I complex suggests a model for vesicle tethering. Cell *127*, 817–830.

Koehler, K., Milev, M.P., Prematilake, K., Reschke, F., Kutzner, S., Jühlen, R., Landgraf, D., Utine, E., Hazan, F., Diniz, G., et al. (2016). A novel TRAPPC11 mutation in two Turkish families associated with cerebral atrophy, global retardation, scoliosis, achalasia and alacrima. J. Med. Genet.

Lamb, C.A., Nühlen, S., Judith, D., Frith, D., Snijders, A.P., Behrends, C., and Tooze, S.A. (2016). TBC1D14 regulates autophagy via the TRAPP complex and ATG9 traffic. EMBO J. *35*, 281–301.

Leung, A.K.L., Vyas, S., Rood, J.E., Bhutkar, A., Sharp, P.A., and Chang, P. (2011). Poly(ADP-ribose) regulates stress responses and microRNA activity in the cytoplasm. Mol. Cell *42*, 489–499.

Li, C., Luo, X., Zhao, S., Siu, G.K., Liang, Y., Chan, H.C., Satoh, A., and Yu, S.S. (2016). COPI-TRAPPII activates Rab18 and regulates its lipid droplet association. EMBO J.

Liang, W.-C., Zhu, W., Mitsuhashi, S., Noguchi, S., Sacher, M., Ogawa, M., Shih, H.-H., Jong, Y.-J., and Nishino, I. (2015). Congenital muscular dystrophy with fatty liver and infantile-onset cataract caused by TRAPPC11 mutations: broadening of the phenotype. Skelet. Muscle *5*, 29.

Lieschke, G.J., and Currie, P.D. (2007). Animal models of human disease: zebrafish swim into view. Nat. Rev. Genet. *8*, 353–367.

Lipatova, Z., and Segev, N. (2012). A Ypt/Rab GTPase module makes a PAS. Autophagy *8*, 1271–1272.

Lipatova, Z., Majumdar, U., and Segev, N. (2016). Trs33-containing TRAPP IV: A Novel Autophagy-Specific Ypt1 GEF. Genetics.

Lippincott-Schwartz, J., Roberts, T.H., and Hirschberg, K. (2000). Secretory protein trafficking and organelle dynamics in living cells. Annu. Rev. Cell Dev. Biol. *16*, 557–589.

Littler, D.R., Harrop, S.J., Goodchild, S.C., Phang, J.M., Mynott, A.V., Jiang, L., Valenzuela, S.M., Mazzanti, M., Brown, L.J., Breit, S.N., et al. (2010). The enigma of the CLIC proteins: Ion channels, redox proteins, enzymes, scaffolding proteins? FEBS Lett. *584*, 2093–2101.

Loh, E., Peter, F., Subramaniam, V.N., and Hong, W. (2005). Mammalian Bet3 functions as a cytosolic factor participating in transport from the ER to the Golgi apparatus. J. Cell Sci. *118*, 1209–1222.

Lynch-Day, M.A., Bhandari, D., Menon, S., Huang, J., Cai, H., Bartholomew, C.R., Brumell, J.H., Ferro-Novick, S., and Klionsky, D.J. (2010). Trs85 directs a Ypt1 GEF, TRAPPIII, to the phagophore to promote autophagy. Proc. Natl. Acad. Sci. U. S. A. *107*, 7811–7816.

Mahfouz, H., Ragnini-Wilson, A., Venditti, R., De Matteis, M.A., and Wilson, C. (2012). Mutational analysis of the yeast TRAPP subunit Trs20p identifies roles in endocytic recycling and sporulation. PloS One *7*, e41408.

Malhotra, V., and Erlmann, P. (2015). The pathway of collagen secretion. Annu. Rev. Cell Dev. Biol. *31*, 109–124.

Mali, P., Yang, L., Esvelt, K.M., Aach, J., Guell, M., DiCarlo, J.E., Norville, J.E., and Church, G.M. (2013). RNA-guided human genome engineering via Cas9. Science *339*, 823–826.

McEwen, E., Kedersha, N., Song, B., Scheuner, D., Gilks, N., Han, A., Chen, J.-J., Anderson, P., and Kaufman, R.J. (2005). Heme-regulated inhibitor kinase-mediated phosphorylation of eukaryotic translation initiation factor 2 inhibits translation, induces stress granule formation, and mediates survival upon arsenite exposure. J. Biol. Chem. *280*, 16925–16933.

McGourty, C.A., Akopian, D., Walsh, C., Gorur, A., Werner, A., Schekman, R., Bautista, D., and Rape, M. (2016). Regulation of the CUL3 Ubiquitin Ligase by a Calcium-Dependent Co-adaptor. Cell *167*, 525–538.e14.

Meiling-Wesse, K., Epple, U.D., Krick, R., Barth, H., Appelles, A., Voss, C., Eskelinen, E.-L., and Thumm, M. (2005). Trs85 (Gsg1), a component of the TRAPP complexes, is required for the organization of the preautophagosomal structure during selective autophagy via the Cvt pathway. J. Biol. Chem. *280*, 33669–33678.

Melville, D.B., and Knapik, E.W. (2011). Traffic jams in fish bones: ER-to-Golgi protein transport during zebrafish development. Cell Adhes. Migr. *5*, 114–118.

Molliex, A., Temirov, J., Lee, J., Coughlin, M., Kanagaraj, A.P., Kim, H.J., Mittag, T., and Taylor, J.P. (2015). Phase separation by low complexity domains promotes stress granule assembly and drives pathological fibrillization. Cell *163*, 123–133.

Morozova, N., Liang, Y., Tokarev, A.A., Chen, S.H., Cox, R., Andrejic, J., Lipatova, Z., Sciorra, V.A., Emr, S.D., and Segev, N. (2006). TRAPPII subunits are required for the specificity switch of a Ypt-Rab GEF. Nat. Cell Biol. *8*, 1263–1269.

Morsomme, P., and Riezman, H. (2002). The Rab GTPase Ypt1p and tethering factors couple protein sorting at the ER to vesicle targeting to the Golgi apparatus. Dev. Cell *2*, 307–317.

Mourelatos, Z., Adler, H., Hirano, A., Donnenfeld, H., Gonatas, J.O., and Gonatas, N.K. (1990). Fragmentation of the Golgi apparatus of motor neurons in amyotrophic lateral sclerosis revealed by organelle-specific antibodies. Proc. Natl. Acad. Sci. U. S. A. *87*, 4393–4395.

Moutaoufik, M.T., El Fatimy, R., Nassour, H., Gareau, C., Lang, J., Tanguay, R.M., Mazroui, R., and Khandjian, E.W. (2014). UVC-induced stress granules in mammalian cells. PloS One *9*, e112742.

Nazarko, T.Y., Huang, J., Nicaud, J.-M., Klionsky, D.J., and Sibirny, A.A. (2005). Trs85 is required for macroautophagy, pexophagy and cytoplasm to vacuole targeting in Yarrowia lipolytica and Saccharomyces cerevisiae. Autophagy *1*, 37–45.

Nemet, I., Ropelewski, P., and Imanishi, Y. (2015). Rhodopsin Trafficking and Mistrafficking: Signals, Molecular Components, and Mechanisms. Prog. Mol. Biol. Transl. Sci. *132*, 39–71.

Novick, P., Field, C., and Schekman, R. (1980). Identification of 23 complementation groups required for post-translational events in the yeast secretory pathway. Cell *21*, 205–215.

Ohn, T., Kedersha, N., Hickman, T., Tisdale, S., and Anderson, P. (2008). A functional RNAi screen links O-GlcNAc modification of ribosomal proteins to stress granule and processing body assembly. Nat. Cell Biol. *10*, 1224–1231.

Panas, M.D., Kedersha, N., and McInerney, G.M. (2015). Methods for the characterization of stress granules in virus infected cells. Methods San Diego Calif *90*, 57–64.

Peretti, M., Angelini, M., Savalli, N., Florio, T., Yuspa, S.H., and Mazzanti, M. (2015). Chloride channels in cancer: Focus on chloride intracellular channel 1 and 4 (CLIC1 AND CLIC4) proteins in tumor development and as novel therapeutic targets. Biochim. Biophys. Acta *1848*, 2523–2531.

Puri, S., and Linstedt, A.D. (2003). Capacity of the golgi apparatus for biogenesis from the endoplasmic reticulum. Mol. Biol. Cell *14*, 5011–5018.

Ramaswami, M., Taylor, J.P., and Parker, R. (2013). Altered ribostasis: RNA-protein granules in degenerative disorders. Cell *154*, 727–736.

Reineke, L.C., and Lloyd, R.E. (2013). Diversion of stress granules and P-bodies during viral infection. Virology *436*, 255–267.

Reineke, L.C., and Lloyd, R.E. (2015). The stress granule protein G3BP1 recruits protein kinase R to promote multiple innate immune antiviral responses. J. Virol. *89*, 2575–2589.

Reineke, L.C., Kedersha, N., Langereis, M.A., van Kuppeveld, F.J.M., and Lloyd, R.E. (2015). Stress granules regulate double-stranded RNA-dependent protein kinase activation through a complex containing G3BP1 and Caprin1. MBio *6*, e02486.

Rossi, G., Kolstad, K., Stone, S., Palluault, F., and Ferro-Novick, S. (1995). BET3 encodes a novel hydrophilic protein that acts in conjunction with yeast SNAREs. Mol. Biol. Cell *6*, 1769–1780.

Sacher, M., Jiang, Y., Barrowman, J., Scarpa, A., Burston, J., Zhang, L., Schieltz, D., Yates, J.R., Abeliovich, H., and Ferro-Novick, S. (1998). TRAPP, a highly conserved novel complex on the cis-Golgi that mediates vesicle docking and fusion. EMBO J. *17*, 2494–2503.

Sacher, M., Barrowman, J., Schieltz, D., Yates, J.R., and Ferro-Novick, S. (2000). Identification and characterization of five new subunits of TRAPP. Eur. J. Cell Biol. *79*, 71–80.

Sacher, M., Barrowman, J., Wang, W., Horecka, J., Zhang, Y., Pypaert, M., and Ferro-Novick, S. (2001). TRAPP I implicated in the specificity of tethering in ER-to-Golgi transport. Mol. Cell *7*, 433–442.

Saito, K., Chen, M., Bard, F., Chen, S., Zhou, H., Woodley, D., Polischuk, R., Schekman, R., and Malhotra, V. (2009). TANGO1 facilitates cargo loading at endoplasmic reticulum exit sites. Cell *136*, 891–902.

Salama, N.R., Yeung, T., and Schekman, R.W. (1993). The Sec13p complex and reconstitution of vesicle budding from the ER with purified cytosolic proteins. EMBO J. *12*, 4073–4082.

Santos, A.J.M., Raote, I., Scarpa, M., Brouwers, N., and Malhotra, V. (2015). TANGO1 recruits ERGIC membranes to the endoplasmic reticulum for procollagen export. ELife *4*.

Satoh, W., Matsuyama, M., Takemura, H., Aizawa, S., and Shimono, A. (2008). Sfrp1, Sfrp2, and Sfrp5 regulate the Wnt/beta-catenin and the planar cell polarity pathways during early trunk formation in mouse. Genes. N. Y. N 2000 *46*, 92–103.

Shirahama-Noda, K., Kira, S., Yoshimori, T., and Noda, T. (2013). TRAPPIII is responsible for vesicular transport from early endosomes to Golgi, facilitating Atg9 cycling in autophagy. J. Cell Sci. *126*, 4963–4973.

Simpson, J.C., Joggerst, B., Laketa, V., Verissimo, F., Cetin, C., Erfle, H., Bexiga, M.G., Singan, V.R., Hériché, J.-K., Neumann, B., et al. (2012). Genome-wide RNAi screening identifies human proteins with a regulatory function in the early secretory pathway. Nat. Cell Biol. *14*, 764–774.

Soo, K.Y., Halloran, M., Sundaramoorthy, V., Parakh, S., Toth, R.P., Southam, K.A., McLean, C.A., Lock, P., King, A., Farg, M.A., et al. (2015). Rab1-dependent ER-Golgi transport dysfunction is a common pathogenic mechanism in SOD1, TDP-43 and FUS-associated ALS. Acta Neuropathol. (Berl.) *130*, 679–697.

Souquere, S., Mollet, S., Kress, M., Dautry, F., Pierron, G., and Weil, D. (2009). Unravelling the ultrastructure of stress granules and associated P-bodies in human cells. J. Cell Sci. *122*, 3619–3626.

Stagg, S.M., Gürkan, C., Fowler, D.M., LaPointe, P., Foss, T.R., Potter, C.S., Carragher, B., and Balch, W.E. (2006). Structure of the Sec13/31 COPII coat cage. Nature *439*, 234–238.

Storrie, B., White, J., Röttger, S., Stelzer, E.H., Suganuma, T., and Nilsson, T. (1998). Recycling of golgi-resident glycosyltransferases through the ER reveals a novel pathway and provides an explanation for nocodazole-induced Golgi scattering. J. Cell Biol. *143*, 1505–1521.

Sundaramoorthy, V., Sultana, J.M., and Atkin, J.D. (2015). Golgi fragmentation in amyotrophic lateral sclerosis, an overview of possible triggers and consequences. Front. Neurosci. *9*, 400.

Takahara, T., and Maeda, T. (2012). Transient sequestration of TORC1 into stress granules during heat stress. Mol. Cell *47*, 242–252.

Taussig, D., Lipatova, Z., and Segev, N. (2014). Trs20 is required for TRAPP III complex assembly at the PAS and its function in autophagy. Traffic Cph. Den. *15*, 327–337.

Thedieck, K., Holzwarth, B., Prentzell, M.T., Boehlke, C., Kläsener, K., Ruf, S., Sonntag, A.G., Maerz, L., Grellscheid, S.-N., Kremmer, E., et al. (2013). Inhibition of

mTORC1 by astrin and stress granules prevents apoptosis in cancer cells. Cell *154*, 859–874.

Tisdale, E.J., Bourne, J.R., Khosravi-Far, R., Der, C.J., and Balch, W.E. (1992). GTP-binding mutants of rab1 and rab2 are potent inhibitors of vesicular transport from the endoplasmic reticulum to the Golgi complex. J. Cell Biol. *119*, 749–761.

Tourrière, H., Chebli, K., Zekri, L., Courselaud, B., Blanchard, J.M., Bertrand, E., and Tazi, J. (2003). The RasGAP-associated endoribonuclease G3BP assembles stress granules. J. Cell Biol. *160*, 823–831.

Townley, A.K., Schmidt, K., Hodgson, L., and Stephens, D.J. (2012). Epithelial organization and cyst lumen expansion require efficient Sec13-Sec31-driven secretion. J. Cell Sci. *125*, 673–684.

Unsworth, H., Raguz, S., Edwards, H.J., Higgins, C.F., and Yagüe, E. (2010). mRNA escape from stress granule sequestration is dictated by localization to the endoplasmic reticulum. FASEB J. Off. Publ. Fed. Am. Soc. Exp. Biol. *24*, 3370–3380.

Venditti, R., Scanu, T., Santoro, M., Di Tullio, G., Spaar, A., Gaibisso, R., Beznoussenko, G.V., Mironov, A.A., Mironov, A., Zelante, L., et al. (2012). Sedlin controls the ER export of procollagen by regulating the Sar1 cycle. Science *337*, 1668–1672.

Venditti, R., Wilson, C., and De Matteis, M.A. (2014). Exiting the ER: what we know and what we don't. Trends Cell Biol. *24*, 9–18.

Wang, J., Menon, S., Yamasaki, A., Chou, H.-T., Walz, T., Jiang, Y., and Ferro-Novick, S. (2013). Ypt1 recruits the Atg1 kinase to the preautophagosomal structure. Proc. Natl. Acad. Sci. U. S. A. *110*, 9800–9805.

Wang, T., Xu, W., Qin, M., Yang, Y., Bao, P., Shen, F., Zhang, Z., and Xu, J. (2016). Pathogenic Mutations in the Valosin-containing Protein/p97(VCP) N-domain

Inhibit the SUMOylation of VCP and Lead to Impaired Stress Response. J. Biol. Chem. *291*, 14373–14384.

Wang, W., Sacher, M., and Ferro-Novick, S. (2000). TRAPP stimulates guanine nucleotide exchange on Ypt1p. J. Cell Biol. *151*, 289–296.

Westlake, C.J., Baye, L.M., Nachury, M.V., Wright, K.J., Ervin, K.E., Phu, L., Chalouni, C., Beck, J.S., Kirkpatrick, D.S., Slusarski, D.C., et al. (2011). Primary cilia membrane assembly is initiated by Rab11 and transport protein particle II (TRAPPII) complex-dependent trafficking of Rabin8 to the centrosome. Proc. Natl. Acad. Sci. U. S. A. *108*, 2759–2764.

Wheeler, J.R., Matheny, T., Jain, S., Abrisch, R., and Parker, R. (2016). Distinct stages in stress granule assembly and disassembly. ELife *5*.

Wippich, F., Bodenmiller, B., Trajkovska, M.G., Wanka, S., Aebersold, R., and Pelkmans, L. (2013). Dual specificity kinase DYRK3 couples stress granule condensation/dissolution to mTORC1 signaling. Cell *152*, 791–805.

Yamasaki, A., Menon, S., Yu, S., Barrowman, J., Meerloo, T., Oorschot, V., Klumperman, J., Satoh, A., and Ferro-Novick, S. (2009). mTrs130 is a component of a mammalian TRAPPII complex, a Rab1 GEF that binds to COPI-coated vesicles. Mol. Biol. Cell *20*, 4205–4215.

Yoshihisa, T., Barlowe, C., and Schekman, R. (1993). Requirement for a GTPase-activating protein in vesicle budding from the endoplasmic reticulum. Science *259*, 1466–1468.

Yu, S., Satoh, A., Pypaert, M., Mullen, K., Hay, J.C., and Ferro-Novick, S. (2006). mBet3p is required for homotypic COPII vesicle tethering in mammalian cells. J. Cell Biol. *174*, 359–368.

Zacharogianni, M., Kondylis, V., Tang, Y., Farhan, H., Xanthakis, D., Fuchs, F., Boutros, M., and Rabouille, C. (2011). ERK7 is a negative regulator of protein secretion in response to amino-acid starvation by modulating Sec16 membrane association. EMBO J. *30*, 3684–3700.

Zacharogianni, M., Aguilera-Gomez, A., Veenendaal, T., Smout, J., and Rabouille, C. (2014). A stress assembly that confers cell viability by preserving ERES components during amino-acid starvation. ELife *3*.

Zhang, Y., Liu, S., Wang, H., Yang, W., Li, F., Yang, F., Yu, D., Ramsey, F.V., Tuszyski, G.P., and Hu, W. (2015). Elevated NIBP/TRAPPC9 mediates tumorigenesis of cancer cells through NFκB signaling. Oncotarget *6*, 6160–6178.

Zou, S., Chen, Y., Liu, Y., Segev, N., Yu, S., Liu, Y., Min, G., Ye, M., Zeng, Y., Zhu, X., et al. (2013). Trs130 participates in autophagy through GTPases Ypt31/32 in Saccharomyces cerevisiae. Traffic Cph. Den. *14*, 233–246.